EXPLORATION OF PEROXISOME PROLIFERATOR-ACTIVATED RECEPTOR GAMMA AGONIST IN ALZHEIMER'S DISEASE THERAPY – A THERAPEUTIC ENIGMA

CHANG KAI LUN

(B. Sc. Pharm (Hons), NUS)

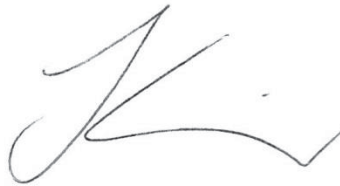A THESIS SUBMITTED

FOR THE DEGREE OF JOINT DOCTOR OF PHILOSOPHY

DEPARTMENT OF PHARMACY

NATIONAL UNIVERSITY OF SINGAPORE

AND

DEPARTMENT OF SURGERY AND CANCER

IMPERIAL COLLEGE LONDON

2014

Declaration

I hereby declare that this thesis is my original work and it has been written by me in its entirety. I have duly acknowledged all the sources of information which have been used in the thesis.

This thesis has also not been submitted for any degree in any university previously.

_____

Chang Kai Lun

31 July 2014

Acknowledgements

Table of contents

Summary

Recent failures of several phase III Alzheimer's disease (AD) clinical trials that were based on amyloid cascade hypothesis prompted researchers to look for alternatives in understanding the disease and finding an effective treatment for it. Pathological events that are associated with early-stage AD are of particular interest to the AD research community, as these represent potential drug targets that could allow clinical interventions to be initiated while AD has not deteriorated beyond the point of no return. In this thesis, I capitalised the high sensitivity offered by metabolic profiling approach, to study the early-stage AD pathological alterations in two different AD models, namely Chinese hamster ovarian cells transfected with amyloid precursor protein (CHO-APP_{695}) and transgenic mice carrying APP and presenilin-1 transgenes (APP/PS1).

My work in chapter 2 using CHO-APP_{695} allowed me to detect metabolic changes that occurred prior to any observable accumulation of extracellular amyloid-β in this model. Majority of these metabolic changes were related to impaired energy metabolism and dysregulated amino acid metabolism. Further biochemical assay data supported the notion of mitochondrial dysfunction in this model, and more interestingly I observed an accumulation of APP itself in the mitochondria of CHO-APP_{695}. This abnormal accumulation of APP at mitochondrial membrane could have mangled the powerhouse organelles, hence rendering the cells incapable of efficient respiration, resulting in impaired energy metabolism. Similar trend was observed in APP/PS1

transgenic mice, where excessive sugar build-up could be detected in their cortex and cerebellum tissue. Coupled with the observations of increased oxidative stress in their cortex, the inefficient energy expenditure and high sugar levels could have contributed to enhancing the oxidation state even further, resulting in subsequent neuronal death and surfacing of AD symptoms.

Intriguingly, pioglitazone (PIO) administration was found to have exerted a larger extent of treatment effect than rosiglitazone (ROSI) in CHO-APP$_{695}$, which was attributed to its dual agonism of both peroxisome proliferator-activated receptor gamma (PPARγ) and PPAR alpha (PPARα) receptors. PIO treatment was also observed to have successfully rescued the state of impaired energy metabolism in APP/PS1 mice, on top of enhancing the anti-oxidative capacity and lowering the amyloid-β in their cortex tissue. Further work in chapter 4 also showed that P-glycoprotein drug efflux transport at the blood-brain-barrier is a significant contributor in keeping PIO away from the brain. I went on to show that (+)-PIO, one of PIO's stereoisomer, afforded the brain of mice a larger exposure to PIO as compared to racemic PIO itself, suggesting that (+)-PIO is potentially a better drug candidate then racemic PIO for treatment of brain diseases. This discovery is particularly relevant now as there are two ongoing clinical trials looking at PIO as treatment for AD and Parkinson's disease. The findings in my thesis contribute substantially to AD research, and support the pursuant of PIO further in the drug pipeline for AD.

List of Tables

List of Figures

APP/PS1 transgenic mice; **(B)** Y-permuted model validation plot for PLS-DA of hippocampus metabolic data; **(C)** OPLS-DA of hippocampus metabolic data (R^2(Y) = 0.986, Q^2(cum) = 0.914).

Figure 9. (A) PCA of cerebellum metabolic profiles for wildtype and APP/PS1 transgenic mice; **(B)** Y-permuted model validation plot for PLS-DA of cerebellum metabolic data; **(C)** OPLS-DA of cerebellum metabolic data (R^2(Y) = 0.966, Q^2(cum) = 0.818).

Figure 10. (A) PCA of cerebellum metabolic profiles for wildtype and APP/PS1 transgenic mice; **(B)** Y-permuted model validation plot for PLS-DA of cerebellum metabolic data; **(C)** OPLS-DA of cerebellum metabolic data (R^2(Y) = 0.966, Q^2(cum) = 0.818).
Figure 11. (A) Discriminant metabolites in cortex tissue that were treated by PIO administration; **(B)** Discriminant metabolites in cerebellum tissue that were treated by PIO administration.

Figure 12. (A) Amyloid-β40 levels in cortex samples; **(B)** Amyloid-β40 levels in plasma samples; **(C)** Amyloid-β42 levels in cortex samples; **(D)** Amyloid-β42 levels in plasma samples; * $P < 0.05$ when compared against non-transgenic wildtype mice; ** $P < 0.05$ when compared against non-treated APP/PS1 mice; All error bars represent one SD.

Figure 13. (A) APP levels in cortex samples harvested from all three groups of mice; **(B)** APP levels in extracted mitochondrial fractions; * $P < 0.05$ when compared against non-transgenic wildtype mice; ** $P < 0.05$ when compared against non-treated APP/PS1 mice; All error bars represent one SD; **(C)** Western blot analysis of 4 organelle markers (100 kDa – plasma membrane; 55 kDa – mitochondria; 36 kDa – cytosol; 15 kDa - nucleus) performed on extracted mitochondrial fractions and cortex tissue homogenate.

Figure 14. LDH activities in cortex samples taken from all three groups of mice; * $P < 0.05$ when compared against non-transgenic wildtype mice; ** $P < 0.05$ when compared against non-treated APP/PS1 mice; All error bars represent one SD.

Figure 15. (A) SOD activities in cortex samples taken from all three groups of mice; **(B)** SOD activities in plasma samples; **(C)** Catalase activities in cortex samples; **(D)** Catalase activities in plasma samples; * $P < 0.05$ when compared against non-transgenic wildtype mice; ** $P < 0.05$ when compared against non-treated APP/PS1 mice; All error bars represent one SD.

Figure 16. (A) PIO levels in plasma samples harvested from mice given intra-peritoneal PIO with or without pre-treatment of P-gp and/or BCRP blocker; **(B)** Ratios of PIO levels in brain-to-plasma in mice with or without pre-treatment of P-gp and/or BCRP blocker; * $P < 0.05$ when compared mice pre-treated with vehicle; Error bars represent one SD.

Figure 17. (A) Chiral separation of (+)-PIO and (-)-PIO in brain samples of mice administered with racemic PIO; chromatogram in box shows (+)-PIO

and (-)-PIO in blank brain samples spiked with racemic PIO; **(B)** Chiral separation of (+)-PIO and (-)-PIO in plasma samples of mice administered with racemic PIO; chromatogram in box shows (+)-PIO and (-)-PIO in blank plasma samples spiked with racemic PIO.

Figure 18. (A) PIO concentration *versus* time (hours) profile for plasma samples harvested from mice fed with either racemic PIO or purified (+)-PIO; **(B)** PIO concentration *versus* time (hours) profile for brain samples harvested from mice fed with either racemic PIO or purified (+)-PIO; Error bars represent one SD.

Figure 19. (A) Representative GC-TOF-MS chromatogram of caffeinated coffee sample; **(B)** Representative GC-TOF-MS chromatogram of decaffeinated coffee sample.

Figure 20. (A) PCA scores plot for caffeinated and decaffeinated coffee samples **(B)** Model validation plot for PLS-DA model between caffeinated and decaffeinated coffee samples **(C)** OPLS-DA between caffeinated and decaffeinated coffee samples (1 predictive component, 1 orthogonal component, $R^2(Y) = 1$, $Q^2(cum) = 0.998$)

List of Abbreviations

AD	Alzheimer's disease
APCI	Atmospheric pressure chemical ionisation
API	Atmospheric pressure ionisation
APP	Amyloid precursor protein
AUC	Area under curve
BACE-1	Beta-secretase
BBB	Blood-brain-barrier
BCRP	Breast cancer resistance protein
CHO	Chinese hamster ovarian
CHO-APP$_{695}$	CHO cells transfected with APP$_{695}$
CHO-WT	CHO cells (wildtype)
CSF	Cerebrospinal fluid
EI	Electron impact
ESI	Electrospray ionisation
FBS	Fetal bovine serum
FC	Fold-change
FDA	Food and Drug Administration
GC-MS	Gas chromatography coupled to mass spectrometry
GC-TOF-MS	GC-Time-of-Flight-MS
HMDB	Human Metabolome Database
HPLC	High performance liquid chromatography
IACUC	Institutional Animal Care and Use Committee (NUS)
IS	Internal standard
KEGG	Kyoto Encyclopedia of Genes and Genomes
LDH	Lactate Dehydrogenase
MCI	Mild cognitive impairment
MOA	Mechanism of action
MRM	Multiple-reaction-monitoring
MS	Mass spectrometry
MSTFA	N-methyl-N-trimethylsilyl trifluoroacetamide
NACLAR	National Advisory Committee on Laboratory Animal Research (Singapore)
NIST	National Institute of Standards and Technology
NMR	Nuclear magnetic resonance
OPLS-DA	Orthogonal partial least squares discriminant analysis
PCA	Principal component analysis
PET	Positron emission tomography
PGC-1α	PPARγ coactivator 1α
P-gp	P-glycoprotein
PIO	Pioglitazone
PLS-DA	Partial least squares discriminant analysis
PPAR	Peroxisome proliferator-activated receptor
PPARα	Peroxisome proliferator-activated receptor alpha

PPARβ	Peroxisome proliferator-activated receptor beta
PPARγ	Peroxisome proliferator-activated receptor gamma
PS1	Presenilin-1
QC	Quality control
ROSI	Rosiglitazone
RT	Retention time
S/N	Signal to noise
SDH	Succinate dehydrogenase
SI	Similarity index
SNP	Single nucleotide polymorphism
SOD	superoxide dismutase
TCMS	Trimethylchlorosilane
TIC	Total ion chromatograms
TRO	Troglitazone
TZD	Thiazolidinedione
UPLC-MS/MS	Ultra performance liquid chromatography coupled to tandem mass spectrometer
VIP	Variable importance in projection

CHAPTER 1: Introductory chapter

1.1.   <u>Overview of Alzheimer's disease</u>

1.1.1. <u>Prevalence and disease characteristics</u>

First discovered by Dr. Alois Alzheimer in 1907, Alzheimer's disease (AD) is now recognised as the most common cause of dementia in our aging population. So far, it is still considered as an irreversible brain disease, which wrecks the brain by bringing with it a progressive deterioration of selective cognitive domains and profound memory decline. Being the most common type of neurodegenerative disorder, AD causes considerable socio-economic impact on the society [1]. The total estimated healthcare cost of AD alone is US$604 billion in 2010 [2], which could have stemmed from 4–5 million individuals in the United States and 100 million worldwide who are afflicted by this dreadful disease [3]. Judging based on the current state of AD research, these numbers are projected to grow to 14 million and 280 million respectively by year 2050 [3]. The rising AD-associated healthcare cost makes it imperative for substantial medical progress to be made in the area of prevention, early diagnosis and treatment of this worldwide pandemic.

AD is defined post mortem by the presence of abundant build-up of amyloid plaques and neurofibrillary tangles in the brain [4]. Amyloid plaques are extracellular deposits consisting primarily of amyloid-β peptides; whereas neurofibrillary tangles are composed of intraneuronal aggregations of hyperphosphorylated tau, a microtubule-associated protein involved in

microtubule stabilization [4]. Some preclinical and clinical evidence suggested that amyloid pathologies precede tau pathologies [4-7], and as a result current AD research work are mainly targeting the amyloid pathology. On the other hand, tau pathology had been shown to be more closely associated with neuronal cell death [6]. However, the mechanistic link between Amyloid-β deposition, tau pathology, and neuronal cell death remains debatable [8]. Nevertheless, one should keep in mind that although plaques and tangles are pathognomonic, they are not the only pathological changes occurring in the brain of AD patients [4]. Numerous other studies also produced evidence of inflammatory reaction, oxidative stress and mitochondrial dysfunction in brain tissues of AD patients [9-11].

Oxidative stress induced damages such as lipid peroxidation, protein oxidation and DNA/RNA oxidation have long been demonstrated to be the hall mark pathological signals in AD [12]. It had already been shown that patients with mild cognitive impairment (MCI) displayed signs of increased brain oxidative damage, and lipid peroxidation markers could potentially be used as a predictor for their increased risk to progress to symptomatic AD [10]. Another major pathological alteration in AD patients is impaired mitochondrial dynamics, which has dangerously close links to the generation of reactive oxygen species in cells [13]. Having both mitochondrial dysfunction and increased oxidative damage is more than just a double whammy, as they could reinforce one another and create a vicious downward spiral that eventually collapses the whole biological system [12]. More and more researchers are investigating these pathological events to hunt for potential therapeutic targets,

in a hope that by preventing oxidative damage and/or rescuing mitochondrial impairment in brain tissue of AD patients, they can slow down or stop AD progression [13, 14].

Regardless of which pathological event unfolds first, it is clear that the combined consequences of all the above-mentioned pathological changes are severe neuronal and synaptic loss, followed subsequently by plummeting cognitive functions and diminishing brain mass in AD patients. It is estimated that at the time of death, one AD patient's brain may weigh only two-third of that of an age-matched, non-demented individual [4]. In view of the heavy social, economic and more importantly emotional impact of AD in our lives, there is a strong urge to tackle this disease and find a treatment strategy that will effectively halt the disease progression. However, the field of AD research is laden with conflicting views of disease pathogenesis, and advancements in finding a successful therapy is constantly inhibited by unceasing reports of catastrophic clinical trials of once promising drug candidates. To put it optimistically, AD researchers have learnt a great deal from these past failures, and the knowledge base is growing tremendously. Nevertheless, there are still numerous obstacles and clinical challenges to overcome in order to see the light at the end of this tunnel (and have faith that it is not the light of an oncoming train).

1.1.2. Clinical challenges in diagnosing and treating AD

Although a century has passed since the first case of AD was described by Dr. Alois Alzheimer, diagnosis and treatment of AD remain clinically challenging.

Complicated further by a lack of specific biomarkers and elusive mechanism of AD pathogenesis, there is currently no absolute clinical guidelines for diagnosing and treating AD patients. Although doctors now have several tools to help them determine whether a dementia patient has possible or probable AD, it can only be definitively diagnosed after death by linking clinical measures with an examination of brain tissue and pathology in an autopsy [15]. Recent developments in the field of amyloid-β positron emission tomography (PET) imaging had been facilitated by the availability of florbetapir F-18 (Amyvid, Eli Lilly) approved by the Food and Drug Administration (FDA). However, its implications in clinical settings are fairly limited by the sparse number of studies that have evaluated this imaging technique [16]. Besides the high level of skills required to carry out and interpret a PET scan, its clinical application is severely hampered by high proportion of false positive scan results. In particular, one study showed that 30% of cognitively normal older subjects recruited were diagnosed to have "AD-positive" PET scan results [17]. Therefore, there is still a lack of specific biomarkers that can be used to screen the population for AD or to diagnose the disease in a suspected clinical case. This limitation also poses a great challenge to AD clinical trials, given the difficulty in recruiting accurately diagnosed AD patients and the lack of tools to properly measure their therapeutic responses to experimental drug compounds.

To further exacerbate this situation, the exact pathogenesis of AD remains elusive, though it is now generally thought to be a multifactorial disease. Several hypotheses have been proposed, and among them the amyloid cascade

hypothesis [18, 19] gathered the most evidence in preclinical and clinical studies and it is currently considered the most widely accepted hypothesis underlying the AD pathogenesis [20]. It postulates that a mutation in the amyloid precursor protein (APP) gene results in increased expression of membrane-spanning APP, which is a target for two enzymes, namely beta-secretase (BACE-1) and gamma-secretase. Cleavage of APP by these two enzymes leads to increased production of amyloid-β, and subsequently formation of more amyloid-β plaques in the brain, which entails inflammation and ultimately results in neurodegeneration [19]. Despite the well-established evidence to support amyloid cascade hypothesis, clinical significance of the amyloid-β paradigm has been undermined recently by the increasing number of failed clinical trials which were based on the amyloid cascade hypothesis. The more prominent one includes phase III clinical trial for Eli Lilly's Semagacestat, which is a small molecule inhibitor of gamma-secretase enzyme [21]. The trial ended in dismay as it was halted by Eli Lilly after an interim analysis showed that AD patients dosed with semagacestat had a worse cognitive decline as compared to the placebo group [21]. More interestingly, their data showed that patients administered with semagacestat had a lower level of amyloid-β in their plasma, indicating that drug target was successfully engaged but failed to elicit any meaningful therapeutic response [21]. More recently, another two closely-watched drug candidates, namely bapineuzumab (Pfizer and Johnson & Johnson) and solanezumab (Eli Lilly) also failed their multiple phase III clinical trials. Both candidates are humanized anti-amyloid-β monoclonal antibodies, and they both failed to perform any better than placebo in their own respective phase III trials [22, 23]. All these failed

attempts led some researchers to focus their effort on alternative drug target such as pathological tau, which is a brain-specific protein associated with microtubules [24, 25]. On the other hand, some believe that interactions between both amyloid-β and tau are the true culprits behind the destructive biochemistry unfolded in the brain tissues of AD patients [26].

Coming up with a disease modifying therapy that is effective in treating the disease is also another uphill task in AD research. Besides the failures of more prominent anti-amyloid clinical trials discussed above, numerous other drug candidates that engage different drug targets had not demonstrated efficacy in their own clinical trials as well. These include the anti-inflammatory ibuprofen [27], cholesterol-lowering simvastatin [28], and anti-diabetic rosiglitazone (ROSI) [29], just to name a few. Meanwhile, a group of researchers are approaching a different treatment strategy of AD. They are attempting to administer the drug to research participants even before any symptoms of cognitive decline characteristic of AD can be observed. The goal is to nip the disease in the bud while it is still in the "preclinical", asymptomatic phase of AD [30]. These participants are recruited because they carry the Presenilin-1 (PS1) mutation, which predisposes them to development of AD later in life due to the detrimental downstream effect on the activity of gamma-secretase. This is the first preventive trial in the field of AD and its results can be potentially enlightening to AD drug researchers. The outcome of this trial would help to clear the doubts surrounding amyloid cascade hypothesis, and yield information that is vital to the advancement of AD research.

Clearly, the pathogenesis and pathophysiological process of AD is currently still unclear, and the field is in dire need for an effective disease modifying drug compound. More recent advancements in high throughput analytical instruments have made possible the extraction of enormous datasets from a single sample within a reasonably short analysis run time, and gave rise to the "-omics" era. Metabolic profiling technique (also known as metabolomics or metabonomics) is one relatively newer member of the "-omics" family, and has since been increasingly adopted to study biochemical consequences of different pathophysiological processes [31] and to understand the mechanism of action (MOA) of therapeutic compounds [32]. When applied on a carefully chosen disease model, these strategies are able to produce comprehensive data that allow further hypotheses to be generated and tested using the same model. In the following sections, I will elaborate in detail the background of metabolic profiling and what it can offer over the other "-omics" techniques. I will also discuss briefly the applicability and advantages offered by gas chromatography coupled to mass spectrometry (GC-MS) in metabolic profiling studies, and how GC-MS can be used as a potential study tool to help me elucidate the pathogenesis and pathophysiological processes of AD and better understand the therapeutic mechanism of compound of interest in my project, the peroxisome proliferator-activated receptor gamma (PPARγ) agonists.

1.2. Metabolic profiling as a tool to better understand AD

1.2.1. The era of "-omics" and metabolic profiling

Since the advent of "genomics" and "transcriptomics" about two decades ago, the scientific research community has stepped into the "-omics" era, where studies involve generation of large datasets followed by multivariate data analyses that focus on holism instead of reductionism. Metabolomics is a relatively newer "-omics" in the field of system biology, with the term "metabolome" first appearing in the literature in 1998 [33]. This technique is built upon original works that measured metabolites in unmodified biological fluids using GC-MS or nuclear magnetic resonance (NMR) spectroscopy, and made possible with the development of pattern recognition methods [31]. The term "metabonomics" was later coined by Professor Jeremy Nicholson and his colleagues at the Imperial College London as "*the quantitative measurement of the dynamic multiparametric metabolic response of living systems to pathophysiological stimuli or genetic modification*" [34]. The difference between metabonomics and metabolomics is mainly philosophical, rather than technical, and both terms were often used interchangeably as the analytical science and statistical methods powering both techniques are the same [31]. In this respect, I will use the term "metabolic profiling" throughout my thesis to avoid confusion in readers.

Subsequently, the "-omics"-driven research received increasing acceptance in various fields of research, and becomes the widely used approach in biomarker discovery [31]. Biomarkers can be broadly defined, according to National Institute of Health (NIH), as "*a characteristic that is objectively measured and evaluated as an indicator of normal biological processes, pathological processes, or pharmacological responses to a therapeutic intervention*" [35].

When compared against other "-omics"-driven research, metabolic profiling offers several distinct advantages. Firstly, owing to its small size and low molecular weight, metabolites are structurally conserved across species [36], unlike protein and gene expressions which usually involve different isoforms that often carry notably different properties. Secondly, since the metabolome lies downstream of genomes, transcriptomes, and proteomes, the metabolic signal was shown to be amplified [37]. This allows metabolic profiling approach to detect subtle fluctuations in the system, and therefore represents a more sensitive platform for probing into the early disease stages, as well as for detecting and monitoring the therapeutic response to drug treatment. However, regulation in this "-omics" cascade was found to be rarely hierarchical [38], thus being closer to the phenotypic outcome gives metabolic profiling a vast advantage over other "-omics" techniques.

1.2.2. GC-MS in metabolic profiling studies

With the availability of a variety of high throughput analytical instruments, metabolic profiling approach is beginning to gain traction, especially in the field of biomarker discovery. A variety of analytical methods can be employed in metabolic profiling studies, with some of the common ones being NMR spectroscopy and Mass spectrometry (MS) [31]. One analytical tool that has been widely used in metabolic profiling studies is GC-MS. As compared to other analytical platforms, GC-MS offers high sensitivity, powerful peak resolution and reproducibility [39]. On top of that, GC-MS uses electron impact (EI) ionisation, a hard ionisation technique, to turn analyte into ions which can then be detected by mass analysers. This affords GC-MS its biggest

advantage over other analytical platforms in metabolic profiling studies – the availability of large commercial EI spectral libraries for fast and straightforward metabolite identification. EI ionisation is carried out based on gas-phase physical mechanism, under conditions of high temperature and high vacuum. Upon collision of GC-eluted analyte by a high-energy electron beam standardised at 70 eV, the gaseous analyte molecule is fragmented in a highly reproducible manner, generating almost identical mass spectra for the same compound analysed under the standard set of analytical conditions. As a result, large commercial EI spectral libraries such as National Institute of Standards and Technology (NIST) [40] and FiehnLib [41] mass spectral database could be put together to provide straightforward metabolic peak identification. This makes GC-MS a suitable analytical platform for metabolic profiling studies as the analyses carried out are often untargeted, where analytes of interest are not known beforehand. The availability of a transferable mass spectral database enables the analyst to identify the unknown metabolites with ease and confidence, and also contribute more spectral to the database for the benefits of other analysts.

This distinct advantage of EI ionisation is unfortunately not applicable for other atmospheric pressure ionisation (API) methods, such as electrospray ionisation (ESI) and atmospheric pressure chemical ionisation (APCI), which are commonly used with LC-MS systems. These ionisation interfaces are based on low-energy chemical processes, thus also known as soft ionisation methods. These ionisation methods produce protonated (positive mode) or deprotonated (negative mode) molecular ions (with or without adducts), and

fragmentation of analyte molecule is minimum. Tandem MS (MS/MS) or high resolution MS are often used to account for the loss of information given by fragmentation pattern, but these require more complex and costly MS instrumentation [42]. On top of that, one major constraint imposed on API methods is the impact of co-eluting matrix compounds on the degree of analyte ionisation (more commonly known as matrix effects), and it could result in either ionisation suppression or enhancement [43]. Another drawback of API methods is that polarity of the analyte molecule can also have an impact on its signal response to matrix effects [43]. These limitations make it challenging to create a mass spectral library that can be applicable to different analytical instruments or when analysing different biological fluids, even if the analysis is operated under the same set of conditions. As a result, analytical platform that commonly employ API interface such as LC-MS has limited utility in untargeted metabolic profiling studies, and has better applicability in targeted screening, where analytes of interest are known beforehand. Operating conditions required for EI methods are contradictory to the operating environment of LC-MS interface, therefore making LC-EI-MS an unlikely analytical set-up. Although some groups have attempted to employ EI ion source in a LC system to reap the benefits of mass spectral database availability, its applicability is often compromised by trying to strike a balance between the divergent requirements of LC and EI ionisation [42].

In spite of the advantages conferred by GC-MS in metabolic profiling studies, GC-MS analysis is not without its limitations. The analytical procedure usually entails extensive sample preparation which could introduce variability

into sample analyses. The majority of metabolites also require chemical derivatisation at elevated temperature to add volatility and thermal stability to the metabolites and make them compatible with GC-MS analysis, but the derivatisation step itself could be detrimental to thermal-labile metabolites [44]. On top of that, the metabolic profiling analysis run time often stretch into the range of 30 to 60 minutes for each individual sample, making this analytical platform less suitable for large sample batch. Therefore, choosing the right platform for metabolic profiling analysis is often dependent on the analytes of interest, sample types, sample batch size, as well as research purpose of the metabolic profiling studies. Interestingly, different analytical platforms, such as NMR and GC-MS-based analyses, were found to cover different metabolic spaces when applied together [45]. This suggests that both platforms are complementary to each other in metabolic profiling studies and may be used in tandem to gain a more comprehensive understanding about the disease of interest.

1.2.3. Metabolic profiling in AD studies

In an attempt to unravel the pathological changes behind AD pathogenesis and identify the drug targets that can effectively slow down or halt AD progression, more and more researchers have recently been focusing their effort on investigating and characterising early-stage AD phenotypes [46]. Such effort could potentially give rise to reliable early-stage AD diagnostic tools, which can then be used to assist clinicians and researchers in positioning drug interventions at the right temporal therapeutic window for effective detection of treatment effects in AD clinical trials [47]. Therefore, tools that

allow investigation of early-stage AD would prove to be invaluable, and metabolic profiling technique, given its capability to detect the subtle fluctuations in a biological system as discussed above, presents itself as a promising approach in the field of AD research [48]. Applied on a carefully chosen disease model, metabolic profiling strategies could produce comprehensive data that allow further hypotheses to be generated and tested using the same model. This technique had also been employed on its own [49] or in conjunction with other "-omics" technique [50] to give a more complete understanding of the MOA powering a therapeutic compound. Therefore, it represents a valuable study tool in this project that metabolic profiling technique was employed for better understanding the AD pathophysiology using both the *in vitro* and *in vivo* AD models, as well as for better discerning the therapeutic mechanisms of PPARγ agonists in the AD therapy.

One of the more commonly used disease model in AD research is the APP model, where cells (*in vitro* model) or animals (*in vivo* model, often mice are used as models) having the APP transgene would overexpress the membrane protein APP, which will then lead to accumulation of neurotoxic amyloid-β protein. The accumulation of amyloid-β is then assumed to be responsible for cell death or biochemical changes that are reflective of AD pathology in these disease models, an assumption that is supported by the widely accepted amyloid cascade hypothesis. Due to alternative splicing of exons, APP exists in three major isoforms that are used widely in AD research [51]. Choosing between different APP isoforms is an important factor that should be taken into consideration when an APP model is employed in AD research. Among

the three major APP isoforms, APP_{695} is considered to be the most appropriate isoform for AD research as amyloid-β and AICD (APP intracellular domain) were observed to be preferentially synthesized from APP_{695} [51].

To generate a more aggressive APP model, another transgene PS1 could be added to amplify the toxicity induced by APP in the disease models. PS1 mutation is responsible for increasing expression of PS1, a part of presenilin complex which regulate the proteolytic activity of gamma secretase. Together with the increased expression of APP, the enhanced activity of gamma secretase will lead to more rapid generation of neurotoxic amyloid-β, therefore producing observable AD phenotypes in the disease models at a much earlier time point [52]. The APP/PS1 double transgenic mouse model has now been widely used in the field of AD research to understand the disease better [53], and has also been used routinely as an *in vivo* screening model for therapeutic compounds [54]. Then with the recent reports of failed clinical trials that are based on amyloid cascade hypothesis, there is an increasing research interest to look into triple transgenic mouse, which bears mutated APP gene, PS1 gene, and P301L tau gene. However, this led some to question the physiological relevance of triple transgenic mouse, since it is clear that no clinical case of AD is associated with triple mutations on APP, PS1 and tau genes [53]. The relevance of different AD mouse models will be further elaborated in chapter 3, where I will discuss my work on AD metabolic profiling studies using the *in vivo* AD model.

A thorough search among published literatures revealed relatively few studies that employ GC-MS-based metabolic profiling approach to study AD, as compared to studies that used NMR-based metabolic profiling technique. Two studies employed GC-MS-based metabolic profiling tool on APP/PS1 transgenic AD mice. One study used GC-quadrupole-MS to reveal the metabolic profiles of whole brain and plasma of TASTPM mice, which carries the mutant human APP_{695} (with K670N/M671L double mutation) and PS1 (with M146V single mutation) transgenes [55]. Another study also used GC-quadrupole-MS on APP/PS1 transgenic AD mice, but they chose to focus their analyses on hippocampal tissue [56]. Besides studies that looked at transgenic mouse models, one study used GC-MS-based metabolic profiling strategy to investigate the metabolic changes in cerebrospinal fluid (CSF) of AD patients [57]. The strengths and limitations of each paper will be discussed further in chapter 3, as they formed the basis for my selection of AD model and analytical instrument for analysis.

Studies that used NMR-based metabolic profiling strategy in AD research are more abundant in the literature. In one paper by Lalande et al.,^{1}H-NMR was used to look at the metabolic profile changes in four brain regions (cortex, hippocampus, midbrain and cerebellum) of tg2576 AD mice [58]. In another study, ^{1}H-NMR was employed to investigate the metabolic changes in extracts taken from eight brain regions (cortex, frontal cortex, cerebellum, hippocampus, olfactory bulb, pons, midbrain and striatum) of CRND8 transgenic mice [59]. Tg2576 and CRND8 mice both carry the human mutant APP_{695} with Swedish mutation (K670N, M671L), with the latter one having

additional Indiana mutation (V717F). Other mouse model has also been investigated, such as the senescence-accelerated SAMP8 mouse which has its serum metabolic profiles measured using ^{1}H-NMR [60]. ^{1}H-NMR has also been employed in metabolic profiling of clinical samples that consisted of serum samples taken from patients with MCI, a condition associated with increased risk for developing AD [61].

So far, there is a lack of study that used GC-MS-based metabolic profiling technique to look at metabolic changes in different brain regions in an AD model. On top of that, most GC-MS-based metabolic profiling studies employed GC-quadrupole-MS, which in general has a lower sensitivity than GC-Time-of-Flight-MS (GC-TOF-MS) due to the compromised duty cycle (which will be further explained in chapter 2). Therefore, a GC-TOF-MS-based metabolic profiling of an appropriately chosen APP_{695} models could generate useful findings that will complement existing knowledge and several other NMR-based AD metabolic profiling studies to allow for a better understanding of AD pathophysiology. On top of that, metabolic profiling studies of such AD model will also allow one to investigate the therapeutic mechanism for selected compound of interest.

1.3. PPARγ agonists in AD research

1.3.1. PPARγ agonist as a promising therapeutic compound for treating AD

Initial studies exploring the actions of PPARγ in AD were based on the ability of non-steroidal anti-inflammatory drug (NSAID) to activate this nuclear

receptor [62]. Epidemiological studies showed that NSAID treatment reduces AD development risk by as much as 80% and it was suggested that these effects arise from the ability of these drugs to activate PPARγ and inhibit inflammatory responses in the AD brain [63-67]. PPARγ nuclear receptors present themselves as attractive therapeutic targets for the treatment of AD as they are able to regulate several cellular processes, such as amyloid-β degradation, mitochondrial activation and anti-inflammatory response [68-70]. Among the nuclear receptors, activation of PPARγ nuclear receptor holds the most promising therapeutic potential for AD therapy [70, 71], and has garnered tremendous interest in developing PPARγ agonists into therapeutic molecules for AD [72-74]. PPARγ agonism's impact is mostly on lipogenic pathways and it influences storage of fatty acids, while agonism of another PPAR isoform, PPAR-alpha (PPARα), is mainly responsible for catabolism of fatty acids [75]. There is another isoform of PPAR, PPAR-beta (PPARβ), but it has received little research interest, mainly due to lack of association of its agonism to important clinical manifestations [75]. Nevertheless, interaction between the different PPAR isoforms has been suggested to bring about a stronger pharmacological effect, especially in regulating the anti-inflammatory activity in brain tissue [76], thus implying that regulation of more than one PPAR isoform might be needed to achieve therapeutic effect of clinical significance.

PPARγ agonism is better known for its anti-diabetic effects. One class of drug, thiazolidinedione (TZD), is a PPARγ agonist that has been widely prescribed to treat type II diabetes mellitus, but its effects in the brain remained largely

unknown [71]. More recently, TZDs such as ROSI and pioglitazone (PIO) have seen their preclinical applications in AD studies [77, 78]. These PPARγ agonists have been suggested to have significant roles in regulating different pathological aspects of AD, such as amyloid-β accumulation, inflammatory response, impaired energy utilization and perturbed lipid homeostasis [70, 79]. Agonism of PPARγ nuclear receptors also activate PPARγ coactivator 1α (PGC-1α) pathway, which was revealed to be down regulated in AD patients' brain tissues [80]. On top of that, PPARγ agonists such as ROSI had also been reported to play a role in mitochondrial biogenesis, hence carrying with it the potential to alleviate mitochondrial dysfunction which is likely to be a significant contributor to AD pathogenesis [81]. A recent discovery of a centrally penetrating partial PPARγ agonist only goes to demonstrate the growing research interest in PPARγ agonist's application for brain diseases such as AD [82].

1.3.2. <u>A gloomy outlook on the clinical development of PPARγ agonist for AD therapy</u>

Even though the therapeutic benefits of PPARγ agonist for AD were well documented in preclinical trials, these therapeutic observations did not translate well into positive clinical trial outcomes. Research interest on PPARγ agonists was particularly heightened after ROSI demonstrated promising treatment effects in a preliminary clinical trial for AD patients [74]. This pilot trial was quickly followed up and supported by another successful phase II clinical trial for ROSI in AD patients [72]. However, ROSI disappointingly failed a subsequent large phase III trial, which did not detect any evidence of

18

efficacy for ROSI in the entire AD patient population recruited for the study [29]. To account for their failure to observe therapeutic effect of ROSI, the authors reasoned that therapeutically effective level of ROSI was not achieved in the target tissues of AD patient's brain [29]. They continued to explain that this could be due to ROSI being a substrate to P-glycoprotein (P-gp), a major drug efflux transporter famously labelled as a "gatekeeper" in the blood-brain-barrier (BBB) [83]. P-gp is a drug transporter that actively pumps drugs away from the brain tissue, therefore rendering many drug compounds ineffective for treating brain diseases [83]. On top of that, neuroinflammation, which is a common occurrence in AD patient's brain tissue, could up-regulate expression of P-gp and such condition could limit brain exposure to ROSI and obviate its potential benefit [29]. Accordingly, the authors suggested that other PPARγ agonist with higher brain penetration should be investigated to support application of PPARγ agonist in AD therapy.

However, PIO, the only alternative PPARγ agonist available in the market, also demonstrated low brain penetration in preclinical studies [84]. Similar to ROSI, PIO had also gathered considerable preclinical evidence of its therapeutic potential for treatment of AD [78, 85, 86] . At the time of writing, two preliminary clinical trials for PIO in AD patients had been reported, but with contradictory outcomes. A pilot clinical trial designed to study PIO's long-term drug safety profile in AD patient population did not detect any treatment effect in its exploratory analysis of clinical efficacy, although the authors cautioned that the study was not powered to detect treatment effects [87]. On the other hand, another preliminary clinical trial reported positive

treatment outcome when AD patients with comorbid type II diabetes were given PIO [73]. The discrepancies between the PIO's performances in preclinical and clinical studies remain as a hindrance to its drug development process in AD research. Taking a lesson from ROSI's failure in phase III AD clinical trial, much work is still needed to understand the factors behind poor brain penetration observed with PIO, as well as to devise a strategy to overcome this limitation. Such knowledge is especially relevant now, since Takeda had recently just started recruiting 5800 subjects for a 5-year phase III clinical trial to look at therapeutic potential of PIO in AD [88].

1.3.3. <u>Metabolic profiling as a tool to understand therapeutic mechanisms</u>

Despite the substantial engagement of PPARγ agonists in AD clinical trials, therapeutic effects of PPARγ agonists in the brain are still not fully understood [71]. Since metabolic profiling technique can potentially be used as a valuable tool to better understand MOA of therapeutic compounds [49], I postulated that GC-TOF-MS-based metabolic profiling approach could be employed as a powerful study platform to elucidate the therapeutic effects of PPARγ agonists in treating AD. By studying the treatment effects of PPARγ agonists on metabolic profiles of AD models, I could then hypothesise which particular enzymatic pathways were affected or "treated", and led to the final snapshot of metabolic picture observed in the treated AD models. I would then run selected enzymatic assays to gather evidence in support of these hypotheses, and propose them as therapeutic mechanisms of PPARγ agonists studied in this project. By shedding more light on pathways that are affected by PPARγ agonists, my study will provide useful insights into the MOA of PPARγ

agonists on cellular processes, as well as to help uncovering novel pharmacological mechanistic pathway of PPARγ agonist in the treatment of AD.

In addition to that, by choosing to investigate two closely related PPARγ agonists, namely ROSI and PIO, this study allowed me to investigate the therapeutic effects of the two major PPAR isoforms, namely the PPARγ and PPARα. Owing to its recent failure to demonstrate treatment efficacy in phase III clinical trial [29], as well as its withdrawal from market due to reports of adverse drug reactions [89], ROSI has fallen out of favour as drug candidate for AD. However, it remains attractive as a probe compound to be employed in PPARγ research given its high selectivity for PPARγ nuclear receptor [90]. On the other hand, PIO is currently being investigated in several clinical trials, including a large phase III trial for AD patients [88], and another pilot study looking at PIO in Parkinson's disease patients [91]. Interestingly, PIO has been demonstrated to be a dual agonist of both PPARγ and PPARα nuclear receptors [92]. By investigating both ROSI and PIO, I would be able to explore the treatment effects of both PPARγ and PPARα agonism in AD. With the help of suitably chosen specific blockers of PPARγ and PPARα nuclear receptors, I could then pin-point which observed treatment effects could be attributed specifically to agonism of each individual PPAR nuclear receptor. Such information would come in handy for researchers currently engaged in PIO research for AD treatment, as well as for other researchers in the field of PPAR research.

1.4. <u>Research gaps in existing knowledge on AD and PPARγ agonists</u>

As illustrated above, there exist several research gaps in our existing knowledge on AD pathogenesis, and how PPARγ agonists such as ROSI and PIO exert their treatment effects on AD. In particular, the AD research community has a growing interest in understanding more about the pathophysiological processes associated with the early-stage AD, which could be very helpful in both early diagnosis of AD patients and allowing clinicians to initiate clinical intervention before the disease goes beyond the point of no return.

There are several research gaps in drug development of PPARγ agonists for treatment of AD as well. As the AD research community witnessed the rise and fall of ROSI in AD research, this particular drug candidate has generally fallen out of favour in the field of AD, especially after the surfacing of its drug toxicity reports [89]. Nevertheless, research interest in developing PPARγ agonists as therapeutic compound for AD remains, evident from the ongoing clinical trials for PIO in both AD [88] and Parkinson's disease [91], as well as the recent discovery of PPARγ agonist that penetrate the BBB [82]. However, the poor brain penetration of PIO remains a concern for drug development of PIO in AD research, as this limitation could have been the Achilles' heel that doomed ROSI in its own phase III AD clinical trial [29]. Since being a substrate to P-gp drug efflux transporter is a major factor that explains ROSI's poor brain penetration [29], there is a research need to investigate if PIO is also a substrate to P-gp and whether this limits PIO's brain penetration, given that both ROSI and PIO are similar structural analogues. On top of that, a

strategy to overcome PIO's limitation of poor brain penetration needs to be devised to support PIO's drug development in AD research.

1.5. <u>Research objectives in this PhD project</u>

In my PhD project, I proposed to use GC-TOF-MS-based metabolic profiling as a systematic bottom-up approach to explore the amyloid cascade hypothesis further using suitably chosen AD model. This would be achieved by employing metabolic profiling technique on two different AD models, one is a model of Chinese hamster ovarian cells (CHO) stably transfected with mouse APP_{695} to create an *in vitro* model for AD (CHO-APP_{695}), and the other AD model is an *in vivo* model, which is a double transgenic mouse expressing chimeric mouse/human APP (APP_{695} with K670N, M671L Swedish mutation) and mutant human presenilin 1 (PS1). Metabolic profiling studies using these two AD models would allow me to explore the possibility of capturing the early-stage AD signals, since metabolic profiling has been demonstrated to be a sensitive tool capable of capturing subtle fluctuations in a biological system [37]. Metabolic findings from my studies using both AD models would give me several clues of which cellular processes were affected by APP or amyloid-β, which I could then gather further evidence using biochemical assays to confirm my metabolic findings.

Besides trying to study the AD pathogenesis and its pathophysiological alterations, I also investigated the therapeutic mechanisms of PPARγ agonists, namely ROSI and PIO, using the two abovementioned AD models. Similarly, metabolic profiling tool was first employed as a bottom-up study approach to

first obtain a snapshot of the metabolic picture in my AD models, then I gathered further evidence to learn more about the cellular processes that could have occurred to give the metabolic picture I observed. Differential treatment effects of PPARγ and PPARα agonisms were investigated to determine which drug compound warrant my further investigation using *in vivo* AD model. Findings generated from my *in vitro* experiments would help guiding my research direction in my experiment using AD transgenic mice, which allowed me to validate my *in vitro* findings using a more holistic biological *in vivo* system.

Therefore, the specific objectives in this PhD are:

1)   To establish GC-TOF-MS as a suitable analytical platform in metabolic profiling studies of biological samples harvested from *in vitro* (culture media) and *in vivo* experiments (plasma and brain tissues).

2)   To employ GC-TOF-MS-based metabolic profiling technique in studying early-stage AD pathophysiological processes using CHO-APP$_{695}$ as my *in vitro* AD model.

3)   To study the therapeutic effects of ROSI and PIO in CHO-APP$_{695}$ using metabolic profiling approach.

4)   To investigate differential therapeutic effects of PPARγ and PPARα agonisms in *in vitro* AD model, using ROSI and PIO as probe drugs and selective blockers of each nuclear receptor.

5)   To employ GC-TOF-MS-based metabolic profiling technique in studying pathophysiological processes in APP/PS1 transgenic mice, focusing on detecting early-stage AD signals.

6)   To elucidate therapeutic effects of PIO in APP/PS1 transgenic mice using metabolic profiling approach.

7)   To determine whether PIO is a substrate to P-gp or other major drug efflux transporters at the BBB, and their impact on limiting brain penetration of PIO in an *in vivo* biological system.

8)   To investigate stereoselectivity exerted by P-gp on PIO stereoisomers, and to devise a strategy utilises stereoselectivity of P-gp to overcome poor brain penetration of PIO.

1.6.   Significance of project

This project contributed to the field of AD research in several ways. Firstly, findings from both my *in vitro* and *in vivo* studies helped to shed more light on understanding AD pathogenesis and pathological alterations underlying AD, especially those associated with early-stage AD. GC-TOF-MS-based metabolic profiling findings generated in both *in vitro* and *in vivo* AD models complement existing knowledge and several other NMR-based AD metabolic profiling studies, allowing for a better understanding of AD pathophysiology. On top of that, I have also uncovered differential treatment effects of PPARγ and PPARα agonism in AD models. My data strongly indicated that PIO exerted a larger extent of treatment effects than ROSI in my *in vitro* AD model, suggesting therapeutic superiority of PPARγ and PPARα dual agonism over PPARγ agonism alone. Further exploration on interactions between PIO brain penetration and two major drug efflux transporters present at the BBB (P-gp and breast cancer resistance protein) also confirmed that P-gp contributed significantly to limiting brain penetration of PIO. More

interestingly, I discovered that (+)-PIO, one of the two PIO stereoisomers, is a better brain penetrant, and upon dosing the mice with purified (+)-PIO, I managed to double the presence of PIO in brain of mice when compared against racemic PIO. My findings on brain penetration of PIO are especially relevant now as there are several ongoing clinical trials investigating PIO for brain diseases. This project as a whole contributed to understand the early-stage AD better, and supported the development of PIO as a therapeutic molecule for AD. It also paves the path for future research to determine the biological relevance of dosing with purified (+)-PIO, which could potentially be a more promising drug candidate than racemic PIO for treatment of AD.

1.7. Thesis outline

Chapter 2: GC-TOS-MS-based metabolic profiling in CHO-APP$_{695}$ for discovery of early-stage AD signals and elucidation of ROSI's and PIO's therapeutic effects in AD

In this chapter, I discussed mainly about my *in vitro* metabolic profiling work using CHO-APP$_{695}$ as my AD model. Several factors were considered before the project was initiated, such as the type of cell line to be used for investigation, and which APP isoform is appropriate for generation of AD model. For this *in vitro* project, I chose to focus my effort on extracellular metabolic profiling technique (also known as "metabolic footprinting"), which involves the profiling of metabolites that are either released by cells into culture medium, or metabolites that are not consumed by the cells and remain in the culture medium [93]. Intracellular metabolic profiling (also known as

"metabolic fingerprinting") was carefully avoided due to possibility of introducing procedural artefacts into analyses (explained further under section 2.2). Culture media used for metabolic profiling studies were optimized to give reproducible and reliable metabolic peaks in GC-TOF-MS analytical runs. I also explored the treatment effects of selective PPARγ agonist (ROSI) and PPARγ/PPARα dual agonist (PIO) on CHO-APP$_{695}$, and employed the usage of selective blockers of each nuclear receptor to pin-point the treatment effects exerted by activation of these nuclear receptors individually. Metabolic data generated from this *in vitro* experiment gave me clue of what to look out for in subsequent *in vivo* experiment, and my observation that PIO is therapeutically more superior than ROSI served as a justification for focusing on PIO in the subsequent work for this PhD project.

Chapter 3: GC-TOF-MS-based metabolic profiling in APP/PS1 transgenic mice to uncover early-stage pathological alterations and to shed light on therapeutic mechanisms of PIO in AD therapy

In chapter 3, the research was focused on employing similar GC-TOF-MS-based metabolic profiling technique to study the metabolic pictures in plasma and brain tissues harvested from 5-month old APP/PS1 transgenic mice and their wildtype counterparts. Since different brain regions were expected to have their own distinct metabolic signals, four different brain regions, namely the cortex, hippocampus, mid brain and cerebellum tissues, were dissected and had their metabolic profiles inspected separately. Biochemical assays were also performed on plasma and brain cortex tissue of transgenic mice and wildtype mice, with a focus on mitochondrial health. APP and amyloid-β

levels in plasma, brain cortex tissue, and mitochondria fractions isolated from brain cortex were measured to assess the amyloid pathology. This *in vivo* experiment was employed to investigate the therapeutic effects of PIO in APP/PS1 transgenic mice, and ROSI was not studied and reported in this chapter as my previous *in vitro* experiments (chapter 2) had demonstrated that PIO is therapeutically more superior than ROSI, which is attributed to its dual agonisms of both PPARγ and PPARα nuclear receptors. Discussion in this chapter would revolve around the metabolic signals that are characteristic of the early-stage AD, and the therapeutic effects of 14-day PIO treatment regimen on these early-stage disease phenotypes.

Chapter 4: Overcoming barriers to brain penetration of PIO

In both my *in vitro* and *in vivo* experiments with AD models, I have observed clear signs of therapeutic effects exerted by PIO on these AD models. My observations are largely in agreement with other preclinical evidence of PIO's treatment effects on AD. Taken together, these findings support the pursuant of PIO further in the AD drug pipeline. However, poor brain penetration of PIO remains a significant concern since we have already learnt that this limitation is possibly the factor for ROSI's failure in its own phase III AD clinical trial. Given the close structural similarity between ROSI and PIO, I proceeded to determine whether is PIO a substrate to P-gp, and would this be a significant factor in limiting brain penetration of PIO in an *in vivo* biological system. My findings demonstrated that partial inhibition of P-gp at the BBB increased brain penetration of PIO significantly, given the higher brain-to-plasma ratios of PIO with the mice were pre-treated with P-gp inhibitor. To

overcome this limitation, I explored the possibility of stereoselectivity exerted by P-gp on PIO stereoisomer. Interestingly, I observed higher levels of (+)-PIO in mice brain after they were dosed with racemic PIO, and the opposite trend is observed in their plasma samples. This represents an attractive dosing strategy from a pharmacokinetics point of view, as higher level in the brain and lower level in the plasma could translate to a targeted dosing of PIO to the brain tissue, and lesser of PIO to the peripheral or other unintended organs. Finally, by dosing the mice with purified (+)-PIO, I observed that the presence of PIO in brain tissues of mice was almost doubled as compared to dosing with racemic PIO. This exciting finding is especially relevant now since there are several ongoing clinical trials looking at therapeutic application of PIO in both AD and Parkinson's disease. Future work that helps to ascertain the biological relevance of this increased PIO's brain penetrance could support the usage of (+)-PIO in treating AD or other brain diseases.

Chapter 5: GC-TOF-MS-based metabolic profiling of caffeinated and decaffeinated coffee and its implications for AD

In chapter 5, I ventured into a slightly different research area within the therapeutic research field of AD. Being a coffee addict myself, reports of neuroprotection against development of AD offered by coffee consumption are always welcome. More interestingly, a recent study showed that caffeinated coffee exerted a stronger treatment effect against AD as compared to decaffeinated coffee or caffeine alone [94], and the authors reasoned that caffeine acts in synergy with another unknown compound present in coffee to enhance its therapeutic potential against AD. Based on their findings, I

hypothesised this unknown synergistic compound had been stripped away from the coffee beans during the decaffeination process, therefore rendered decaffeinated coffee ineffective against AD. To test this hypothesis, I compared the metabolites present in commercially available caffeinated and decaffeinated coffee using GC-TOF-MS-based metabolic profiling approach. Remarkably, I discovered 69 distinct metabolites that differentiate metabolic profiles of the two types of coffee, and the list includes several benzoate and cinnamate-derived phenolic compounds, organic acids, sugar, fatty acids, and amino acids. Clearly the difference between the two types of coffee is not just caffeine, which had been assumed in numerous papers that compare the two coffee types for other purposes. Findings in this chapter demonstrated the utility of metabolic profiling tool in nutritional research, and pave the path for future work on elucidating the mysterious synergistic compound that could hold the key for nutritional therapy against AD.

CHAPTER 2: GC-TOS-MS-based metabolic profiling in CHO-APP$_{695}$ for discovery of early-stage AD signals and elucidation of ROSI's and PIO's therapeutic effects in AD

2.1.   Chapter summary

In this chapter, I applied GC-TOF-MS-based metabolic profiling study approach on an *in vitro* AD model as a hypothesis generating tool to better understand the AD pathogenesis and shed light on the therapeutic mechanisms of ROSI and PIO in AD therapy. The *in vitro* AD model, or more specifically the APP model, used in this chapter is the CHO-APP$_{695}$. It should be noted that only extracellular metabolic profiling was performed in this chapter, where metabolic profiles of culture medium samples harvested from CHO-APP$_{695}$ and CHO-wildtype (CHO-WT) were compared. Intracellular metabolic profiling was carefully avoided due to the high risk of procedural artefacts being introduced into the analyses. Principal component analysis (PCA) and Y-permuted model validation were used to check for separation between groups and validity of discriminant analysis model. If these are satisfactory, orthogonal partial least squares discriminant analysis (OPLS-DA) was then used to identify the discriminant metabolites, which gave the clues about the effects of APP transgene on cellular processes. To confirm the hypotheses generated based on metabolic data, I then performed selected biochemical assays to gather further evidence to support my metabolic data findings.

To summarise my findings in this chapter, the OPLS-DA between CHO-APP$_{695}$ and CHO-WT showed a robust differentiation after 24 hours of

postseeding incubation (Q^2(cum) = 0.884), and 15 discriminant metabolites were identified based on the OPLS-DA model. In contrast, extracellular amyloid-β42 only increased significantly in CHO-APP$_{695}$ after the postseeding incubation time was extended to 48 hours. The observed 24-hour metabolic alterations were associated with increased accumulation of APP in mitochondria and reduced mitochondrial viabilities, events which all occurred before accumulation of extracellular amyloid-β42 in CHO-APP$_{695}$. In addition, I also investigated the therapeutic potential of PPARγ agonists, namely ROSI and PIO, by using the same GC-TOF-MS-based extracellular metabolic profiling approach to characterize the metabolic profiles of the ROSI-treated and PIO-treated CHO-APP$_{695}$, with or without their respective PPARγ and/or PPARα receptor blockers. Interestingly, treatment with PIO was found to restore perturbations of discriminant metabolites in CHO-APP$_{695}$ to a larger extent than treatment with ROSI. Subsequent experiments also attributed the amyloid-β42 lowering effect, and restoration of mitochondrial activity to PPARγ and PPARα agonism, respectively. Taken together, PIO was shown to be therapeutically superior to ROSI. Findings in this chapter contribute to the AD research community by providing further insights into early disease stages in this APP model, and support the advancement of PIO in AD therapeutic research.

2.2. Introduction

In this chapter, I first illustrated my attempt to use metabolic profiling as a tool in trying to understand the pathophysiological processes related to AD using an *in vitro* AD model, with a focus on unravelling pathological phenotypes associated with the early-stage AD. An important factor to be considered in this chapter's work would naturally be the selection of an appropriate *in vitro* AD model. My experiments in this chapter employed the APP model, specifically the cell model that is stably transfected with mouse APP_{695}. *In vitro* AD models that are transfected with APP transgene are widely used in AD research, and I decided to focus my investigation on the APP_{695} isoform since amyloid-β and AICD were observed to be preferentially synthesized from APP_{695}, making it the most appropriate isoform for AD research [51].

Another important consideration when choosing an *in vitro* AD model in this study is the selection of cell line used to carry the APP transgene for experimentation. In this chapter's work, I used CHO cells that are stably transfected with APP as my APP model. While some may argue that the neuronal-like cell line should be used for such purpose instead of CHO cells, it should be noted that many neuronal-like cells may not be suitable for metabolic profiling work. Firstly, most neuronal cells available today are primary cells which differentiate terminally and can no longer propagate, thus making them not suitable for *in vitro* metabolic profiling experiments. There are also neuronal-like cells that are derived from malignant tumours. One example is SH-SY5Y neuroblastoma cell, but this cell line has two limitations: 1) SH-SY5Y grows as both adherent and non-adherent cells, and 2) SH-SY5Y

cells form two morphologically distinct phenotypes when cultured, the neuroblast-like cells and epithelial-like cells [95]. These two properties could give rise to mixed phenotypes in a cultured population of SH-SY5Y cells, and thus are unable to offer a stable metabolic baseline for metabolic profiling experiments. A stable metabolic baseline is required for *in vitro* metabolic profiling experiments, as metabolic profiling is a very sensitive study tool that will pick up small fluctuations in metabolites. On the other hand, given its resilient growth and reproducible metabolic profiles, transfected CHO cells became a suitable host to lend its cellular machinery for investigation of APP transgene's biological effects on different cellular organelles. In my study, APP transgene insertion was observed to have no significant impact on CHO cells' growth rate, therefore making the metabolic profiles of both CHO-APP_{695} and CHO-WT directly comparable. The resilient growth rates of both CHO-APP_{695} and CHO-WT also came in handy when I performed follow-up experiments, as there will be minimal risk of procedural artefacts due to altered growth rates being introduced into my data analyses. For these reasons, CHO cells were chosen as the cell line for transfection work in this study.

Prior to my experiments, I conducted a trial analysis of quality control (QC) sample using GC-TOF-MS, and confirmed the suitability of this platform for the metabolic profiling of CHO-APP_{695} and CHO-WT. For this *in vitro* experiment, extracellular metabolic profiling technique was used to capture the metabolic signals of both CHO-APP_{695} and CHO-WT. Also termed as "metabolic footprinting", this type of analysis involves the profiling of extracellular metabolites that are either released by the cell into its

surrounding, or metabolites that are remaining in the culture medium as a result of not being consumed or metabolised by the cells [93]. Intracellular metabolic profiling (also known as metabolic fingerprinting) was carefully avoided in this project due to the high risk of introducing procedural artefacts into analyses, which could lead to data misinterpretations. One possible source for these procedural artefacts could be inconsistent rinsing of cells (to remove traces of culture medium from cell membrane surfaces) where small metabolic molecules could easily escape into the rinsing solution down their concentration gradients. Another source of procedural artefacts could be the method of detachment of adherent cells from culture vessels, as both mechanical and chemical detachment could introduce variability into their metabolic profiles.

Composition of the culture medium used in the extracellular metabolic profiling experiments was also optimised to ensure reliability in the sample preparation and derivatisation for the GC-TOF-MS analyses. Using low-glucose culture media is important in ensuring good analytical variation in GC-TOF-MS-based metabolic profiling analyses. This is because glucose molecules consume large quantity of derivatising agents, and could undergo incomplete derivatization when derivatising agents become limited or depleted. HEPES buffer system was also avoided as I observed that high level of HEPES buffer salts gave rise to inconsistency in the drying process during sample preparation for GC analysis. On top of that, all glassware used in this metabolic profiling experiment is carefully silanised (if not pre-silanised during manufacturing process) as I also observed substantial improvement in

analytical variations if silanised glassware is used. This is because metabolite could easily adsorb onto exposed, non-silanised glass surface during samples derivatization process. By taking all these steps into consideration, I obtained a good level of coefficient of variations for most metabolites detected in my pilot analyses of QC samples, which gave me the assurance of reliable data in my subsequent metabolic profiling experiments.

After I had optimised the experimental conditions and instrumentations for my investigation, I started the metabolic profiling experiment with my *in vitro* AD model. In the first part of this chapter, extracellular metabolic profiles of CHO-APP$_{695}$ were compared against CHO-WT, and 15 "APP-perturbed metabolites" were identified based on the comparison between the extracellular metabolic profiles of these two cell lines. Further hypotheses were generated based on this list of 15 metabolites, which were then confirmed using an array of biochemical assays. My data clearly showed that accumulation of APP in the mitochondria and impairment of mitochondrial viability took place before accumulation of extracellular amyloid-β42 could be observed. Therefore, these two pathological events could potentially be further investigated as pathophysiological processes that define early-stage AD.

In the second part of this chapter, I explored the mechanistic therapeutic pathways of PPARγ agonists by examining their effects on the above-mentioned 15 metabolites identified in the first part of this chapter. Originally, I planned to investigate the three closely related PPARγ agonists, namely troglitazone (TRO), ROSI and PIO. However, preliminary test in my

experiments showed that TRO exerted drug induced toxicity on CHO cell viability when used at the same concentration as the other two compounds, and therefore it was excluded from subsequent experiments. As PIO also possesses PPARα agonism activity which was not observed with ROSI [92], I could study differential treatment effects of both PPARγ and PPARα agonisms by comparing therapeutic effects of ROSI and PIO on metabolic profiles of CHO-APP$_{695}$. My findings in this chapter demonstrated for the first time that PIO is a more promising drug candidate than ROSI in AD therapy, and this observation was attributable to PIO being a dual agonist of both PPARγ and PPARα nuclear receptors. Since Takeda has just started recruiting 5800 subjects for a 5-year phase III clinical trial to look at the therapeutic potential of PIO in AD [88], the information acquired in this study could prove to be useful for the research scientists involved in this particular phase III clinical trial.

2.3. Materials and Methods

2.3.1. Chemicals and Reagents used

Ingredients for cell culture media used in this study (DMEM culture medium D1152, DMEM low-glucose culture medium D2902, sodium bicarbonate, Penicillin G sodium salt, Streptomycin sulfate salt, DMEM D5030, L-glutamine, sodium pyruvate, D-(+)-galactose) were purchased from Sigma-Aldrich (St. Louis, MO, USA). ROSI and PIO were purchased from Cell Molecular Pharmaceutical R&D (Xi'an, China). TRO and T0070907 (T007, PPARγ blocker) were purchased from Cayman Chemical Company (Ann

Arbor, MI). GW6471 (PPARα blocker) was purchased from Tocris Bioscience (Bristol, UK). MOX reagent (2% Methoxamine hydrochloride in pyridine) and MSTFA (N-methyl-N-trimethylsilyl trifluoroacetamide) derivatising reagent with 1% trimethylchlorosilane (TCMS) were purchased from Thermo Fisher Scientific (Waltham, MA). All other reagents used were of analytical grades.

2.3.2. Cell Culture conditions for *in vitro* APP model

This project was blessed with a kind donation of Chinese hamster ovary (CHO) cells stably transfected with mouse *APP 695* (CHO-APP$_{695}$) and its wildtype (CHO-WT) from Professor Gavin Dawe's research group (National University of Singapore, Singapore). Both cell lines were grown at 37°C, in the presence of 5% CO_2 for all subsequent *in vitro* work. Cell lines were maintained and subcultured in DMEM culture medium (Sigma D1152) containing 3.7 g/L sodium bicarbonate and 10% heat-inactivated fetal bovine serum (FBS) and supplemented with 100 units/ml of penicillin and 100 μg/ml of streptomycin. When cell lines were used for any *in vitro* experiments in this chapter, they were all standardised at third passage. Both cell lines were harvested for seeding when they were at the log-phase of growth curve. For all metabolic profiling experiments in this chapter, seeding of cells was done on 24-well cell culture plates (at cell density of 1×10^5 cell/well) in 0.5 mL of DMEM low-glucose culture medium (Sigma D2902) containing 3.7 g/L sodium bicarbonate and 10% FBS, and supplemented with 100 units/ml of penicillin and 100 μg/ml of streptomycin. Upon completion of seeding after 24 hours (seeding completion was visually inspected under microscope), culture media in all wells were replaced with 0.5 ml of fresh medium (re-constituted

DMEM low-glucose culture medium). Seeded cells were then incubated further for 12 or 24 hours (depending on the experimental design of subsequent investigations) before their culture media were individually harvested and centrifuged at 800 g for 5 minutes (at 4°C) to remove dead floating cells and cell debris. The supernatants were then transferred individually into clean 1.8 ml cryogenic vials and snap frozen in liquid nitrogen. All harvested samples were stored at -80°C until analysis.

2.3.3. Monitoring cellular proliferation rates to assess metabolic baseline

To compare the metabolic data gathered from both CHO-APP$_{695}$ and CHO-WT in the subsequent experiment, I first had to ensure that both cell lines have comparable metabolic baseline, which can be assessed based on their cellular proliferation rates. To measure their cellular proliferation rates, both CHO-APP$_{695}$ and CHO-WT were seeded on 6-well plate (n = 6 for each group) at 1 × 10^5 cells/well in 2.0 ml of DMEM culture medium (supplemented with 3.7 g/L sodium bicarbonate, 10% FBS, 100 units/ml of penicillin and 100 μg/ml of streptomycin). Additional wells (n = 6) of CHO-APP$_{695}$ cells were also seeded in similar manner using culture media added with 10 μM of individual or combination of test compounds (TRO, ROSI, ROSI + T007, PIO, PIO + T007, and PIO + GW6471). Culture media were replaced with fresh ones after 24 hours of seeding and incubated for another 48 hours before the cells were harvested by trypsinization. Cell numbers for all wells were then enumerated by cell counting using hemocytometer.

2.3.4. Extracellular metabolic profiling experiments

To characterize the metabolic profiles of CHO-APP$_{695}$ and compare them against metabolic profiles of CHO-WT, both cell lines were seeded in DMEM low-glucose culture media and subjected to 12 hours (n = 12 per group) and 24 hours (n = 10 per group) postseeding incubation before their culture medium samples were harvested for metabolic profiling. GC-TOF-MS was used to analyse the metabolites present in culture medium samples, and metabolic profiles of both cell lines at two different harvesting time points were compared using multivariate data analysis (detailed under section 2.3.7). In order to study treatment effects of ROSI and PIO on CHO-APP$_{695}$, additional groups (n = 10 per group) of CHO-APP$_{695}$ cells were seeded in culture media containing 10 μM of either ROSI or PIO, which is a concentration that had been shown to elicit therapeutic responses in *in vitro* experiments conducted by other researchers [96]. Then, I proceeded to make sure that which particular treatment effects observed were due to PPARγ agonism. In order to do so, separate treatment groups of CHO-APP$_{695}$ cells were seeded with culture media containing either ROSI or PIO, supplemented with T007, a selective inhibitor of PPARγ nuclear receptor. T007 was co-administered at 10 μM, which is also a concentration known to inhibit PPARγ receptors and have insignificant effect on cellular proliferation rate or cellular viability [97, 98]. Interestingly, my data showed that PPARγ agonism did not account for majority of treatment effects observed with PIO treatment of CHO-APP$_{695}$ (discussion detailed under section 2.4.3). This observation prompted me to investigate further if treatment effects observed were due to other non-PPARγ agonism mechanisms, such as PPARα agonism since PIO is a dual agonist of PPARγ and PPARα nuclear receptors. Therefore, additional groups of CHO-

APP$_{695}$ cells were seeded with culture medium containing PIO supplemented with 10 μM of GW6471, a known selective inhibitor of PPARα nuclear receptor when used at this concentration [99, 100]. CHO-APP$_{695}$ cells in all treatment groups were subjected to 24 hours of postseeding incubation in DMEM low-glucose culture media before their culture medium samples were harvested and centrifuged at 800 g for 5 minutes (at 4°C) to remove dead floating cells and cell debris. The supernatants were then transferred individually into clean 1.8 ml cryogenic vials and snap frozen in liquid nitrogen. All harvested samples were stored at -80°C until analysis.

2.3.5. <u>Sample preparation for GC-TOF-MS-based metabolic profiling analysis</u>

To prepare samples for metabolic profiling experiments, all culture medium samples stored at -80°C were first thawed and kept on ice. After the thawed samples were briefly vortexed, 200 μL of each medium sample was transferred into clean 2-ml centrifuge tubes and 1.0 ml of chilled methanol was added to each centrifuge tube with the culture medium sample for protein precipitation. All mixtures were vortex-mixed at high speed for 5 minutes, followed by centrifugation (14,000 g) for 20 minutes at 4°C to pellet the precipitated protein. For each sample, 950 μL of clear supernatant was then carefully transferred into clean, pre-silanized glass tubes and evaporated to dryness at 50°C under a gentle stream of nitrogen gas using TurboVap nitrogen evaporator (Caliper Life Science, Hopkinton, MA, USA). To ensure complete elimination of water which might interfere with the subsequent sample preparation steps, 100 μL of anhydrous toluene (stored with sodium sulfate)

was added to each dry residue, vortex-mixed for 1 minute, and dried again at 50°C under nitrogen gas. After completion of the drying process, 50 μL of MOX reagent was added to each dried extract, vortex-mixed for 2 minutes and incubated at 60°C for 2 hours as a methoximation step. Following the methoximation step, derivatisation of metabolites was then initiated by adding 100 μL of MSTFA (with 1% TMCS) to each sample, vortex-mixed for 2 minutes, and incubated at 60°C for 1 hour. This step aimed to increase volatility and stability of metabolites present in the samples. Following the completion of derivatisation step, each sample was vortex-mixed again for 2 minutes, and spun at 3000 g at room temperature for 5 minutes to spin down any insoluble solids. Supernatants were then carefully transferred into GC autosampler vials for subsequent injection into the GC-TOF-MS analytical instrument.

2.3.6. GC-TOF-MS data acquisition and preprocessing

Data acquisition for GC-TOF-MS analyses were carried out using an Agilent 7890A Gas Chromatography (Agilent Technologies, Santa Clara, CA) coupled to PEGASUS 4D Time-of-Flight Mass Spectrometer TOF-MS (LecoCorp., St. Joseph, MI). Separations in gas chromatography runs were achieved using a DB-1 GC column (Agilent Technologies) with a altered length of 22.9 m (internal diameter of 250 μm and film thickness of 0.25 μm) was used as the primary column. Carrier gas used to aid separation is helium gas, which was used at constant flow rate of 1.5 ml/min. Injector split ratio was set to 1:10, and total injection volume of 1 μL was used. The injector inlet and ion source temperatures were both maintained at 250°C throughout the entire GC run.

Oven temperature gradient was programmed as follows: first the oven temperature will equilibrate at 70°C for 0.5 minute before sample injection was initiated; upon sample injection, oven temperature was kept at 70°C for another 0.2 minute, and then ramped up at a rate 8 °C/min to 270 °C where it was held at that temperature for 5 minutes; then oven temperature was further increased by 40°C/min to reach 310°C and held for another 5 minutes. The MS detection was operated in EI mode (standard ionisation energy 70 eV) and detector voltage was set at 1800 V. Data were acquired using full scan mode, with mass range set at m/z 50 − 600, and an acquisition rate of 15 Hz was employed. Acquisition delay was set at 195 seconds to prevent the large solvent front peak from entering the mass analyser. GC chromatogram data acquisition, baseline correction, peak deconvolution, analyte alignment, peak area calculation, and preliminary analyte identification by mass spectral searches (based on NIST, Fiehn Rtx5, and in-house libraries built using previous analyses of commercially available metabolite standards) were all performed using LECO ChromaTOF software version 4.21, before the metabolic data were analysed using multivariate data analysis. For preliminary metabolic peak identification, peaks with similarity index (SI) of 70% or more were assigned putative metabolite identities based on the mass spectral libraries matches. To ensure proper matching between sample spectrum and library spectrum, mass spectral from both sample peak and library peak were visually inspected, and retention time (RT) of libraries were checked using a mix of fatty acid methyl esters peak markers that were injected before sample injections. As for integration of area under each metabolite peak, baseline offset, minimum peak width, signal to noise (S/N) ratio and number of

apexing masses were set at 0.5, 2.5 s, 100, and 3, respectively. Calculation of the area under peak for each metabolite was performed based on the unique mass selected from mass spectrum detected for each metabolic peak. Metabolic data matrix was generated using LECO ChromaTOF's Calibration feature as described in previous literature [101], with similarity threshold between analyte peak and reference peak set at 70% instead of 60%. To ensure consistency in sample preparation and data acquisition using the GC-TOF-MS, QC analysis was included in this GC-TOF-MS-based metabolic profiling analytical run. QC analysis was carried out by individually preparing several QC samples (taken from pooled culture medium samples harvested in this study) in similar manner and one QC sample was injected and analysed at interval of every five GC sample injections. Metabolic peaks that were not assigned a putative metabolite identity (SI < 70%) or had coefficient of variation higher than 20% in QC analysis were excluded from subsequent analyses. The resulting metabolic data were then processed by normalising peak area of each analyte based on total integral area calculation performed using an in-house script (Microsoft Office Excel). Total area normalisation was used in this study as one report demonstrated that data-driven normalisation methods are more superior to model-driven normalisation method (such as internal standard normalisation) if insufficient internal standards (IS) were used [102]. To avoid error in normalisation step, metabolic peaks that are also ingredients of constituted culture medium were not included in total integral area calculation.

2.3.7. Multivariate data analysis of metabolic data matrix

Multivariate data analysis of the normalised data were carried out using the SIMCA-P software version 13.0 (Umetrics, Umeå, Sweden). Data were first mean-centered and unit-variance scaled before being subjected to PCA. Purpose of PCA was to observe clustering trends among analysed samples, as well as to identify outliers in the data and exclude them with sufficient justifications based on observation of gross errors that might have been introduced during sample handling or GC-TOF-MS analytical runs. After the initial data overview using PCA, metabolic data were further subjected to partial least squares discriminant analysis (PLS-DA) to build two separate discriminant models between CHO-APP$_{695}$ and CHO-WT at two different harvesting time points (12 hours and 24 hours postseeding incubation). Model validity and potential overfitting of both PLS-DA models were checked by performing 100 observation-dependent randomised permutation tests and visually inspected using model validation plot. As a rule of thumb, model validation plot for this permutation test is considered valid when 1) none of the cumulative Q^2 values calculated for permuted datasets is higher than Q^2 value of original dataset, and 2) the regression line of Q^2 values of original and permuted datasets trend towards zero (or negative values) when the correlation between original dataset and permuted datasets is decreasing. Once PLS-DA model passed model validation step, the same dataset was then analysed using OPLS-DA, which affords a more straightforward identification of discriminant metabolites responsible for differentiation between CHO-APP$_{695}$ and CHO-WT. To select from OPLS-DA model a list of potential discriminant metabolites for further analysis, variable importance in projection (VIP) cut-off value was set to 1.00 to generate a list of potential discriminant metabolites

that could have contributed significantly to the separation between CHO-APP$_{695}$ and CHO-WT in the OPLS-DA model. To determine significance of difference in metabolite levels between the two cell lines, two-tailed independent t-test with Welch's correction was used for statistical comparison of these potential discriminant metabolites between the two groups and Bonferroni-adjusted P-value was used to determine significance. In summary, discriminant metabolites that have VIP $\geq$ 1.00 and P-value lower than Bonferroni-adjusted significance levels were deemed to have contributed significantly to the differentiation of metabolic profiles between CHO-APP$_{695}$ and CHO-WT, and hereafter known as "APP-perturbed metabolites". Fold-change (FC) value for each APP-perturbed metabolite with respect to CHO-WT was calculated using the following **Equation 1**, where x and y represent average metabolite levels calculated for CHO-APP$_{695}$ and CHO-WT, respectively.

$$\textbf{Equation 1}: \text{Fold-change} = x/y$$

Fold-change values were used to assess the degree of alterations for each APP-perturbed metabolite. To interpret the biological meaning behind these alterations, information on APP-perturbed metabolites was sourced from freely available online metabolite databases such as Human Metabolome Database (HMDB) [103] for information on the metabolite itself, and Kyoto Encyclopedia of Genes and Genomes database (KEGG) [104] for metabolic pathway interpretations.

2.3.8. Evaluation of therapeutic effects of ROSI and PIO

To assess therapeutic potential of ROSI and PIO on metabolic perturbation in CHO-APP$_{695}$, I analysed their impact on list of APP-perturbed metabolites established under section 2.4.2. APP-perturbed metabolites were regarded as being normalised or "treated" if their levels in ROSI-treated or PIO-treated CHO-APP$_{695}$ were altered significantly when compared against vehicle-treated CHO-APP$_{695}$, and the direction of change is heading towards metabolite levels observed in CHO-WT. To further determine if treatment effects observed were due to PPARγ or PPARα agonism, I investigated the impact of co-administration of PPARγ and/or PPARα blockers on treatment effects observed with ROSI or PIO in CHO-APP$_{695}$. If a treatment effect observed in ROSI-treated or PIO-treated CHO-APP$_{695}$ was nullified by co-administration of PPARγ or PPARα blocker, then I will attribute this particular treatment effect to the agonism of the nuclear receptor blocker co-administered. Statistical comparison of data for evaluation of treatment effects was performed using two-tailed independent t-test with Welch's correction, and Bonferroni-adjusted *P*-value was used to determine significance.

2.3.9. Measurement of glucose uptake in CHO-APP$_{695}$ and CHO-WT

As one major APP-perturbed metabolite is glucose, I proceeded to measure the glucose uptake in both CHO-APP$_{695}$ and CHO-WT to see if the rate of glucose uptake had been altered in my *in vitro* APP model. Measurements of glucose uptake rates were made using a commercially available glucose uptake assay kit (ab136955 from Abcam, Cambridge, UK). Briefly, both cell lines were first seeded in 96-well plate (5 wells for each group) at 2.1×10^4 cells/well for 24

hours. They were then washed with phosphate buffered saline (PBS) and cultured in serum-free medium for another 24 hours. Glucose uptake assay was then initiated by adding 100 μL of serum-free medium that is supplemented with 10 μL of 2-deoxyglucose (2-DG, 10 mM). 2-DG uptake via glucose transporter into cells was used to simulate glucose uptake in cells. Upon entry into the cells, 2-DG was metabolised by cells into 2-DG-6-phosphate (2-DG6P), which was then oxidised to generate NADPH. To assess this metabolic activity, measurements of NADPH levels were made using a recycling amplification reaction method, and glucose uptake was estimated based on 2-DG uptake. All absorbance readings in this experiment were recorded using Tecan Infinite M200 microplate reader (Tecan, Switzerland).Means of 2-DG uptake data were compared using two-tailed independent t-test with Welch's correction, with $P < 0.05$ to be considered as a significant mean difference.

2.3.10. Measurement of extracellular amyloid-β42 levels

In this experiment, I measured the amyloid-β42 levels in culture media harvested from both CHO-APP$_{695}$ and CHO-WT to assess the downstream processing of increased APP in the transfected cell line. Culture medium samples were harvested from each cell line after 12, 24 and 48 hours (n = 8 per group) of seeding, and amyloid-β42 levels in culture medium samples were measured. For 12-hour and 24-hour time points, both CHO-APP$_{695}$ and CHO-WT were cultured in DMEM low-glucose medium (similar to medium used for extracellular metabolic profiling experiment). For 48-hour time point, both cell lines were cultured in DMEM culture medium (containing 25 mM

glucose) to ensure cells have sufficient resources to sustain their growth beyond the 24-hour time point. Extracellular amyloid-β42 levels were quantitatively measured using colorimetric sandwich ELISA kits, according to the protocols provided by the manufacturer (#SIG-38954 and #SIG-38956 from Covance, Princeton, NJ). All absorbance readings were measured using Tecan Infinite M200 microplate reader (Tecan, Switzerland). Based on findings generated from extracellular metabolic profiling experiments, PPARγ and PPARα dual agonist PIO was observed to be the therapeutically superior. Therefore, treatment effect of PIO on extracellular amyloid-β42 was also evaluated in this part of experiment, and PPARγ and PPARα blockers were used to investigate whether PIO's treatment effect on extracellular amyloid-β42 (if any) was due to agonism of either one of the nuclear receptors or both. To evaluate treatment effects of PIO, amyloid-β42 levels in culture media harvested from additional groups of CHO-APP$_{695}$ treated with PIO, PIO + T007, PIO + GW6471, or PIO + both blockers (following 48 hours of postseeding incubation) were also measured. Measurements for all amyloid-β42 levels in this experiment were performed on undiluted culture media. As CHO-APP$_{695}$ consistently displayed higher level of total protein expression than CHO-WT (even though cellular proliferation rates of both cell lines did not differ significantly), non-normalized extracellular amyloid-β42 data were used for evaluation in this experiment. Data means were statistically compared using two-tailed independent t-test with Welch's correction, with $P < 0.05$ to be considered as a significant mean difference.

2.3.11. Measurement of mitochondrial viability

As my metabolic data is included perturbations in several citric acid cycle components, I proceeded to assess the mitochondrial viability in my treated and non-treated *in vitro* APP model. To evaluate the treatment effects of PIO on mitochondrial viability, CHO-WT and different groups of CHO-APP$_{695}$ (n = 10 per group) treated with vehicle, PIO, PIO + T007, PIO + GW6471, or PIO + both blockers were subjected to mitochondrial viability test after 24 hours of postseeding incubation in respective media. Mitochondrial viability test was performed using indicator dye (7-Hydroxy-3H-phenoxazin-3-one 10-oxide), where mitochondrial viability of tested cells could be measured from their capability to reduce indicator dye into a coloured compound (#ab129732 from abcam, Cambridge, UK). This particular indicator dye had been shown to be reduced by lymphocytes in a time-dependent manner, which was diminished by co-administration of amiodarone, a well-known mitochondrial toxicant [105]. It should be noted that glucose in culture media used in this experiment was replaced entirely with galactose to circumvent the biological phenomenon known as the "crabtree effect" [106]. Crabtree effect is a process where cells generate sufficient ATP for survival from glycolysis alone, eliminating their reliance on mitochondrial oxidative phosphorylation for ATP generation. This effect is much more pronounced when cells are cultured in high glucose environment. Therefore, replacement of glucose with galactose made this indicator dye a sensitive indicator of mitochondrial health. Absorbance readings given by the coloured compound could then be detected using Tecan Infinite M200 microplate reader. Statistical comparison of data was performed using two-tailed independent t-test with Welch's correction, with $P < 0.05$ to be considered as a significant mean difference.

2.3.12. Measurement of APP Levels in mitochondrial fractions

Taken all together, my metabolic profiling and extracellular amyloid-β42 data (detailed under result section below) showed observable perturbations in CHO-APP$_{695}$'s metabolism, even before amyloid-β42 started to accumulate in the culture medium. This led me to hypothesise that an accumulation of APP could have occurred in the mitochondria of CHO-APP$_{695}$ before amyloid-β42 started to gather in the extracellular compartment, since APP is a membrane protein that could also embed itself in mitochondrial membrane. Therefore, I proceeded to assess APP levels in mitochondria fractions harvested from CHO-APP$_{695}$ and CHO-WT (n = 8 per group) after 24 hours of postseeding incubation (a time point where CHO-APP$_{695}$ started to display a significantly different metabolic data as compared to CHO-WT). To harvest sufficient cellular mass for mitochondria extraction to be carried out, both CHO-APP$_{695}$ and CHO-WT were seeded on 6-well plate, each well has a cell density of 5 × 10^5 in 2.0 mL of DMEM low-glucose culture media. After 24 hours of postseeding incubation, cells were harvested by scraping, and the harvested fractions were homogenized on ice using a pre-chilled dounce homogenizer. Mitochondrial fractions were then extracted from the homogenate using differential centrifugation procedure detailed in a commercially available mitochondrial extraction kit (#89874 from Thermo Fisher Scientific, Waltham, MA). It should be noted that, following the recommendation of manufacturer, mitochondrial pellets were obtained using centrifugation at 3,000 g (instead of 12,000 g) to improve purity of extraction. A western blot analysis was performed to assess the purity of mitochondrial fraction by measuring

presence of different organelles in extracted fractions obtained for both CHO-WT and CHO-APP$_{695}$ and compared against whole cell lysate. Presence of different organelles was measured using antibody cocktail suitable for organelle detection (ab133989 from Abcam, Cambridge, UK). Antibodies targeting four different organelle markers were used in the western blot analysis, namely anti-sodium potassium ATPase antibody (plasma membrane), anti-ATP5A antibody (mitochondria), anti-GAPDH antibody (cytosol); and anti-histone H3 antibody (nucleus). Following extraction, the purified mitochondrial fractions were further homogenized using a probe sonicator to completely lyse the mitochondria for analysis of APP using colorimetric sandwich ELISA kit (#KHB0051 from Life Technologies, Carlsbad, CA). The mitochondrial APP data were normalized based on total protein level present in each mitochondrial fraction (measured using micro BCA protein assay kit). All absorbance readings were measured using Tecan Infinite M200 microplate reader. Means between different groups were compared using two-tailed independent t-test with Welch's correction, with $P < 0.05$ to be considered as a significant mean difference.

2.4. Results

2.4.1. Cellular proliferation rates for assessment of metabolic baseline

Cellular proliferation rates of both cell lines with or without treatment were used to evaluate effects of APP transgene insertion and treatment of different compounds (10 μM of TRO, ROSI, ROSI + T007, PIO, PIO + T007, and PIO + GW6471) on metabolic activity of CHO cells. CHO-WT and CHO-APP$_{695}$

treated with vehicle did not show any significant difference in their cellular proliferation rates after 48 hours of postseeding incubation. This implies that the baseline metabolic activities for both cell lines are comparable and metabolic activities of CHO cells were not significantly affected by addition of APP transgene. Treatment of CHO-APP$_{695}$ with 10 μM of TRO significantly reduced proliferation rate by 29.70 %, indicating that TRO administered at this particular concentration induced toxicity that impaired cellular growth of CHO-APP$_{695}$. All other treatments with individual or combination of drug compounds were observed to have no significant effect on cellular proliferation rate of CHO-APP$_{695}$. Data for cellular proliferation rate experiment for both cell lines were summarised in **Figure 1**.
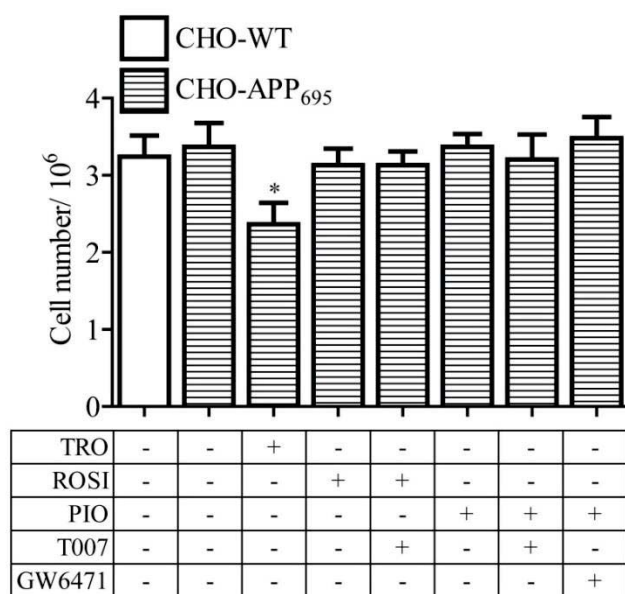
Figure 1. Cellular proliferation rates of CHO-WT and CHO-APP$_{695}$ treated with vehicle or other drug compounds; * $P < 0.05$ against vehicle-treated CHO-APP$_{695}$; Error bars represent one SD.

2.4.2. Comparing metabolic profiles of CHO-APP$_{695}$ and CHO-WT

After 12 hours of postseeding incubation, PCA for extracellular metabolic profiles of CHO-APP$_{695}$ and CHO-WT did not display any visible clustering trend on scores plot, suggesting only slight or no difference between the metabolites in their culture medium samples (**Figure 2A**). A PLS-DA model generated using the same 12-hour metabolic data did not pass the model validation plot as randomly permuted datasets gave higher Q^2 values than the Q^2 value calculated for original dataset (**Figure 2B**), which indicates high risk of model over-fitting and little interpretability for the dataset. OPLS-DA model constructed using the same data is presented in **Figure 2C** (1 predictive and 1 orthogonal components, R^2(Y) and Q^2(cum) were 0.735 and 0.101, respectively). R^2(Y) is the fraction of the sum of squares of all Y-values explained by the current latent variables, and Q^2(cum) is the cumulative Q^2 for the extracted latent variables, which is given by the expression defined in **Equation 2**.

$$\text{Equation 2}: Q^2 = 1 - \Sigma(Y_{predicted} - Y_{true})^2 / \Sigma Y_{true}^2$$

Judging based on the OPLS-DA model, the small Q^2(cum) value also indicates that separation between metabolic profiles of the two cell lines after 12 hours of postseeding incubation is not clear. Nevertheless, a list of 38 potential discriminant metabolites (VIP ≥ 1.00) was generated based on the OPLS-DA model, and two-tailed independent t-tests with Welch's correction was used to compare their means. Expectedly, none of the 38 metabolites achieved significance as determined by $P < 0.0013$ (Bonferroni-adjusted significance level).
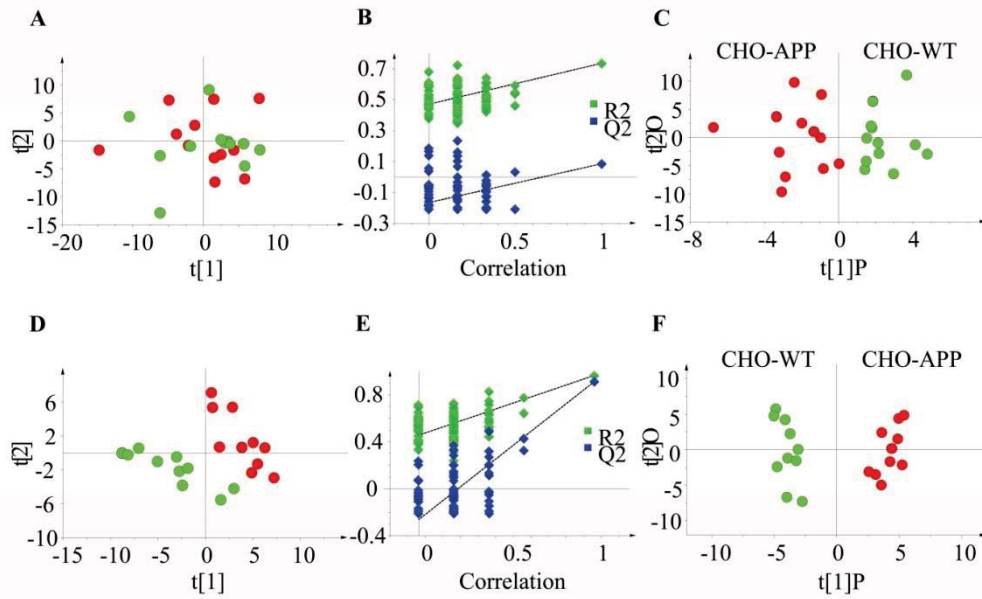
Figure 2. (A) PCA of 12-hour postseeding metabolic profiles of CHO-APP$_{695}$ (red) and CHO-WT (green); **(B)** Y-permuted model validation plot for PLS-DA of 12-hour metabolic profiles; **(C)** OPLS-DA of 12-hour metabolic profiles (2 LV, $R^2(Y)$ = 0.735, Q^2(cum) = 0.101); **(D)** PCA of 24-hour metabolic profiles of CHO-APP$_{695}$ (red) and CHO-WT (green); **(E)** Y-permuted model validation plot for PLS-DA of 24-hour metabolic profiles; **(F)** OPLS-DA of 24-hour metabolic profiles (2 LV, $R^2(Y)$ = 0.957, Q^2(cum) = 0.884).

I then performed another analysis on the extracellular metabolic profiles of the two cell lines after postseeding incubation time was extended by another 12 hours to 24 hours. PCA of their metabolic profiles displayed two distinct clusters on the scores plot (**Figure 2D**). Model validation plot for PLS-DA model generated using the same dataset indicated clearly the model is valid, as all Q^2 values calculated for randomly permuted datasets were lower than actual Q^2 value itself, and the regression line of Q^2 values intersected y-axis below zero (**Figure 2E**). The corresponding OPLS-DA model (**Figure 2F**) generated using the same dataset demonstrated robust separation between the metabolic profiles of the two cell lines (1 predictive and 1 orthogonal components, $R^2(Y)$ and Q^2(cum) were 0.957 and 0.884, respectively). Based

on this OPLS-DA model, a list of 20 potential discriminant metabolites (VIP ≥ 1.00) that were responsible for separation was generated and presented in **Table 1**. 15 out of these 20 metabolites achieved significance when means were compared between CHO-APP$_{695}$ and CHO-WT, as determined by $P < 0.0025$ (Bonferroni-adjusted significance level). These 15 discriminant metabolites will hereafter be referred to as "APP-perturbed metabolites".

Table 1. List of potential discriminant metabolites that differentiate CHO-APP$_{695}$ from CHO-WT following 24 hours of postseeding incubation

	Metabolite	Metabolite Class	FC	P value [a]	SI(%) [b]
1	D-glucose	Monosaccharides	1.71	< 0.0001*	91.3
2	Malonic acid	Dicarboxylic acids	1.08	< 0.0001*	73.8
3	Succinic acid	Dicarboxylic acids	0.92	< 0.0001*	89.8
4	Methylmalonic acid	Dicarboxylic acids	1.16	< 0.0001*	74.5
5	Citric acid	Tricarboxylic acids	1.15	< 0.0025*	73.8
6	2-Oxoglutaric acid	Keto acids	1.07	< 0.0001*	80.5
7	Pyruvic acid	Keto acids	0.98	< 0.01	77.6
8	L-Lysine	Amino acids	0.86	< 0.0001*	78.3
9	L-Alanine	Amino acids	0.86	< 0.0001*	90.8
10	L-Serine	Amino acids	1.26	< 0.0001*	81.8
11	L-Proline	Amino acids	0.83	< 0.0005*	81.4
12	L-Ornithine	Amino acids	0.75	< 0.0005*	80.3
13	L-Isoleucine	Amino acids	0.95	< 0.0005*	88.3
14	Glycine	Amino acids	0.93	< 0.001*	85.7
15	L-Tryptophan	Amino acids	0.77	< 0.0025*	80.8
16	L-Threonine	Amino acids	0.93	< 0.01	91.4
17	L-Leucine	Amino acids	0.91	< 0.05	86.8
18	L-Cystine	Amino acids	1.18	< 0.05	72.3
19	Uracil	Pyrimidines	0.87	< 0.0001*	85.8
20	Glycerol	Sugar alcohols	0.93	< 0.05	91.4

[a] P values were calculated for means compared between CHO-APP$_{695}$ and CHO-WT using independent t-tests (two-tailed) with Welch's correction
[b] SI indicates percentage matched between the mass spectrum of identified metabolic peak in GC chromatogram versus mass spectrum in libraries used
* $P < 0.0025$ (Bonferroni-adjusted significance level)

2.4.3. Treatment Effects of ROSI and PIO on APP-Perturbed Metabolites

To assess the therapeutic potential of ROSI and PIO in CHO-APP$_{695}$, I investigated their treatment effects on the list of 15 APP-perturbed metabolites established in previous section. As defined above under section 2.4.2, APP-perturbed metabolite was considered "treated" when its level in ROSI-treated or PIO-treated CHO-APP$_{695}$ was altered significantly when compared against the vehicle-treated CHO-APP$_{695}$, and the direction of change is heading towards metabolite level observed in CHO-WT. Comparisons between ROSI-treated or PIO-treated against vehicle-treated CHO-APP$_{695}$ were performed using two-tailed independent t-tests with Welch's correction, and Bonferroni-adjusted significance level of 0.0033 was employed. PIO successfully exerted its treatment effects on a total of 7 out of 15 (46.67%) APP-perturbed metabolites listed in **Table 1**. On the other hand, ROSI only showed treatment effects on 3 out of the 15 (20%). Treatment effects of PIO and ROSI on APP-perturbed metabolites were summarised in **Table 2**.

Table 2. A summary 24-hour of treatment effects observed in PIO-treated and ROSI-treated CHO-APP$_{695}$

Metabolite	% metabolite levels relative to CHO-WT, mean ± SD			
	CHO-WT	CHO-APP$_{695}$	PIO-treated CHO-APP$_{695}$	ROSI-treated CHO-APP$_{695}$
Glucose	100.00 ± 1.91	170.51 ± 14.26	159.88 ± 22.63	169.13 ± 13.48
Uracil	100.00 ± 4.45	86.52 ± 3.73	84.44 ± 4.16	86.82 ± 3.64
Lysine	100.00 ± 2.82	86.38 ± 5.39	100.09 ± 7.29*$^\gamma$	102.03 ± 5.31*$^\gamma$
Alanine	100.00 ± 2.96	86.42 ± 5.88	73.72 ± 7.20	86.70 ± 5.78
Serine	100.00 ± 5.55	126.43 ± 13.20	120.21 ± 23.72	124.40 ± 11.72
Malonic acid	100.00 ± 1.97	107.72 ± 3.80	106.20 ± 11.20	107.01 ± 3.70
Succinic acid	100.00 ± 3.65	92.24 ± 2.67	97.68 ± 3.06*$^\alpha$	92.25 ± 2.30
Methylmalonic acid	100.00 ± 5.60	115.73 ± 7.36	99.74 ± 6.76*$^{\gamma\alpha}$	117.88 ± 5.50
2-Oxoglutaric acid	100.00 ± 2.75	106.66 ± 3.05	91.22 ± 4.47*$^\alpha$	102.39 ± 3.17
Proline	100.00 ± 8.51	83.37 ± 7.03	75.76 ± 12.87	78.84 ± 6.34
Ornithine	100.00 ± 12.99	75.39 ± 10.65	78.95 ± 13.00	66.50 ± 8.93
Isoleucine	100.00 ± 2.12	95.28 ± 2.56	99.47 ± 2.42*$^\alpha$	100.17 ± 2.83*
Glycine	100.00 ± 1.91	92.73 ± 4.58	85.43 ± 4.85	91.35 ± 4.66
Citric acid	100.00 ± 6.41	114.74 ± 9.78	90.78 ± 9.28*$^\alpha$	100.47 ± 8.04
Tryptophan	100.00 ± 13.57	77.33 ± 14.81	118.25 ± 24.89*$^\gamma$	101.93 ± 13.36*$^\gamma$

* $P < 0.0033$ (Bonferroni-adjusted significance level) against CHO-APP$_{695}$, with direction of change heading towards CHO-WT
$^\gamma$ Observed treatment effect was diminished by co-treatment with T007 (PPARγ blocker)
$^\alpha$ Observed treatment effect was diminished by co-treatment with GW6471 (PPARα blocker)

2.4.4. Contribution of PPARγ and PPARα agonism to treatment effects observed

To further determine if treatment effects observed above were due to PPARγ or PPARα agonism, I co-administered PPARγ and/or PPARα selective blockers with PIO or ROSI in CHO-APP$_{695}$ and observe their impact on PIO's and ROSI's treatment effects. Out of the 7 and 3 APP-perturbed metabolites treated by PIO and ROSI, respectively, I observed that T007 (PPARγ selective blocker) co-administration diminished 3 out of 7 and 2 out of 3 treatment effects observed for PIO and ROSI, respectively (**Table 2**). Treatment effects that were not nullified by co-administration of T007 were subsequently

accounted to mechanisms other than PPARγ agonism itself. As PIO has also been shown to be a partial PPARα agonist [92], I continued to investigate the extent of contribution of PPARα agonism to treatment effects observed with PIO. Co-administration of GW6471 (PPARα selective blocker) diminished 5 treatment effects of PIO, and 4 of them were not attributed to PPARγ agonism (**Table 2**).

2.4.5. Glucose uptake rates in CHO-APP$_{695}$ and CHO-WT

As glucose level is consistently higher in culture medium of CHO-APP$_{695}$ as compared to CHO-WT, I measured glucose uptake rates for both cell lines to investigate the effects (if any) of APP transgene insertion on glucose uptake of CHO cells. After the cells were incubated for 48 hours following cell plating, glucose uptake rates of both cell lines were measured. Interestingly, CHO-APP$_{695}$ (0.235 ± 0.031 pmol/μL) showed a slightly higher rate of glucose uptake than CHO-WT (0.155 ± 0.042 pmol/μL), but the difference did not achieve statistical significance ($P > 0.05$). This implies that glucose uptake of CHO cells remained unchanged, or was only marginally enhanced by APP transgene insertion.

2.4.6. Quantitation of extracellular amyloid-β42 levels

Following 12 and 24 hours of postseeding incubation, no significant difference could be detected between extracellular amyloid-β42 levels measured for CHO-APP$_{695}$ and CHO-WT. When postseeding incubation time was extended to 48 hours, I observed a time-dependent accumulation of extracellular amyloid-β42 in both cell lines, and detected a significantly higher level of

extracellular amyloid-β42 (+42.04%) in CHO-APP$_{695}$ as compared to CHO-WT (**Figure 3A**). PIO's treatment effect on extracellular accumulation of amyloid-β42 was assessed by conducting further experiment that included additional wells of CHO-APP$_{695}$ treated with PIO (with or without PPARγ and PPARα selective blocker to evaluate the contribution of PPARγ agonism and PPARα agonism). In line with my previous observation, higher level of extracellular amyloid-β42 (+75.66%) was again detected in culture media harvested from CHO-APP$_{695}$ as compared to CHO-WT after 48 hours of postseeding incubation. Treatment with PIO reduced extracellular amyloid-β42 to level comparable with CHO-WT, and co-administration with T007 (PPARγ blocker), but not with GW6471 (PPARα blocker), diminished this treatment effect (**Figure 3B**).
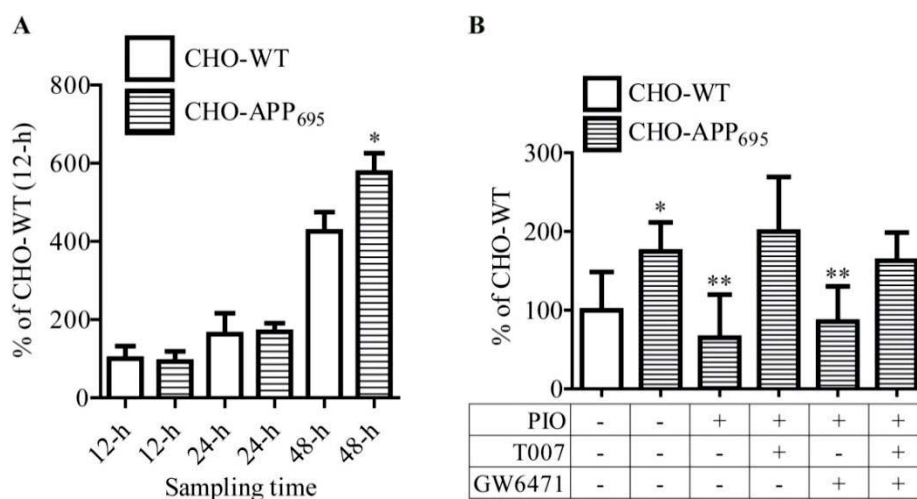
Figure 3. (A) Extracellular amyloid-β42 reported as % of CHO-WT (12-h) after 12, 24 and 48 hours of postseeding incubation; * $P < 0.05$ for means compared between 48-hour CHO-WT and CHO-APP$_{695}$; **(B)** Extracellular amyloid-β42 reported as % of CHO-WT after 48 hours of postseeding incubation in culture media containing vehicle or corresponding drug compounds; * $P < 0.05$ when compared against CHO-WT; ** $P < 0.05$ when compared against vehicle-treated CHO-APP$_{695}$; Error bars represent one SD.

2.4.7. Measurement of mitochondrial viability

Based on observations of perturbed mitochondrial citric acid cycle components, I assessed mitochondrial health of my *in vitro* APP model by measuring its mitochondrial viability (with or without treatment) and compared it against CHO-WT. After 24 hours of postseeding incubation with galactose culture medium, CHO-APP$_{695}$ displayed a significantly reduced mitochondrial viability (-19.82%) as compared to CHO-WT. A complete rescue of mitochondrial viability in CHO-APP$_{695}$ was achieved when PIO was added to the culture medium. Co-administration with GW6471, but not with T007, nullified this treatment effect observed (**Figure 4**).
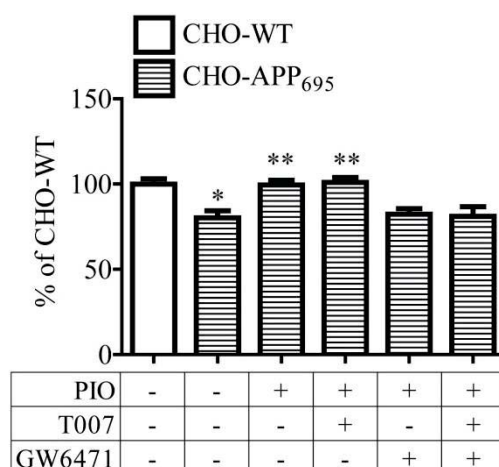
Figure 4. Mitochondrial viability reported as % of CHO-WT after 24 hours of postseeding incubation in galactose culture media containing vehicle or corresponding drug compounds; * $P < 0.05$ when compared against CHO-WT; ** $P < 0.05$ when compared against vehicle-treated CHO-APP$_{695}$; All error bars represent one SD.

2.4.8. Measurement of APP Levels in mitochondrial fractions

Observations from extracellular amyloid-β42 and mitochondrial viability experiments detailed above showed that CHO-APP$_{695}$ displayed an impaired

mitochondrial viability even before any observable accumulation of extracellular amyloid-β42 could be detected. Since APP is a membrane protein, I hypothesised that APP could accumulate in mitochondrial membrane and mangle the mitochondria. Mitochondrial APP was quantitatively measured in mitochondrial fraction harvested from both cell lines after 24 hours of postseeding incubation, and a significantly higher level of mitochondrial APP (+40.80%) was observed in CHO-APP$_{695}$ as compared to CHO-WT (**Figure 5A**). As plasma membrane is another location where APP could accumulate, a western blot analysis was performed on extracted mitochondrial fractions to assess their extraction, and to ensure that APP from plasma membrane did not contribute to measurements of mitochondrial APP. Extracted mitochondrial fractions for both CHO-WT and CHO-APP$_{695}$ showed a clear band at 55 kDa (mitochondrial marker), and a faint band at 15 kDa (nuclear marker); whereas whole cell lysate for both CHO-WT and CHO-APP$_{695}$ gave intense bands at 100 kDa (plasma marker) and 15 kDa (nuclear marker), as well as weaker but visible bands at 55 kDa (mitochondrial marker) and 36 kDa (cytosolic marker) (**Figure 5B**). Western blot data demonstrated high mitochondrial purity in extracted fractions, and ruled out possibility of contamination from plasma membrane APP in mitochondrial APP measurements.
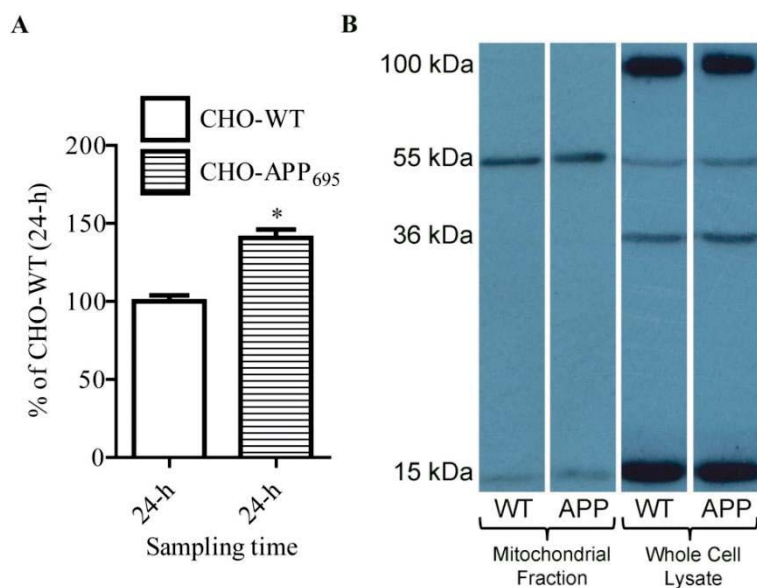
Figure 5. (A) Mitochondrial APP level reported as % of CHO-WT after 24 hours of postseeding incubation; * $P < 0.05$ against 24-hour CHO-WT; Error bar represents one SD **(B)** Western blot analysis of 4 organelle markers (100 kDa – plasma membrane; 55 kDa – mitochondria; 36 kDa – cytosol; 15 kDa - nucleus) carried out on extracted mitochondrial fraction and whole cell lysate of CHO-WT and CHO-APP$_{695}$.

2.5. Discussion

2.5.1. APP transgene and drug treatment had little effect on cellular proliferation rates

Since cellular proliferation rate is directly associated with cellular metabolism, the growth rates of CHO-APP$_{695}$ and CHO-WT with or without drug treatments need to be ascertained before any meaningful comparison can be made between the extracellular metabolic profiles. In this study, growth rates of CHO-WT were not affected by APP transgene insertion, allowing direct comparison to be made between their extracellular metabolic profiles. Treatment of CHO-APP$_{695}$ with 10 µM TRO reduced its cellular proliferation rate by 30 %, indicating drug induced toxicity that impaired growth of CHO-

63

APP_{695}. Treatment with all other compounds (10 μM of ROSI, ROSI + T007, PIO, PIO + T007, and PIO + GW6471) did not affect growth rate of CHO-APP_{695} in any significant manner. Similar to PIO, TRO is known to activate both PPARγ and PPARα nuclear receptors [107]. However, as it displayed drug induced toxicity on *in vitro* APP model, TRO is eliminated from list of drug compounds to be examined in this study. Subsequent analyses will focus on investigation of PIO as a probe drug for dual agonism of PPARγ and PPARα nuclear receptors.

2.5.2. <u>Mitochondrial dysfunctions occurred prior to extracellular amyloid-β accumulation</u>

Although I observed time-dependent and clear changes in the extracellular metabolic profiles of CHO-APP_{695} as compared to CHO-WT after 24 hours of postseeding incubation, I did not detect any significant difference between their extracellular amyloid-β42 levels at the 24-hour time point. A significantly higher level of extracellular amyloid-β42 in CHO-APP_{695} can only be detected after incubation time was extended to 48 hours. This observation suggests that the amyloid-β42 induced toxicities were not responsible for extracellular metabolic changes that differentiate CHO-APP_{695} and CHO-WT at 24-hour time point, which could be reflective of more upstream processes, or might even be due to toxicities induced by APP itself. Although amyloid-β cleavage products were more widely known to exert toxicities in AD research, APP had also been identified as primary culprit before. It was first reported in 2003 that mitochondrial membrane is a target location of APP [108], and researchers are getting more and more interested in

studying the toxicities induced by accumulation of APP in the mitochondrial membrane.

In this study, I utilised CHO-APP$_{695}$ as an *in vitro* APP model and its wildtype counterpart CHO-WT as its control. Since both CHO-APP$_{695}$ and CHO-WT were derived from the same cell line, any differences in their extracellular metabolic profiles can be attributed to the addition of APP transgene and/or the resulting amyloid toxicities. My metabolic profiling findings (discussed in the next section) strongly indicate the impaired energy metabolism that is characteristic of a perturbed citric acid cycle, which occurs principally in the mitochondria. Encouraged by this piece of information, I followed up by measuring mitochondrial viability and mitochondrial APP levels in both CHO-APP$_{695}$ and CHO-WT after 24 hours of postseeding incubation. Interestingly, my data showed both impaired mitochondrial viability and accumulation of mitochondrial APP in CHO-APP$_{695}$ at this particular time point (24-hour postseeding incubated).

As this sampling time point occurred before significant accumulation of amyloid-β42 could be detected, these observations were attributed to earlier pathological processes that occurred prior to amyloid-β induced toxicities. My findings were supported by prior study from Trushina et al., where they observed alterations in mitochondrial dynamics which occurred prior to the onset of memory decline and formation of amyloid deposits in APP mice [56]. Another study by Pavlov et al. also corroborates these findings, where they reported contributions of mitochondria-associated APP metabolism to

mitochondrial dysfunction in AD via intracellular pathways [109]. More specifically, they demonstrated that mitochondrial APP is a substrate for gamma-secretase associated with mitochondria [109]. Taken all together, the evidence gathered in this study substantially validates CHO-APP$_{695}$ as a suitable APP model for investigating and pin-pointing early-pathological effects of APP induced toxicities on cellular processes. By performing a global extracellular metabolic profiling to characterize CHO-APP$_{695}$, I have identified a list of APP-perturbed metabolites representative of pathological events that occurred prior to extracellular amyloid-β42 accumulation.

2.5.3. Impaired energy metabolism in CHO-APP$_{695}$

It was reported that impaired energy metabolism is one of the earlier events that occur in AD [110]. There is also a rapidly growing body of evidence to demonstrate that mitochondrial dysfunction is fundamentally involved in the AD pathogenesis [56, 111]. Therefore, the information gathered from metabolic profiling experiments in this chapter will prove to be helpful in understanding the pathological processes underlying impaired energy metabolism in AD.

Both HMDB [103] and KEGG [104] were used to check for metabolic pathways associated with APP-perturbed metabolites. Several APP-perturbed metabolites detected in this study play important roles in cellular energy metabolism, and one of these metabolites is the fuel to cellular metabolism itself, glucose. CHO-APP$_{695}$ consistently displayed higher levels of extracellular glucose in the culture medium after incubation, suggesting a

lower rate of glucose uptake into CHO-APP$_{695}$ cells from the culture medium. Interestingly, subsequent experiments showed that glucose uptake rate remained largely unchanged in CHO-APP$_{695}$ as compared to CHO-WT. However, it should also be noted that the different culture conditions in metabolic profiling and glucose uptake experiments could disconnect the findings from both experiments. Nevertheless, the data implied an impaired glucose metabolism in CHO-APP$_{695}$. Interestingly, reduction of glucose metabolism had been reported to be expedited in early-onset AD patients [112]. Other APP-perturbed metabolites detected which are closely associated with energy metabolism are citric acid, succinic acid, and 2-oxoglutaric acid. These metabolites are key components of the citric acid cycle itself (KEGG reference pathway, KO00020), a main cornerstone of cellular energy metabolism. Earlier study reported that 2-oxoglutarate dehydrogenase, an enzyme responsible for converting 2-oxoglutaric acid to succinyl-CoA through decarboxylation, displayed diminished activity in AD patients [113, 114]. This corroborates with my findings on increased levels of 2-oxoglutaric acid detected in CHO-APP$_{695}$, since conversion of 2-oxoglutaric acid could have been rate-limited by the reduced activity of 2-oxoglutarate dehydrogenase. Increased citric acid and decreased succinic acid levels in CHO-APP$_{695}$ could also be explained by the same bottleneck effect.

Another APP-perturbed metabolite that also participates in energy metabolism is malonic acid, which was shown to be increased in CHO-APP$_{695}$. Malonic acid is a selective and reversible competitive inhibitor that acts against succinate dehydrogenase (SDH), a key enzyme in the citric acid cycle

responsible for oxidative phosphorylation in the respiratory electron transport chain. At higher concentrations, malonic acid is considered to be a mitochondrial toxin and it had been shown to induce brain lesions and subsequent excitotoxic death, caused by SDH inhibition and subsequently excessive NMDA receptor activation [115, 116]. Methylmalonic acid is also an interesting metabolite, which was identified as one of the APP-perturbed metabolites that accumulates in culture medium samples harvested from CHO-APP$_{695}$. It is a component of methylmalonyl CoA, which is an intermediate of a metabolic pathway responsible for converting valine and isoleucine into succinyl-CoA before they enter the citric acid cycle for energy production. In line with my observation, other reports demonstrated that increased concentration of methylmalonic acid in the serum is associated with inhibited energy metabolism [117], as well as deteriorating cognitive functions [118]. Coupled with evidence of a perturbed citric acid cycle, findings in this study lend support to the suitability of CHO-APP$_{695}$ as a platform to study pathological contributions of impaired energy metabolism to AD pathogenesis and therapeutic strategies to overcome it.

2.5.4. Dysregulation of amino acids metabolism in CHO-APP$_{695}$

Metabolism of several amino acids was shown to be adversely affected in CHO-APP$_{695}$. In general, extracellular amino acids (lysine, alanine, proline, ornithine, isoleucine, glycine and tryptophan) were all observed to be present in lower levels in culture media harvested from CHO-APP$_{695}$, with the exception of serine. Taking into account the reservoir of amino acids available in culture medium, this translates to an increased uptake or consumption of

amino acids by CHO-APP$_{695}$, therefore suggesting a possibility of amino acids degradation as compensatory fuel to sustain growth for CHO-APP$_{695}$. Trushina et al. reported increased levels of alanine and glycine in brain tissues of APP mouse model, and this could possibly be due to increased uptake of these amino acids from extracellular space as suggested by my metabolic findings [56]. In another report, lower levels of lysine, isoleucine, and tryptophan were detected in CSF samples taken from probable AD patients when compared against age-matched control patients [119]. Remarkably, the same study reported higher levels of these three amino acids in plasma [119], clearly demonstrating the compartmentalization of amino acids metabolism between brain and plasma. In this respect, my findings could provide useful clues to help understand contributions of amino acids metabolism dysregulation to AD pathogenesis.

2.5.5. PIO exerts a larger extent of treatment effects than ROSI

There is mounting evidence that PPARγ agonists, namely ROSI and PIO, have shown therapeutic potentials in AD [70, 77, 78]. Following the failure of ROSI to demonstrate treatment effect in a phase III AD clinical trial [29], recent studies had been focusing on investigation of PIO as therapeutic agent against AD [85, 120]. This chapter provides supplementary findings as I compared treatment effects of both ROSI (selective PPARγ agonist) and PIO (dual agonist of PPARγ and PPARα) in an APP model. Both compounds demonstrated significant treatment effects on APP-perturbed metabolites, which is in line with their beneficial effects reported in afore-mentioned studies. As ROSI is the stronger and more selective PPARγ agonist [121], I

originally postulated that ROSI would induce a stronger pharmacological response in CHO-APP$_{695}$ as compared to PIO. However, I observed that PIO exerted a noticeably larger extent of treatment effects than ROSI. Metabolite levels of lysine, isoleucine and tryptophan were treated by both ROSI and PIO, suggesting their ability in minimizing dysregulation in amino acids metabolism. However, PIO also successfully restored the metabolic levels of succinic acid, methylmalonic acid, 2-oxoglutaric acid and citric acid, all of which are associated with citric acid cycle and energy metabolism. Taken together, these findings strongly suggest that both ROSI and PIO exerted therapeutic effects on dysregulated amino acids metabolism, while PIO brought about additional treatment effects on mitochondrial dysfunction and impaired energy metabolism observed in CHO-APP$_{695}$.

2.5.6. <u>Contribution of PPARγ and PPARα agonisms to PIO's treatment effects</u>

Therapeutic superiority of PIO observed in this study could be due to other non-PPARγ mechanisms, and since PIO also possesses PPARα agonism activity [92], I hypothesised that PPARα agonism could have been an addition to PIO's therapeutic mechanism in my *in vitro* APP model. This was confirmed by further analyses, where co-administration of T007, a selective blocker of PPARγ receptor, only partially diminished treatment effects observed with both PIO and ROSI, which are mostly amino acids (lysine and tryptophan). Interestingly, T007 co-administration also reversed PIO's treatment effect on methylmalonic acid, a treatment effect which was not observed with ROSI administration, hence suggesting the co-participation of

both PPARγ and non-PPARγ mechanisms in this particular treatment effect. To further pinpoint the mechanistic therapeutic effects observed with PIO, I co-administered GW6471, a selective PPARα blocker, together with PIO to CHO-APP$_{695}$ and studied its extracellular metabolic profiles. Intriguingly, co-administration of GW6471 diminished treatment effects of PIO on metabolites characteristically associated with energy metabolism, namely succinic acid, methylmalonic acid, 2-oxoglutaric acid and citric acid. In line with my observations, previous report demonstrated association of PPARα regulation with citric acid cycle fluxes [122], and treatment with PPARα agonist enhanced hepatic citric acid cycle activity in diabetic rats [123].

In order to gather further evidence to support the therapeutic potential of PIO, I investigated the extent of contribution of PPARγ agonism and PPARα agonism to its treatment effects using two biochemical markers, namely mitochondrial viability and extracellular amyloid-β42. In agreement with my metabolic profiling data, I observed restoration of mitochondrial viability in CHO-APP$_{695}$ with PIO treatment, which was diminished when GW6471 was co-administered. I also detected amyloid-lowering effect of PIO on extracellular amyloid-β42, which was nullified by co-administration of T007. Interestingly, these data on treatment effects associated with both PPARγ and PPARα agonism corroborates findings from previous reports. Sastre et al. demonstrated that PPARγ activation reduced amyloid-β generation via inflammatory modulation and repression of beta secretase gene transcription [86]. In addition to beta secretase expression, Liu et al. observed that PPARγ activation also suppressed APP expression which led to reduction of brain

amyloid-β in diabetic mouse model [124]. On the other hand, it had been shown that PPARα agonism was able to stimulate mitochondrial oxidation of fatty acids in liver [125] and muscle tissues [125, 126], therefore potentially providing an efficient source of alternative fuel for the energy-impaired brain cells in AD patients. It is also worth noting that beneficial effects of PIO on mitochondria in AD model had recently been reported by Masciopinto et al. [120], although the study did not look further into the differential therapeutic effects of PPARγ and PPARα activation by PIO. My study in this chapter generated complementary and useful insights to help understanding better the therapeutic potential of both PPARγ and PPARα agonisms in AD therapy, and supported further pursuant of PIO as a promising drug candidate for treatment of AD.

2.5.7. PIO could be a better drug candidate than ROSI for AD treatment

ROSI had once been studied extensively for treatment of AD, having completed a preliminary clinical trial [74] and a phase II clinical trial in AD patients [72]. However, given its failure in its phase III clinical trial completed in 2010 [29], and recent reports of adverse drug reactions which resulted in the withdrawal of ROSI from the market [89], ROSI has largely fallen out of favour in the field of AD therapeutic research. On the other hand, PIO is another PPARγ agonist which has been gaining traction as drug candidate for AD treatment. My findings in this chapter present an encouraging evidence for further research on PIO as therapeutic agent for AD therapy. To date, one preliminary clinical trial designed to investigate treatment effects of PIO in AD had been completed and the study reported cognitive and functional

improvements in PIO-treated AD patients [73]. On top of that, there is minimal drug safety concern for long-term PIO treatment in AD patients, as an 18-month clinical trial had established its safety profile in AD population [87]. My findings lend strength to support PIO as a potential candidate for AD therapy, and these findings came in a timely manner as Takeda has just initiated its 5-year phase III clinical trial of PIO in AD patients [88]. More carefully designed experiments need to be conducted to gather additional evidence in order to better understand how PIO works. This information could be valuable for interpretation of the clinical trial data, and help to advance PIO further in the pipeline.

2.6.   Conclusions

This chapter generated findings that contribute to the field of AD research in several respects. Firstly, I established CHO-APP$_{695}$ as a suitable *in vitro* APP model for early-stage AD research, which proved to be a useful tool for investigating therapeutic effects of ROSI and PIO in this chapter's work. Secondly, extracellular metabolic profiling data generated from my *in vitro* APP model help to better understand metabolic fluctuations underlying AD, especially when it comes to impaired energy metabolism and amino acid dysregulation. Thirdly, I demonstrated two clear pathological events that occurred before accumulation of extracellular amyloid-β, namely increased mitochondrial APP and reduced mitochondrial viabilities, and both could potentially be further investigated as pathophysiological processes that define early-stage AD. Last but not the least, findings in this chapter demonstrated for the first time that PIO is a more promising drug candidate than ROSI in

AD therapy, and this observation was attributable to PIO being a dual agonist of both PPARγ and PPARα nuclear receptors.

The above findings serve as an informative platform for planning of future experiments aimed at pinpointing the affected metabolic pathways in early-stage AD, and provide a clear support for further advancement of PIO as drug candidate for AD. Therefore in my next chapter, I followed up by performing metabolic profiling experiments on brain tissue samples (cortex, hippocampus, midbrain and cerebellum) and plasma samples harvested from APP/PS1 transgenic mice and compare them against their wildtype counterparts. Using clues generated from *in vitro* experiments in this chapter, I focused my effort on elucidating metabolic alterations and other early-stage AD pathophysiological processes in my *in vivo* AD model, which will be discussed in more detail in the next chapter. Since findings in this chapter clearly demonstrated the therapeutic superiority of PIO over ROSI, subsequent chapters will focus on investigating PIO further to gather more evidence in support of its development as a drug candidate in AD therapy.

CHAPTER 3: GC-TOF-MS-based metabolic profiling in APP/PS1 transgenic mice to uncover early-stage pathological alterations and to shed light on MOA of PIO in AD therapy

3.1.   Chapter summary

In the previous chapter, I used an *in vitro* AD model to look into the effects of APP transgene on cellular metabolism, and studied the therapeutic effects of PPARγ agonists, namely ROSI and PIO, in this APP cell model. Briefly, I observed metabolic alterations closely associated with impaired energy metabolism in the APP cell model, and detected an accumulation of APP in their mitochondrial membrane, which could have mangled their mitochondria. I also showed that PIO is therapeutically superior to ROSI, which could be attributed to PIO's dual agonisms of both PPARγ and PPARα nuclear receptors.

In this chapter, I employed an *in vivo* AD model to continue studying the AD pathophysiological processes, and to investigate further the therapeutic effects of PIO. The AD model used in this chapter's work is APP/PS1 transgenic mouse, which is a commonly used AD model that carries both APP and PS1 transgenes. In an attempt to validate my findings from chapter 2 using this *in vivo* AD model, a similar metabolic profiling approach was used to study the transgenic mouse and compared against their wildtype counterparts. PIO's treatment effects were assessed based on its ability to alleviate or rescue some of the metabolic alterations that were observed in AD transgenic mice used in

this study. Selected biochemical assays were also performed to assess some common AD-related pathology in APP/PS1 mice used in this study.

Some findings in this chapter include the observation of extensive metabolic alterations in cortex and cerebellum of APP/PS1 mice, but not in their hippocampus, midbrain and plasma. The major pathways affected in cortex and cerebellum of APP/PS1 mice were closely related to impaired energy metabolism and perturbation of amino acid metabolism in these mice. APP/PS1 mice also exhibited higher amyloid-β40 and amyloid-β42 in their cortex, accumulation of mitochondria APP in their cortex, and present an altered oxidative state in their brain. PIO treatment had successfully restored the energy metabolism, lowered the amyloid-β peptides, and afforded the APP/PS1 mice a better anti-oxidative capacity in their cortex.

This chapter's work successfully validated some main findings from chapter 2, and continued to support the development of PIO as a therapeutic molecule for AD. In the next chapter, I will attempt to tackle a limitation which could be an obstacle to PIO's drug development process – its poor brain penetration.

3.2. Introduction

In chapter 2, I studied AD pathophysiological processes using an *in vitro* AD model and observed several disease phenotypes that are associated with early-stage disease induced by APP transgene in the cell model. In particular, these phenotypes are associated mainly with impaired energy metabolism, and my findings suggest that an accumulation of APP in mitochondrial membrane could have been responsible for the reduced mitochondrial viability observed in AD cell model. On top of that, my work in chapter 2 also revealed the therapeutic superiority of PIO over ROSI, which could be attributed to PIO being a dual agonist of both PPARγ and PPARα nuclear receptors. This finding is of particular relevance now, as Takeda has just started to recruit 5800 subjects for a phase III AD clinical trial to look into therapeutic effects of PIO [88].

In this chapter, I studied the AD pathophysiological processes further using a different AD model, with a similar focus on early-stage disease phenotypes. In order to study the disease phenotypes in a more intact biological system, an *in vivo* AD model would be employed in this chapter's work. More specifically, the AD models used in this study are C57BL/6 mice that carry two transgenes, APP and PS1 which encodes for APP and presenilin-1 (PS1), respectively. Presence of PS1 transgene increases the activity of gamma-secretase in the model, resulting in enhanced cleavage of APP to form amyloid-β and faster progression to AD in the model. In an attempt to validate some of my findings in chapter 2 in an *in vivo* system, I studied the APP/PS1 mice using the same metabolic profiling approach, and investigated the ability of PIO in

minimising or reversing the metabolic alterations observed in APP/PS1 transgenic mice. Selected biochemical assays were then performed to follow up on findings generated from metabolic data in this study. Accumulation of APP in cortical mitochondria was also assessed in this study, since mitochondrial APP accumulation was discussed as one of the main early-stage AD phenotypes observed in chapter 2's *in vitro* AD model. On top of that, I also attempted to take a look at the oxidative state in APP/PS1 transgenic mice by measuring activities of two major antioxidative enzymes, namely superoxide dismutase (SOD) and catalase, in their cortex and plasma tissue and compare against activities observed in non-transgenic wildtype mice.

To gather a more comprehensive metabolic data using biological samples harvested from APP/PS1 transgenic mice and wildtype mice, two different types of tissue, namely plasma and brain samples were collected from the animal experiments in this study. Since different brain regions had been shown to exhibit their own distinctive metabolic alterations [58, 127], I dissected the whole mouse brain into four different brain parts (cortex, hippocampus, cerebellum, and midbrain) and looked into their metabolic profiles changes separately. By investigating different brain part on its own, I can also study PIO's treatment effects in specific brain regions, which would be really useful in evaluating PIO's therapeutic potential in AD research.

To capture the disease phenotypes associated with early-stage AD in this *in vivo* AD model, the sampling time point had to be carefully chosen to take a biological snapshot that allows me to meaningfully interpret my findings

based on this snapshot. The sampling time point that is the most suitable for this study is where AD in these mouse models had progressed enough to elicit pathophysiological alterations when compared against non-transgenic wildtype mice, but had not progressed so much that these mice started to suffer from build-up of amyloid-β plaques in their brain tissue, which is associated more with moderate to late-stage AD. In this study, I sacrificed the APP/PS1 mice and harvested their samples for investigation when they are 20 weeks old, which is a time that is slightly before these mice start to develop sparse amyloid plaques in their brain tissue [128, 129]. By placing my investigation in this time window, I hoped to capture early-stage AD signals in this model before amyloid plaques wreak havoc in their brains, which would then be heavily laden with extensive oxidative damages and neuronal cell death.

One main challenge that I faced while carrying out this chapter's work was the aggressive behaviour observed in both male and female APP/PS1 transgenic mice. My original research work plan was to expand a breeding colony to gather sufficient APP/PS1 transgenic mice for experimentation, but this plan was hampered by the aggressive behaviours observed in these mice, which made animal husbandry and breeding more challenging than expected. Upon reviewing the literature, I noticed that such aggressive behaviours had been reported in APP transgenic mice before [130, 131]. This observation is also not limited to preclinical AD models, as clinical studies had also reported similar traits among AD patients and looked into ways to improve these symptoms [132, 133]. This unexpected challenge severely limited my

capability to expand the breeding colony to reach my original number of expected transgenic mice intended for experimentation. As a result, the sample size for each treatment groups used in this study is relatively small (n = 5), and might not have enough power to detect more subtle biochemical changes in the APP/PS1 mice.

Nevertheless, the work in this chapter generated some interesting findings, and it is particularly revealing on how PIO exerted its therapeutic effects in specific brain regions in this particular AD model. I observed impaired energy metabolism, oxidative stress, and accumulation of APP in mitochondria in brain tissues of APP/PS1 mice. Taken together with findings generated in chapter 2's *in vitro* experiments, my PhD project paints a compelling picture of APP's ability to disrupt energy metabolism in a living system, which could couple itself with insidious oxidative stress commonly observed in AD to initiate a downward spiral that results in collapse of the whole biological system. Findings in this chapter help to better understand the effects exerted by APP in a living system and to elucidate PIO's differential treatment effects in different brain regions investigated in this study.

3.3.   Materials and Methods

3.3.1. Chemicals and Reagents used

MOX reagent (2% Methoxamine hydrochloride in pyridine) and MSTFA derivatising reagent with 1% TCMS were purchased from Thermo Fisher Scientific (Waltham, MA). PIO was purchased from Cell Molecular

Pharmaceutical R&D (Xi'an, China). All other reagents used were of analytical grades.

3.3.2. <u>Animal husbandry</u>

APP/PS1 transgenic male and female breeders were used to generate breeding colony to obtain APP/PS1 transgenic mice for experiments in this study. Transgenic breeders were generous gifts given by Professor Gavin Dawe's research group (National University of Singapore, Singapore). The mice were paired for breeding in separate cages, and pups were weaned 4 weeks after birth. Mouse tail genotyping was used to confirm the presence of APP and PS1 transgene in offsprings. To carry out the genotyping, PureLink Genomic DNA Mini kit (Life Technologies, Carlsbad, CA, US) was first used to extract DNA from sampled mouse tails. DNA extractions were then subjected to PCR amplification with primers (separately for APP, PS1, and internal control) and GoTaq Green Master Mix (Promega, Madison, WI, US). Mixtures were then resolved by DNA gel electrophoresis, whereas gel imaging was done using Molecular Imager Gel Doc XR and analysed using Image Lab Software (Bio-Rad, Hercules, CA, US). APP/PS1 transgenic mice intended for experiments were housed in groups (maximum of 5 mice per cage) under standard conditions of humidity, temperature and 12-h light/dark cycle with ad libitum access to food and water. All mice were maintained under constant conditions for 4 days prior to experiments. All animal handling protocols were carried out in accordance with Singapore National Advisory Committee on Laboratory Animal Research (NACLAR) guidelines and approved by NUS Institutional Animal care and Use Committee (IACUC) (Reference no. BR10/11, 074-11).

3.3.3. Animal experiment and sample collection

A total of 10 male APP/PS1 transgenic mice (18 weeks old) were split into two treatment groups (n = 5), where one group received PIO treatment and the other group received vehicle treatment as disease control. Another 5 male wildtype mice (18 weeks old, taken from the same breeding colony) were also given vehicle treatment and they serve as healthy control in this experiment. PIO was dissolved in DMSO and diluted 20 times with 1% (w/v) methyl cellulose to be administered via oral gavage (p.o.). PIO treatment was given as single p.o. administration every day for 14 days, and dosage used in this study was 30 mg/kg of PIO. Vehicle-treated APP/PS1 and wildtype mice were given vehicle treatment for 14 days as well. 24 hours after the last dose of the 14-day treatment regimen, all mice (20 weeks old) were sacrificed by CO_2 euthanization and their blood samples were collected via cardiac puncture into eppendorf tubes supplemented with heparin. Transcardial perfusion with saline was then performed on the sacrificed mice to remove traces of blood from their organs before their whole brain tissues were removed from skulls. Immediately after the whole brains were collected, different brain parts (cortex, hippocampus, cerebellum and midbrain) were dissected and transferred into separate clean eppendorf tubes. All biological samples were kept on ice immediately after collection until storage. Blood samples were centrifuged at 4,000 g for 10 minutes and plasma samples were then collected from supernatants into clean eppendorf tubes. Plasma and all brain part samples were stored at -80 °C until analysis.

3.3.4. Sample preparation for GC-TOF-MS-based metabolic profiling analysis

Plasma and brain part samples were thawed and kept on ice before sample preparation. About 20-25 mg of brain part samples (cortex, hippocampus, cerebellum and midbrain) were transferred into new eppendorf tubes, and 10 µL/mg of Milli-Q water was added to each tube containing the brain part sample before they were lysed with bead homogeniser. 150 µL of each tissue homogenate was then transferred into new tubes for subsequent sample preparation. 100 µL of plasma samples were used without dilution for sample preparation. To prepare biological samples for GC-TOF-MS analyses, 950 µL of chilled methanol (containing 50 µM of myristic-d_{27} acid as IS) was first added to each brain part and plasma samples for protein precipitation. All mixtures were vortex-mixed at high speed for 5 minutes, followed by centrifugation (14,000 g) for 20 minutes at 4°C to pellet the precipitated protein. 900 µL of clear supernatant was then transferred into pre-silanized glass tubes for drying, and subsequent procedures for sample derivatisation were similar to GC sample preparation detailed under section 2.3.5.

3.3.5. GC-TOF-MS data acquisition and preprocessing

Brain part and plasma samples were analysed in batches separated according to the types of samples. Within each batch for one particular samples type, sample injections were randomised to minimise procedural artefact during subsequent analyses. Data acquisition and preprocessing for GC-TOF-MS analyses were carried out in a similar fashion as previously described under section 2.3.6. The resulting metabolic data were processed by normalising

peak area of each analyte based on peak area of myristic-d$_{27}$ acid in their own respective sample, followed by another normalisation using total integral area of all included metabolic peaks. Normalised metabolic peak areas were then constructed into a data matrix for subsequent multivariate data analysis.

3.3.6. Multivariate data analysis of metabolic data matrix

Multivariate data analysis of the normalised data was carried out using the SIMCA-P software version 13.0, with separate analyses carried for different types of samples (plasma, cortex, hippocampus, cerebellum, and midbrain). Multivariate data analysis workflow was similar to that reported in section 2.3.7, with a discriminant model built separately for each different type of samples. To interpret the biological meaning behind the observed metabolic alterations, information regarding discriminant metabolites was sourced from freely available online metabolite databases such as HMDB [103], KEGG) [104] and published literature.

3.3.7. Evaluating PIO's therapeutic effects on discriminant metabolites

To assess therapeutic potential of PIO on metabolic perturbation in plasma and different brain parts of APP/PS1 transgenic mice, I analysed PIO's effects on the list of discriminant metabolites identified in above section. Discriminant metabolites for APP/PS1 mice were regarded as being normalised or "treated" if their levels after in PIO-treated transgenic mice were altered significantly when compared against vehicle-treated transgenic mice, and the direction of change is heading towards metabolite levels observed in non-transgenic wildtype mice (healthy control). Since different types of samples (plasma,

cortex, hippocampus, cerebellum, and midbrain) have their own list of discriminant metabolites, PIO's treatment effects on each list were assessed separately. Statistical comparison of data for evaluation of treatment effects was performed using two-tailed independent t-test with Welch's correction, and P-value < 0.05 will be defined as being "treated" to guide the discussion in this chapter.

3.3.8. <u>Measurement of amyloid-β40 and amyloid-β42 levels in cortex and plasma</u>

Amyloid-β40 and 42 levels in cortex and plasma samples of vehicle-treated APP/PS1 mice, PIO-treated APP/PS1 mice, and non-transgenic wildtype mice were quantitatively measured using colorimetric sandwich ELISA kits, according to the protocols provided by the manufacturer (#SIG-38954 and #SIG-38956 from Covance, Princeton, NJ). Cortex tissue samples from all mice were homogenised with PBS supplemented with 1x protease inhibitor cocktail in a ratio of 1:10 before loading into coated plates that came with the ELISA kits. Plasma samples were diluted 30 times with PBS for their amyloid-β40 and 42 measurements to be taken using this method. Similar to *in vitro* AD model used in chapter 2, total protein analysis (using micro BCA protein assay kit) indicated that cortex tissue harvested from APP/PS1 mice consistently displayed higher level of total protein expression than non-transgenic wildtype mice. Therefore, non-normalized cortical amyloid-β40 and 42 data were used for comparison between the three groups of mice, and data were made comparable by loading equal tissue mass into plate before measurements were taken. All absorbance readings were measured using

Tecan Infinite M200 microplate reader (Tecan, Switzerland). Data means were statistically compared using two-tailed independent t-test with Welch's correction, with significance level set at $P < 0.05$.

3.3.9. <u>Measurement of APP Levels in cortex and cortical mitochondrial fractions</u>

One of my observations in chapter 2's *in vitro* experiments was the accumulation of APP in the mitochondria of CHO-APP$_{695}$, which could have mangled its mitochondria and resulted in perturbed energy metabolism in the AD model. In this chapter, I proceeded to assess APP levels in both cortex samples and mitochondria fractions extracted from cortex tissue of APP/PS1 mice, APP/PS1 mice treated with PIO and non-transgenic wildtype mice. Cortex tissue samples were homogenised in a ration of 1:10 with PBS supplemented with 1x protease inhibitor cocktail. To extract mitochondria fractions, cortex tissue samples were first homogenised on ice using a pre-chilled dounce homogenizer, and differential centrifugation procedure detailed in a commercially available kit was used for mitochondria extraction (#89874 from Thermo Fisher Scientific, Waltham, MA). It should be noted that, following the manufacturer's recommendation, mitochondrial pellets were obtained using centrifugation at 3,000 g (instead of 12,000 g) to improve purity of extraction. To assess the purity of mitochondrial fraction, a western blot analysis was used to detect for presence of different organelles in extracted fractions and compared against whole tissue homogenate. Presence of different organelles was measured using antibody cocktail suitable for organelle detection (ab133989 from Abcam, Cambridge, UK). Antibodies

targeting four different organelle markers were used in the western blot analysis, namely anti-sodium potassium ATPase antibody (plasma membrane), anti-ATP5A antibody (mitochondria), anti-GAPDH antibody (cytosol); and anti-histone H3 antibody (nucleus). Following extraction, the purified mitochondrial fractions were further homogenised using a probe sonicator to completely lyse the mitochondria for analysis of APP using colorimetric sandwich ELISA kit (#KHB0051 from Life Technologies, Carlsbad, CA). Cortical APP data were not normalised for the same reason stated in previous section, whereas mitochondrial APP data were normalized based on total protein level present in each mitochondrial fraction (measured using micro BCA protein assay kit). All absorbance readings were measured using Tecan Infinite M200 microplate reader. Means between different groups were compared using two-tailed independent t-test with Welch's correction, with $P < 0.05$ to be considered as a significant mean difference.

3.3.10. Measurement of lactate dehydrogenase (LDH) and citrate synthase activities

Comparison between metabolic data for APP/PS1 and non-transgenic wildtype mice showed that two major discriminant metabolites between these two groups are citric acid and lactic acid (results shown below). Among these two discriminant metabolites, PIO exerted treatment effect on lactic acid but not citric acid. Therefore, I assessed the activities of LDH and citrate synthase in cortex samples taken from APP/PS1 mice, PIO-treated APP/PS1 mice, and non-transgenic wildtype mice. LDH activities were measured using a commercially available colorimetric assay kit (#K726-500, BioVision,

Milpitas, CA, US), where LDH's ability to reduce NAD to NADH was assessed in each sample, and colorimetric probe was used to measure the activity of this reaction. Citrate synthase activities in cortex samples harvested from all three groups of mice were also measured using a commercially available kit (#K318-100, BioVision, Milpitas, CA, US), where citrate synthase activities for all samples were measured based on their ability to convert acetyl-CoA and oxaloacetate into intermediates which would then develop into colored products for detection. All absorbance readings were measured using Tecan Infinite M200 microplate reader, and means between different groups were compared using two-tailed independent t-test with Welch's correction, with $P < 0.05$ to be considered as a significant mean difference.

3.3.11. Measurement of SOD and catalase activities

Since oxidative stress is one pathological phenotype common in most AD models, I attempted to assess the oxidative capacities in cortex and plasma samples of APP/PS1 mice, PIO-treated APP/PS1 mice and wildtype mice, by measuring activities of two major antioxidative enzymes. A commercially available kit (#706002, Cayman Chemical, Ann Arbor, MI, US) was used to measure SOD activity, where a mixture of xanthine oxidase and hypoxanthine was used to generate superoxide radicals which would be scavenged by SOD present in samples. Unreacted superoxide radicals would react with tetrazolium salt to form a detectable coloured dye, thus producing an inverse relationship between amounts of coloured dye formed and SOD activities in samples. Catalase activity was also assessed using a commercially available

kit (#707002, Cayman Chemical, Ann Arbor, MI, US), where reaction of catalase with methanol in presence of H_2O_2 to produce formaldehyde was monitored colorimetrically using a triazole dye. All absorbance readings were measured using Tecan Infinite M200 microplate reader, and means between different groups were compared using two-tailed independent t-test with Welch's correction, with $P < 0.05$ to be considered as a significant mean difference.

3.4. Results

3.4.1. GC-TOF-MS-based metabolic profiling of plasma samples

Metabolic profiles of plasma samples taken from two groups of mice (APP/PS1 transgenic mice and non-transgenic wildtype mice) were scanned in an untargeted fashion using GC-TOF-MS analytical platform. PCA for plasma samples did not display any visible clustering trend on scores plot, suggesting only slight or no difference between the plasma metabolites from the two groups of mice (**Figure 6A**). A PLS-DA model generated using the same metabolic data did not pass the model validation plot as randomly permuted datasets gave higher Q^2 values than the Q^2 value calculated for original dataset (**Figure 6B**), which indicates high risk of model over-fitting and little interpretability for the dataset. OPLS-DA model constructed using the same data is presented in **Figure 6C** (1 predictive and 1 orthogonal components, $R^2(Y)$ and $Q^2(cum)$ were 0.932 and 0.194, respectively). The small $Q^2(cum)$ value indicates that separation of plasma metabolic profiles between the two groups of mice was not clear. Nevertheless, a list of 25 potential discriminant

metabolites (VIP ≥ 1.00) was generated based on the OPLS-DA model, and only two metabolites (L-threonine and L-Valine) have $P < 0.05$. Interestingly, one of them (L-threonine, +28.6 %) has P-value lower than Bonferroni-adjusted significance level (0.002).
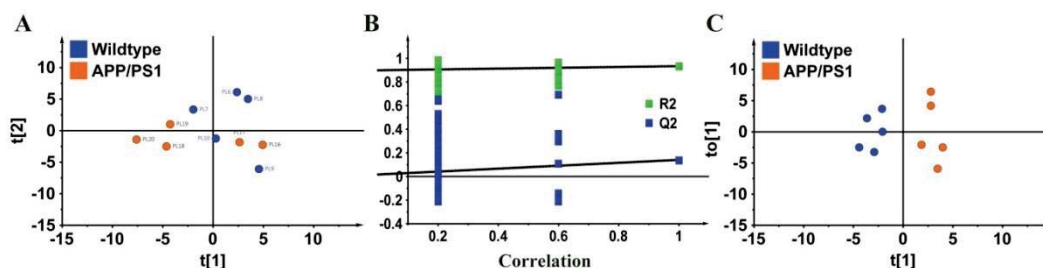
Figure 6. (A) PCA of plasma samples from wildtype and APP/PS1 transgenic mice; **(B)** Y-permuted model validation plot for PLS-DA of same dataset; **(C)** OPLS-DA of their plasma metabolic profiles ($R^2(Y) = 0.932$, $Q^2(cum) = 0.194$).

3.4.2. GC-TOF-MS-based metabolic profiling of cortex samples

PCA for metabolic profiles in cortex samples displayed a clear clustering between APP/PS1 mice and non-transgenic wildtype mice (**Figure 7A**). Model validation plot for PLS-DA model generated using the same dataset showed a valid model, as all Q^2 values calculated for randomly permuted datasets were lower than actual Q^2 value itself, and the regression line of Q^2 values intersected y-axis below zero (**Figure 7B**). OPLS-DA model constructed using the same data is presented in **Figure 7C** (1 predictive and 1 orthogonal components, $R^2(Y)$ and $Q^2(cum)$ were 0.986 and 0.863, respectively). The high $Q^2(cum)$ value indicates that separation of cortical metabolic profiles between the two groups of mice was robust. Based on this OPLS-DA model, a list of 22 potential discriminant metabolites (VIP ≥ 1.00)

that contributed to separation was identified and presented in **Table 3**. 10 out of these 22 metabolites achieved significance when means were compared between APP/PS1 and non-transgenic wildtype mice, as determined by $P <$ 0.0023 (Bonferroni-adjusted significance level).

Figure 7. **(A)** PCA of cortex metabolic profiles for wildtype and APP/PS1 transgenic mice; **(B)** Y-permuted model validation plot for PLS-DA of cortex metabolic data; **(C)** OPLS-DA of cortex metabolic data ($R^2(Y) = 0.986$, $Q^2(cum) = 0.863$).

Table 3. List of potential discriminant metabolites that differentiate cortex tissue of APP/PS1 mice from non-transgenic wildtype mice

	Metabolite	Metabolic class	FC	VIP	P value [a]
1	Citric acid	Carboxylic acid	0.65	1.55	< 0.0001*
2	Glycine	Amino acid	0.80	1.54	< 0.0001*
3	Inosine	Purine nucleoside	1.69	1.54	< 0.0005*
4	Threonine	Amino acid	0.73	1.50	< 0.001*
5	Lactic acid	Hydroxy acid	1.46	1.47	< 0.001*
6	Tyrosine	Amino acid	0.69	1.44	< 0.001*
7	Valine	Amino acid	0.75	1.43	< 0.001*
8	Glucose	Monosaccharide	1.07	1.43	< 0.005*
9	Aspartic acid	Amino acid	0.66	1.42	< 0.005*
10	Malic acid	Carboxylic acid	1.33	1.38	< 0.005
11	Glucose-6-phosphate	Monosaccharide	1.38	1.37	< 0.005*
12	Beta-alanine	Amino acid	0.50	1.36	< 0.01
13	Leucine	Amino acid	0.81	1.31	< 0.005
14	Ribose-5-phosphate	Monosaccharide	1.41	1.30	< 0.01
15	Fumaric acid	Fatty acid	1.18	1.29	< 0.05
16	Ethanolamine	Alkylamine	0.75	1.26	< 0.01

17	Serine	Amino acid	0.86	1.24	< 0.05
18	Pyroglutamic acid	Pyrrolidine	1.16	1.23	< 0.05
19	Glycerol	Sugar alcohol	0.87	1.12	< 0.05
20	Threonolactone	Lactone	1.42	1.10	< 0.05
21	N-Acetyl-L-aspartic acid	Amino acid	1.42	1.09	< 0.05
22	Oleic acid	Fatty acid	1.06	1.07	< 0.05

[a] P values were calculated for mean comparison between APP/PS1 and non-transgenic wildtype using independent t-tests (two-tailed) with Welch's correction
* $P < 0.0023$ (Bonferroni-adjusted significance level)

3.4.3. GC-TOF-MS-based metabolic profiling of hippocampus samples

Similar to cortical metabolic profiles, PCA for hippocampus samples displayed a clear grouping that separates APP/PS1 mice from non-transgenic wildtype mice (**Figure 8A**). Y-permuted validation plot shows that the PLS-DA model built using this dataset is valid (**Figure 8B**). OPLS-DA model (1 predictive and 1 orthogonal components) constructed using the same data gave $R^2(Y)$ and Q^2(cum) values of 0.986 and 0.914, respectively, which indicates that the separation between APP/PS1 mice and wildtype mice based on their hippocampal metabolic profiles is strong (**Figure 8C**). Based on this OPLS-DA model, a list of 21 potential discriminant metabolites (VIP ≥ 1.00) that contributed to separation was identified and presented in **Table 4**. Only 1 out of these 21 metabolites achieved significance when means were compared between APP/PS1 and non-transgenic wildtype mice, as determined by $P < 0.0024$ (Bonferroni-adjusted significance level).
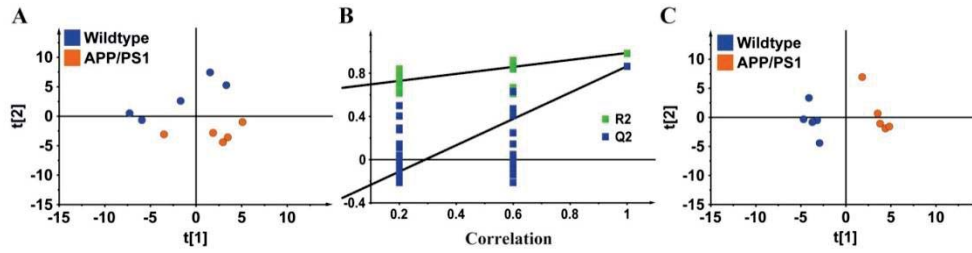
Figure 8. (A) PCA of hippocampus metabolic profiles for wildtype and APP/PS1 transgenic mice; **(B)** Y-permuted model validation plot for PLS-DA of hippocampus metabolic data; **(C)** OPLS-DA of hippocampus metabolic data $(R^2(Y) = 0.986. O^2(cum) = 0.914)$.

Table 4. List of potential discriminant metabolites that differentiate hippocampus tissue of APP/PS1 mice from non-transgenic wildtype mice

	Metabolite	Metabolic class	FC	VIP	P value [a]
1	Ribose-5-phosphate	Monosaccharide	2.11	1.66	< 0.01
2	Lactic acid	Hydroxy acid	1.19	1.62	< 0.0001*
3	Glucose-6-phosphate	Monosaccharide	2.04	1.61	< 0.01
4	Glucose	Monosaccharide	1.58	1.55	< 0.01
5	Aspartic acid	Amino acid	0.77	1.52	< 0.01
6	Creatinine	Lactam	1.41	1.51	< 0.01
7	Uracil	Pyrimidine	0.84	1.46	< 0.05
8	Malic acid	Carboxylic acid	1.16	1.46	< 0.05
9	Succinic acid	Carboxylic acid	1.14	1.45	< 0.05
10	Inosine	Purine nucleoside	1.26	1.42	< 0.05
11	Beta-alanine	Amino acid	0.68	1.41	< 0.05
12	Glycine	Amino acid	0.95	1.40	< 0.05
13	Threonolactone	Lactone	1.55	1.39	< 0.05
14	GABA	Amino acid	0.80	1.33	< 0.05
15	2-Hydroxyglutaric acid	Hydroxy acid	1.15	1.32	< 0.05
16	Urea	Urea	1.23	1.30	< 0.05
17	Proline	Amino acid	1.29	1.24	< 0.05
18	4-Guanidinobutyric acid	Amino acid	0.81	1.24	< 0.05
19	Leucine	Amino acid	0.92	1.22	< 0.05
20	Pyroglutamic acid	Pyrrolidine	1.13	1.20	NS**
21	Glutamic acid	Amino acid	1.47	1.17	NS**

[a] *P* values were calculated for mean comparison between APP/PS1 and non-transgenic wildtype using independent t-tests (two-tailed) with Welch's correction
* $P < 0.0024$ (Bonferroni-adjusted significance level)
** NS (non-significance) is defined by $P > 0.05$

93

3.4.4. GC-TOF-MS-based metabolic profiling of cerebellum samples

PCA for metabolic profiles of cerebellum samples also showed a clear separation between APP/PS1 mice and non-transgenic wildtype mice (**Figure 9A**). Y-permuted validation plot shows that the PLS-DA model built using this dataset is valid (**Figure 9B**). OPLS-DA model (1 predictive and 1 orthogonal components) constructed using the same data showed a robust separation between the two groups of mice, as reflected by their $R^2(Y)$ and $Q^2(cum)$ values of 0.966 and 0.818, respectively (**Figure 9C**). Based on this OPLS-DA model, a list of 16 potential discriminant metabolites (VIP $\geq$ 1.00) that contributed to separation was identified and presented in **Table 5**. 5 out of these 16 metabolites achieved significance when means were compared between APP/PS1 and non-transgenic wildtype mice, as determined by $P <$ 0.003 (Bonferroni-adjusted significance level).
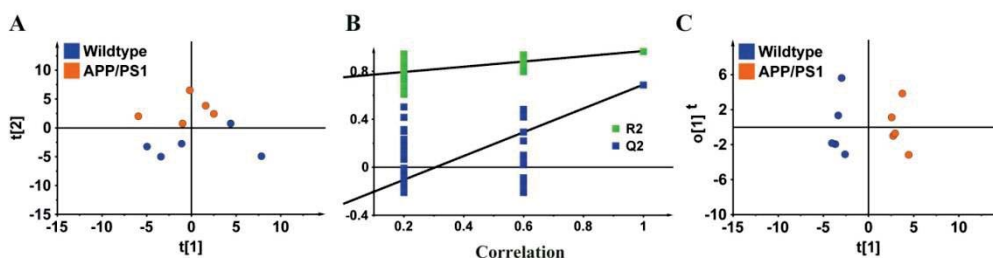
Figure 9. (A) PCA of cerebellum metabolic profiles for wildtype and APP/PS1 transgenic mice; **(B)** Y-permuted model validation plot for PLS-DA of cerebellum metabolic data; **(C)** OPLS-DA of cerebellum metabolic data ($R^2(Y)$ = 0.966, $Q^2(cum)$ = 0.818).

Table 5. List of potential discriminant metabolites that differentiate cerebellum tissue of APP/PS1 mice from non-transgenic wildtype mice

	Metabolite	Metabolic class	FC	VIP	P value [a]
1	Ribose-5-phosphate	Monosaccharide	1.46	1.91	< 0.0005*
2	Glucose-6-phosphate	Monosaccharide	1.35	1.82	< 0.001*

3	Glutamic acid	Amino acid	1.41	1.82	< 0.001*
4	N-acetyl-L-aspartic acid	Amino acid	1.51	1.75	< 0.005*
5	Aspartic acid	Amino acid	0.67	1.73	< 0.005*
6	Leucine	Amino acid	0.81	1.53	< 0.05
7	Ribonic acid	Monosaccharide	0.75	1.32	NS**
8	Succinic acid	Carboxylic acid	1.16	1.29	NS**
9	Threonic acid	Monosaccharide	1.26	1.27	NS**
10	Glycolic acid	Hydroxy acid	1.39	1.25	NS**
11	Fumaric acid	Fatty acid	0.89	1.21	NS**
12	Methylmalonic acid	Carboxylic acid	1.12	1.19	NS**
13	Glyceric acid	Sugar acid	1.33	1.12	NS**
14	Serine	Amino acid	0.85	1.09	NS**
15	Fructose	Monosaccharide	0.86	1.02	NS**
16	Valine	Amino acid	0.85	1.02	NS**

[a] P values were calculated for mean comparison between APP/PS1 and non-transgenic wildtype using independent t-tests (two-tailed) with Welch's correction
* $P < 0.003$ (Bonferroni-adjusted significance level)
** NS (non-significance) is defined by $P > 0.05$

3.4.5. GC-TOF-MS-based metabolic profiling of midbrain samples

Similar to what I had observed with the above three brain regions, PCA for midbrain samples produced a distinct clustering trend that separates APP/PS1 mice from non-transgenic wildtype mice (**Figure 10A**). Validity of PLS-DA model for this metabolic dataset was checked using Y-permuted validation plot (**Figure 10B**), and OPLS-DA model (1 predictive and 1 orthogonal components) constructed using the same dataset gave $R^2(Y)$ and $Q^2(cum)$ values of 0.939 and 0.680, respectively, which indicates that there is also a separation between midbrain metabolic profiles of APP/PS1 mice and wildtype mice (**Figure 10C**). A list of 18 potential discriminant metabolites (VIP ≥ 1.00) was constructed based on this OPLS-DA model, and 3 out of these 18 metabolites achieved significance as determined by $P < 0.0028$ (Bonferroni-adjusted significance level). The list of discriminant metabolites for midbrain samples was summarised in **Table 6**.
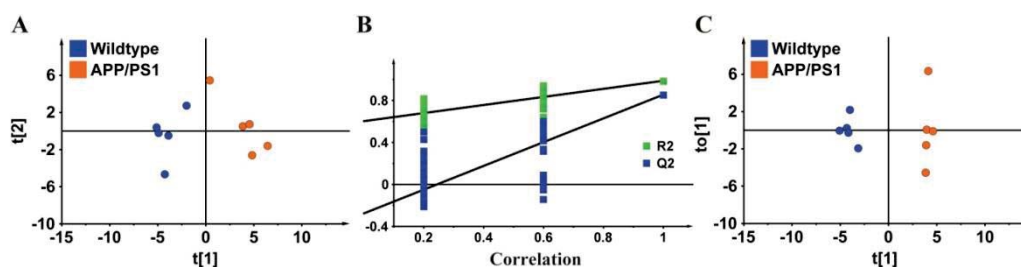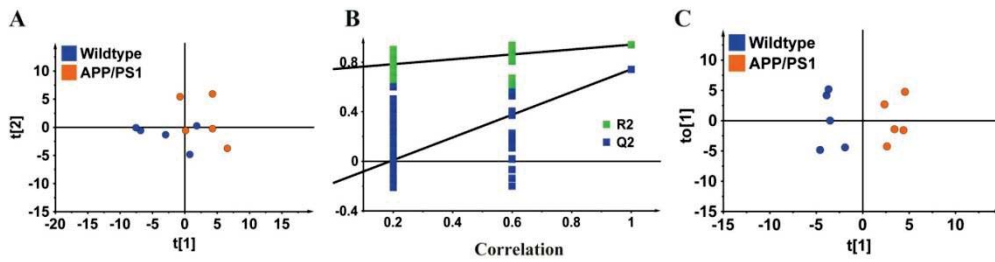
Figure 10. (A) PCA of cerebellum metabolic profiles for wildtype and APP/PS1 transgenic mice; **(B)** Y-permuted model validation plot for PLS-DA of cerebellum metabolic data; **(C)** OPLS-DA of cerebellum metabolic data ($R^2(Y)$ = 0.966, Q^2(cum) = 0.818).

Table 6. List of potential discriminant metabolites that differentiate midbrain tissue of APP/PS1 mice from non-transgenic wildtype mice

	Metabolite	Metabolic class	FC	VIP	P value [a]
1	Urea	Urea	1.55	1.85	< 0.0005*
2	Uracil	Pyrimidine	0.72	1.73	< 0.005*
3	Inosine	Purine nucleoside	1.52	1.73	< 0.01
4	Aspartic acid	Amino acid	0.73	1.69	< 0.05
5	N-acetyl-L-aspartic acid	Amino acid	3.93	1.68	NS**
6	Glucose-6-phosphate	Monosaccharide	1.58	1.52	< 0.05
7	Pyroglutamic acid	Amino acid	0.63	1.39	< 0.05
8	Ribose-5-phosphate	Monosaccharide	1.51	1.38	< 0.05
9	Tyrosine	Amino acid	0.63	1.33	< 0.005*
10	Lactic acid	Hydroxy acid	1.20	1.31	NS**
11	Serine	Amino acid	0.82	1.29	NS**
12	Threonine	Amino acid	0.87	1.19	NS**
13	Succinic acid	Carboxylic acid	1.19	1.14	NS**
14	Docosahexaenoic acid	Fatty acid	1.15	1.11	NS**
15	Sorbitol	Fatty alcohol	1.18	1.09	NS**
16	Glycolic acid	Hydroxy acid	1.22	1.05	NS**
17	Alanine	Amino acid	0.77	1.04	NS**
18	Leucine	Amino acid	0.86	1.03	NS**

[a] P values were calculated for mean comparison between APP/PS1 and non-transgenic wildtype using independent t-tests (two-tailed) with Welch's correction
* $P < 0.0028$ (Bonferroni-adjusted significance level)
** NS (non-significance) is defined by $P > 0.05$

3.4.6. Evaluating PIO's therapeutic effects on discriminant metabolites

To assess therapeutic potential of PIO in the AD model used in this study, I investigated PIO's ability to alleviate or reverse the discriminant metabolites identified in plasma and different brain parts of APP/PS1 mice. PIO was observed to exert no therapeutic effect on discriminant metabolites that were identified in plasma (L-threonine), hippocampus tissue (lactic acid) and midbrain tissue (urea and uracil). On the other hand, PIO successfully treated 4 out of 10 discriminant metabolites (lactic acid, L-valine, glucose and glucose-6-phosphate) which characterised cortex tissue of APP/PS1 mice. On top of that, out of the 5 discriminant metabolites that differentiated cerebellum tissue of APP/PS1 mice from their wildtype counterparts, PIO successfully treated 4 of them (ribose-5-posphate, glucose-6-phosphate, L-glutamic acid and N-acetyl-L-aspartic acid). It is also worth noting that among the "treated" discriminant metabolites, those that are associated with energy metabolism (lactic acid, glucose, glucose-6-phosphate and ribose-5-phosphate) were completely rescued by treating APP/PS1 mice with PIO. Treatment effects exerted by PIO on discriminant metabolites are graphically summarised in **Figure 11**.
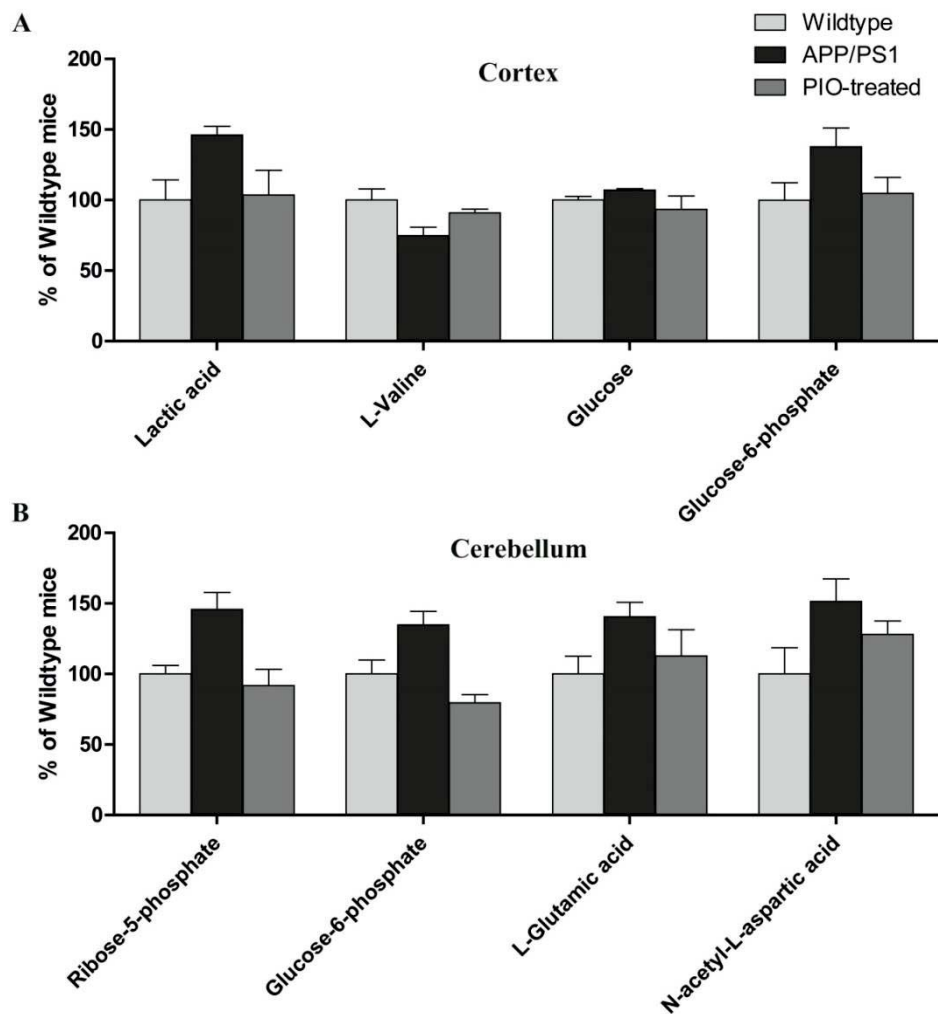
Figure 11. (A) Discriminant metabolites in cortex tissue that were treated by PIO administration; **(B)** Discriminant metabolites in cerebellum tissue that were treated by PIO administration.

3.4.7. Measurement of amyloid-β (40 and 42) levels in cortex and plasma

Amyloid-β40 and amyloid-β42 levels in plasma of APP/PS1 mice and their non-transgenic wildtype counterparts did not show any significant difference, and PIO treatment had no effect on both amyloid-β in plasma of APP/PS1 mice. On the other hand, amyloid-β40 was observed to increase by 19 % in cortex tissue of APP/PS1 mice as compared to non-transgenic wildtype mice, which was reversed by PIO treatment. Remarkably, amyloid-β42 levels in cortex tissue of APP/PS1 mice increased by as much as 364 % when compared

against non-transgenic wildtype mice. The increase in cortical amyloid-β42 was partially reduced by PIO treatment in the transgenic mice. All data for amyloid-β40 and amyloid-β42 in cortex and plasma samples were graphically summarised in **Figure 12**.
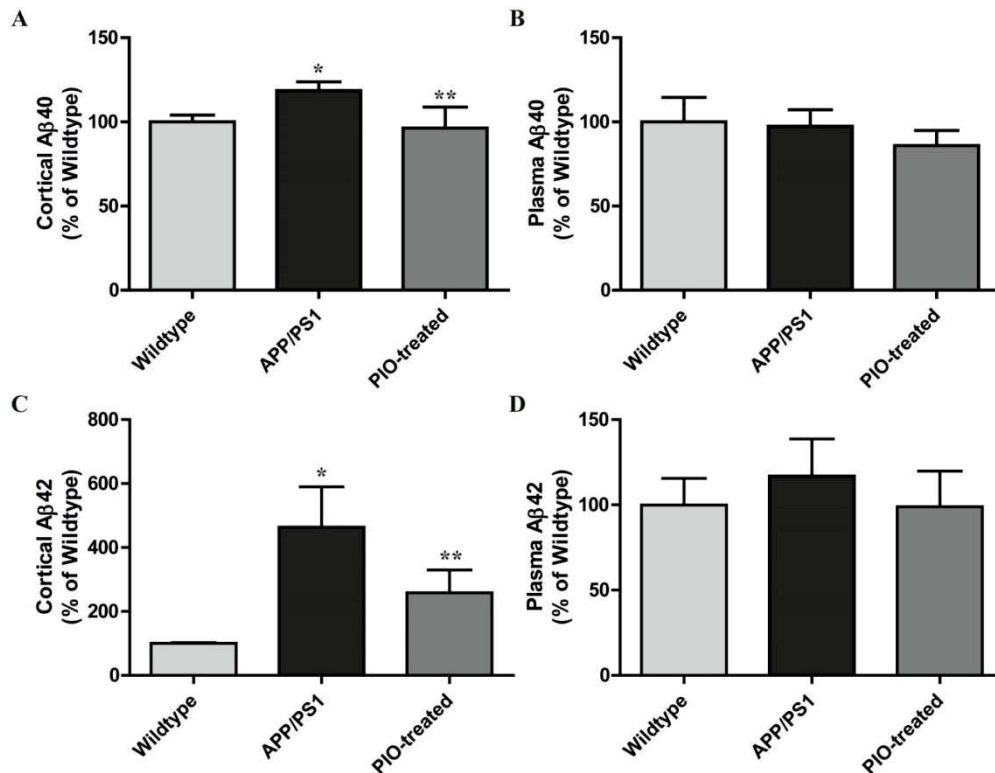
Figure 12. (A) Amyloid-β40 levels in cortex samples; **(B)** Amyloid-β40 levels in plasma samples; **(C)** Amyloid-β42 levels in cortex samples; **(D)** Amyloid-β42 levels in plasma samples; * $P < 0.05$ when compared against non-transgenic wildtype mice; ** $P < 0.05$ when compared against non-treated APP/PS1 mice; All error bars represent one SD.

3.4.8. Measurement of APP Levels in cortex and cortical mitochondria

In this study, I measured the amount of APP present in cortex tissue and mitochondrial extracts of cortex tissue taken from APP/PS1 mice, PIO-treated APP/PS1 mice and non-transgenic wildtype mice. Cortical APP was observed to be higher in APP/PS1 mice by 33 %, although this increase did not achieve

significance. Interestingly, PIO treatment significantly reduced the cortical APP in APP/PS1 mice (**Figure 13A**). APP was also observed to have accumulated significantly (+31 %) in mitochondria extracted from cortex tissue of APP/PS1 mice. However PIO treatment did not have any obvious effect on the accumulation of mitochondrial APP in transgenic mice (**Figure 13B**). To ensure that there was no contaminant of plasma membrane (a considerable source of APP) in the mitochondrial extracts, a western blot analysis was used to assess the purity of extracted mitochondria fractions. Extracted mitochondrial fractions for cortex tissue showed an intense band at 55 kDa (mitochondrial marker), and a very faint band at 15 kDa (nuclear marker); whereas analysis of tissue homogenate gave intense bands at both 100 kDa (plasma marker) and 55 kDa (mitochondrial marker), as well as a faint band 15 kDa (nuclear marker) (**Figure 13C**). My western blot analysis demonstrated excellent mitochondrial purity in extracted fractions, and ruled out possibility of contamination from plasma membrane APP in mitochondrial APP measurements.

Figure 13. (A) APP levels in cortex samples harvested from all three groups of mice; **(B)** APP levels in extracted mitochondrial fractions; * $P < 0.05$ when compared against non-transgenic wildtype mice; ** $P < 0.05$ when compared against non-treated APP/PS1 mice; All error bars represent one SD; **(C)** Western blot analysis of 4 organelle markers (100 kDa – plasma membrane; 55 kDa – mitochondria; 36 kDa – cytosol; 15 kDa - nucleus) performed on extracted mitochondrial fractions and cortex tissue homogenate.

3.4.9. Measurement of LDH and citrate synthase activities

Citrate synthase activities in cortex samples of all three groups of mice (APP/PS1 mice, PIO-treated APP/PS1 mice and non-transgenic wildtype mice) did not show any significant difference. On the other hand, activities of LDH were observed to have decreased significantly in cortex tissue of APP/PS1 mice when compared against their non-transgenic wildtype mice, and PIO treatment was observed to have reversed this reduction in LDH activities in APP/PS1 mice. Data for measurement of LDH activities in cortex samples from all three groups of mice were graphically summarised in **Figure 14**.
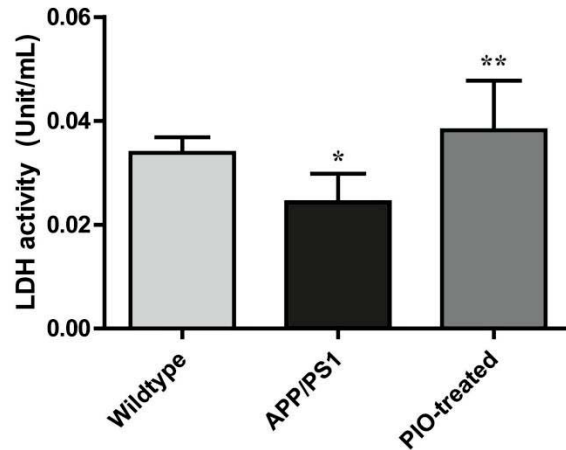
Figure 14. LDH activities in cortex samples taken from all three groups of mice; * $P < 0.05$ when compared against non-transgenic wildtype mice; ** $P < 0.05$ when compared against non-treated APP/PS1 mice; All error bars represent one SD.

3.4.10. <u>Measurement of SOD and catalase activities</u>

SOD activities were observed to have dropped significantly in cortex samples of APP/PS1 mice when compared against wildtype mice, and PIO treatment successfully reversed this reduction of SOD activities in cortex tissue (**Figure 15A**). There was no reduction in SOD activities in plasma samples, but PIO treatment was observed to have an up-regulating effect on SOD activities in plasma of APP/PS1 mice (**Figure 15B**). On the other hand, no significant difference could be observed in catalase actitvities in cortex tissue of all three groups of mice (**Figure 15C**), while catalase activities were observed to have increased significantly in plasma of APP/PS1 mice, which was also completely rescued by PIO treatment in the transgenic mice (**Figure 15D**).
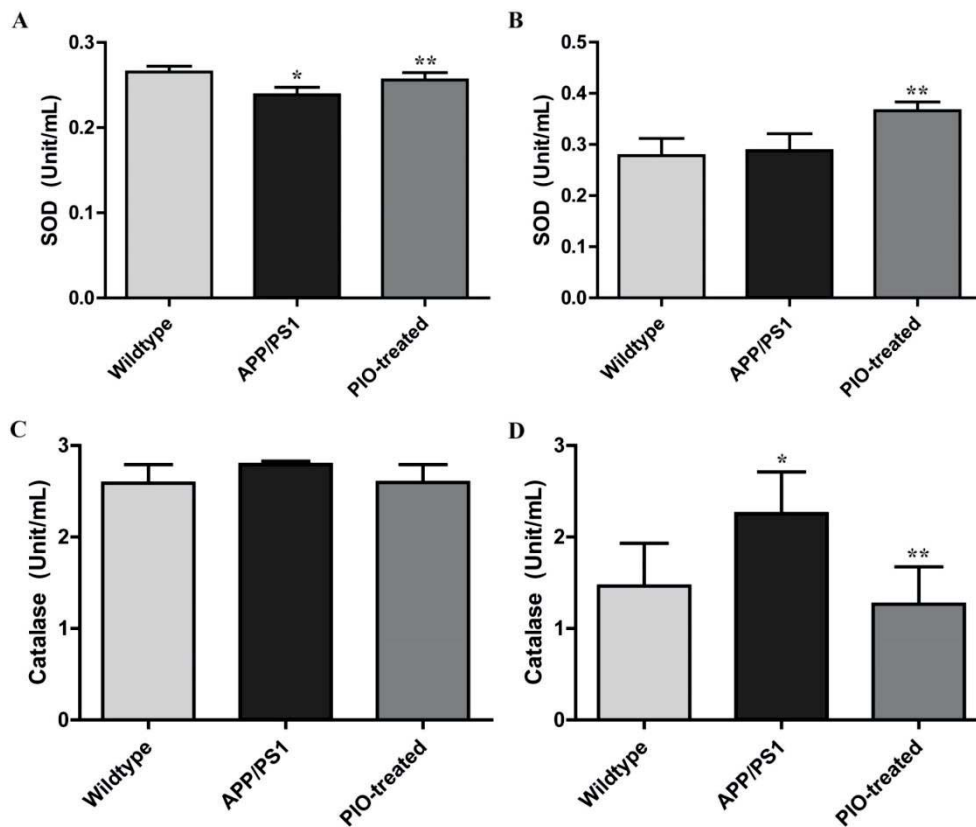
Figure 15. (A) SOD activities in cortex samples taken from all three groups of mice; **(B)** SOD activities in plasma samples; **(C)** Catalase activities in cortex samples; **(D)** Catalase activities in plasma samples; * $P < 0.05$ when compared against non-transgenic wildtype mice; ** $P < 0.05$ when compared against non-treated APP/PS1 mice; All error bars represent one SD.

3.5. Discussion

3.5.1. Metabolic profiling of plasma and brain tissue samples

In this study, I studied the metabolic profiles of plasma and four different brain parts (cortex, hippocampus, cerebellum and midbrain) of APP/PS1 mice and compare their metabolic profiles against non-transgenic wildtype mice. PCA of plasma metabolic profiles did not show any clear sign of separation between these two groups of mice, and the subsequent OPLS-DA did not produce any strong separation between them. This indicates that plasma in

APP/PS1 mice at 20 weeks of age is not a sample matrix that could yield a lot of useful information about the pathological processes occurring in this disease model. Nevertheless, I proceeded with mean comparison between the metabolites with VIP > 1.00, which surprisingly gave one discriminant metabolite that differentiates plasma profiles of APP/PS1 mice form wildtype mice significantly (Bonferroni-adjusted). L-threonine was observed to be significantly higher in plasma of APP/PS1 mice, which was inversely related to level of L-threonine in their brains where lower levels of L-threonine were seen in cortex tissues of APP/PS1 mice (discussed below). This indicates a clear compartmentalisation of metabolic activities between brain parts and plasma, although in this study plasma samples were found to be not so helpful in understanding the disease using metabolic profiling when sample at 20 weeks of age. Higher plasma level of L-threonine had also been reported in AD patients before [134], but no clear explanation was given to explain this observation.

When sampling and analysing brain tissues harvested from APP/PS1 mice in this chapter's experiment, I made the additional effort to look into metabolic profiles in different brain regions separately, as it had been reported that different brain regions exhibit distinct metabolic signals of their own when placed under stresses of APP-induced or age-induced toxicities [58, 127]. In this chapter's work, I investigated the metabolic alterations in four brain regions of APP/PS1 mice, namely cortex, hippocampus, cerebellum and midbrain. As expected, I observed different metabolic alterations in among these four brain parts, with cortex tissue being the most informational among

these four as judged by the highest number of discriminant metabolites observed in cortex tissue (citric acid, glycine, inosine, L-threonine, lactic acid, L-tyrosine, L-valine, glucose, L-aspartic acid and glucose-6-phosphate). Cerebellum and midbrain sample matrices also yielded considerable metabolic information, with cerebellum giving 5 discriminant metabolites (ribose-5-phosphate, glucose-6-phosphate, L-glutamic acid, N-acetyl-L-aspartic acid and L-aspartic acid) and midbrain giving three discriminant metabolites (urea, uracil and L-tyrosine). Another brain part that I had investigated is the hippocampus, but this particular sample matrix only produced one discriminant metabolite (lactic acid) in my analysis, indicating that the metabolic alterations in this particular brain region is not extensive in this mouse model at the sampling time point employed in this study (20 weeks of age). Another study that looked into metabolic changes in hippocampus tissue of APP/PS1 mice (16 weeks old) reported the P values for their top 30 discriminant metabolites they detected using univariate analysis [56]. However, none of them achieved significance if Bonferroni correction for multiple testing was applied on this set of 30 metabolites, suggesting that the metabolic changes were very limited in the hippocampus tissue of APP/PS1 mice, which is in agreement with my observations in this chapter. Although hippocampus was one of the main brain regions affected in AD, this was not reflected in APP/PS1 transgenic mice sampled at the time point used in this study. This highlights the caveats of employing a disease model to understand a disease, and caution should be exercised when interpreting the data generated based on this disease model.

3.5.2. <u>Impaired energy metabolism in cortex and cerebellum of APP/PS1 mice</u>

Analyses of metabolic data harvested from cortex, cerebellum and midbrain tissues generated some interesting findings. Among the discriminant metabolites that described cortex tissue of APP/PS1 mice, compounds that are closely linked in the energy metabolism and glycolysis pathway (KEGG, map00010), namely lactic acid, glucose and glucose-6-phosphate were observed to have increased considerably. In cerebellum of APP/PS1 mice, glucose-6-phosphate and ribose-5-phosphate also shot up significantly. The higher levels of monosaccharides observed in cortex and cerebellum of APP/PS1 mice were strikingly similar to my observations in chapter 2's *in vitro* experiments, where an excessively high level of extracellular glucose was detected for my AD cell model. On the other hand, citric acid, another component closely associated with energy metabolism, was found to have dropped by as much as 35 % in cortex tissue of APP/PS1 mice when compared against wildtype control. An opposite trend was observed for citric acid in chapter 2's *in vitro* experiments, but this could be due to the very dissimilar physiological conditions between interstitial fluid and culture medium. This illustrates clearly the differences between *in vitro* and *in vivo* experiments, highlighting the caveats when carrying out data interpretation for such experiments. Increased lactic acid in cortex of APP/PS1 mice could be explained by the reduction in their cortical LDH activities, which was measured in this study using LDH assay that assessed their rates of converting NAD+ to NADH. This observation was well corroborated by another study which reported increased lactic acid in cortex of APP/PS1 mice which were

harvested at 9 months of age [135], and by another study which reported high brain lactic acid as a biomarker for aging [136]. Taken altogether, there is a clear signal of impaired energy metabolism in cortex tissue of 20-week-old APP/PS1 mice, making them good model for therapeutic intervention which focuses on these particular brain region and disease mechanism.

3.5.3. Dysregulated amino acid metabolism in cortex and cerebellum of APP/PS1 mice

Looking at amino acids (glycine, L-threonine, L-tyrosine, L-valine and L-aspartic acid) that discriminated cortex tissue of APP/PS1 mice against wildtype control, I noticed that they were all lowered in APP/PS1 mice. This trend was similar to my observations in *in vitro* AD model employed in the previous chapter. Both could be similarly explained by the possibility of brain cells (or AD cell model) using up amino acids as compensatory fuel to sustain growth, since they all suffered from impaired energy metabolism. Among these amino acids, glycine and L-threonine are closely linked in the glycine, serine and threonine metabolism pathway (KEGG, map00260). Reduction in both glycine and L-threonine indicates that this pathway was severely affected by the APP and PS1 transgenes. It should be noted that L-serine was detected in this study, but their levels were not significantly different between cortex tissue of APP/PS1 and wildtype mice. More interestingly, I observed an inverse relation between L-aspartic acid and N-acetyl-L-aspartic acid, two discriminant metabolites detected in cerebellum tissue of APP/PS1 mice. L-aspartic acid was observed to have decreased in cerebellum of APP/PS1 mice, while the opposite is true for N-acetyl-L-aspartic acid. The relation between

these two discriminant metabolites suggests that the enzyme that link them both, aspartate N-acetyltransferase (KEGG, K18309), could have been affected by the APP or PS1 transgene insertion. In agreement with what I had observed, lower levels of N-acetyl-aspartic acid in cerebellum of APP transgenic mice had been reported before [59]. Similar trend was observed in cortex tissue of APP/PS1 mice in my study as well, although N-acetyl-L-aspartic acid did not achieve significance after Bonferroni's correction was applied. However, since N-acetyl-L-aspartic acid was frequently reported to be reduced in brains of AD patients [137, 138], the interpretability for my observations is limited. The differences between observations in disease models and clinical cases help to highlight the limitations of APP/PS1 mice as AD model, which should be employed with careful considerations for such differences.

3.5.4. PIO exerted treatment effects in cortex and cerebellum tissues

One interesting discovery in this study was the specificity of PIO's treatment effects to cortex and cerebellum of APP/PS1 mice. In the cortex tissue of APP/PS1 mice, PIO administration for 14 days completely rescued the metabolic alterations related to impaired energy metabolism, namely lactic acid, glucose, and glucose-6-phosphate. Similar effects were also observed in cerebellum of APP/PS1 mice, where pathological changes in ribose-5-phosphate and glucose-6-phosphate were completely reversed by treatment of APP/PS1 mice with PIO. Treatment effect of PIO on cortical lactic acid could be explained by PIO's therapeutic efficacy in rescuing LDH activities on cortex tissue of APP/PS1 mice. These findings were supported by previous

reports, where one reported normalisation of glucose metabolism with PIO treatment [85], and another study reported PIO's therapeutic benefits on glucose metabolism and LDH activities [120]. More importantly, this is the first study to demonstrate specificity of PIO's treatment effects on metabolic alterations in two particular brain regions, namely the cortex and cerebellum. PIO exerted no treatment effects in hippocampus and midbrain tissue of APP/PS1 mice used in this study, but this could be due to the occurrence of limited metabolic alterations in these two brain regions when mice were 20 weeks old. PIO's treatment effects on metabolic fluctuations in cortex and cerebellum of APP/PS1 mice shed light on therapeutic mechanisms of PIO, and one such example in this study was PIO's reversing effect on the impaired cortical LDH in APP/PS1 mice. These information could prove to be useful for interpretation of PIO's treatment effects observed in other studies, and contribute to the field of therapeutic research for PPARγ agonist in AD.

3.5.5. Measurements of Amyloid-β40, amyloid-β42, cortical APP and mitochondrial APP

At 20 weeks of age, amyloid-β40 and amyloid-β42 levels in plasma of APP/PS1 mice did not increase significantly as compared to their wildtype counterparts. On the other hand, both amyloid-β, in particular amyloid-β42, had increased considerably in their cortex tissue. This has an important implication as the soluble form of amyloid-β40 and amyloid-β42 had been discussed to better correlate with severity of cognitive symptoms in AD [139], making APP/PS1 transgenic mice a suitable model for researching on these soluble amyloid-β peptides. PIO administration was observed to have

successfully treated the pathological increase in amyloid-β40 and amyloid-β42 levels in the cortex of APP/PS1 mice. This amyloid-lowering effect of PIO had been reported before [124], which lends support to my findings in this study.

As one of the main findings based on my *in vitro* AD model in chapter 2 was the accumulation of APP in mitochondria, I measured the APP levels in cortex tissue and mitochondrial extracts from cortex tissues harvested from APP/PS1 mice and compared them against wildtype control. Cortical APP was observed to be higher in APP/PS1 transgenic mice, but this increase did not achieve significance. Interestingly, PIO administration appears to have suppressed APP expression in cortex tissue of APP/PS1 mice, an observation that had been reported in previous study [124]. Similar to what I had observed in chapter 2's *in vitro* experiments, a higher level of mitochondrial APP was detected in cortex tissue of APP/PS1 mice, although PIO treatment did not appear to have a significant treatment effect on this increase. A western blot analysis was carried out to confirm the purity of mitochondria in the isolated extracts, which gave satisfying results and showed that there is little possibility of contamination from plasma APP in mitochondrial APP readings. Therefore, findings for mitochondrial APP in this chapter validates my findings in chapter 2, suggesting that mitochondrial APP could potentially be a marker for assessing AD in its early disease stage.

3.5.6. Assessing the oxidation state in APP/PS1 mice

Neuroinflammation had been reported to be a common observation in several preclinical and clinical studies of AD [14, 68]. In this study, I assessed the oxidation state in cortex tissue of APP/PS1 mice, by measuring the activities of two major antioxidant enzymes in their cortical and plasma tissue samples, namely SOD and catalase. SOD activities were found to have decreased in cortex of APP/PS1 mice, though it remained unchanged in their plasma. PIO treatment enhanced the activities of SOD in both cortex and plasma of APP/PS1 mice, which could have given the APP/PS1 mice more anti-oxidative power in these two tissue compartments to resist the oxidative stress coming from all the destructive biochemical processes that occurred in this AD model. On the other hand, catalase activities increased in both cortex and plasma of APP/PS1 mice, although this increase did not achieve significance in their cortex tissue. Once again, PIO treatment normalised activities of catalase in plasma of APP/PS1 mice, bringing catalase activities to level similar to non-transgenic wildtype mice. Although the data in this study is insufficient to pin-point the actual cause for fluctuations in SOD and catalase activities, previous study had demonstrated the protective role of SOD and cytotoxic role of catalase in a cell model of Parkinson's disease [140]. All these observations indicate that oxidative stress had already been exhibited in APP/PS1 at 20 weeks of age, and PIO had effectively exerted its treatment effects by regulating the activities of these two major antioxidant enzymes.

3.6.   Conclusions

In this chapter, I employed GC-TOF-MS-based metabolic profiling in studying the metabolic alterations in plasma and brain part samples (cortex,

hippocampus, cerebellum and midbrain) of APP/PS1 mice and compared their metabolic profiles against wildtype control. At 20 weeks old, their plasma, hippocampus and midbrain tissue do not yield a lot of useful metabolic profiling data, indicating the limitation in using this model to study the metabolic alterations in these particular sample matrices and sampling time point. On the other hand, their cortex and cerebellum samples displayed extensive metabolic changes, which were all closely associated with impaired energy metabolism and a perturbed amino acid metabolism in both brain regions. PIO was observed to have exerted its treatment effects on metabolic alterations occurring in both cortex and cerebellum of APP/PS1 mice. PIO administration helped to normalise glucose metabolism, as well as their lactic acid levels by enhancing LDH activities in cortex of APP/PS1 mice. Selected biochemical assays were also conducted to assess other AD-related parameters in these mice. In brief, I observed that amyloid-β40 and amyloid-β42 levels were higher in cortex of APP/PS1 mice, which were both treated by PIO administration. APP was also observed to have accumulated in the cortical mitochondria of APP/PS1 mice, and PIO treatment did not have any effect on accumulation of mitochondrial APP. SOD activities were also observed to have been lowered in cortex of APP/PS1 mice, which were also normalised by PIO treatment.

Taken all together, APP/PS1 transgenic mice represents a suitable model to study AD pathophysiological processes, although some cautions have to be exercised during data interpretation as the model suffers from some limitations which were highlighted in this study. PIO administration was observed to have

exerted a range of therapeutic effects in this AD model, and present itself as a promising therapeutic compound to be developed further for treatment of AD. Next, I endeavoured to tackle a potential obstacle that could limit PIO's drug development process in AD research – its poor brain penetration, which was the Achilles' heel for rosiglitazone's development in AD therapeutic research. In the next chapter, I attempted to shed light on factor that could have contributed to PIO's poor brain penetration, and devise a strategy to overcome this limitation.

CHAPTER 4: Overcoming barriers to brain penetration of PIO

4.1.   Chapter summary

In the previous chapters, I have discussed at length about the therapeutic potential of PPARγ agonists in treating AD, and demonstrated both *in vitro* and *in vivo* data to support the therapeutic application of PPARγ agonists, namely ROSI and PIO, in the field of AD. My findings are in agreement with other preclinical findings in existing literatures, where a wealth of information demonstrates the wide-ranging therapeutic strength of PPARγ agonists against AD, from lowering Aβ plaque load to alleviating mitochondrial dysfunction associated with AD. Taken together, PPARγ agonists represent a promising class of drugs that could be developed into therapeutic molecules in the field of AD, where currently there exists no approved therapy that can effectively halt the disease progression in AD.

However, despite the well-established preclinical evidence of their therapeutic benefits in AD therapy, ROSI's and PIO's developments in clinical trials are less encouraging. In particular, ROSI's failure in its phase III AD clinical trial promptly ended its development in AD research, and one main reason cited for the failure was ROSI's poor brain penetration.

Given the similar preclinical establishment of PIO in AD therapy, there is a tremendous interest in pursuing this compound further as a therapeutic molecule for AD, which is evident in the ongoing phase III trial of PIO for AD, and an active pilot clinical trial of PIO in Parkinson's disease. However,

PIO is also haunted by the same brain penetrability problem which brought ROSI down in its phase III clinical trial. Therefore, poor brain penetrability of PIO becomes an important caveat in its drug development process in AD.

My research effort in this chapter revolved around investigating contributions of drug efflux transporters at the BBB in keeping PIO away from the brain. I noticed increased presence of PIO in the brain with P-gp inhibition, which was not observed with BCRP inhibition. Co-administration of P-gp regulator together with PIO could in theory be a viable dosing strategy to enhance presence of PIO in the brain for treatment of brain diseases. However, clinical utility of P-gp inhibitors is severely limited by its poor solubility and nonspecific toxicity of even the third generation P-gp inhibitors currently available in the market. This represents an even more pronounced problem for chronic disease like AD, since the patients may have to be put under the drug treatment regimen for the rest of their lives.

Therefore, I continued to explore alternative strategies for enhancing the PIO's brain penetration. Subsequently, I discovered stereoselectivity in brain penetration of PIO, and gathered evidence to show that (+)-PIO is a better brain penetrant than racemic PIO, thus making it an even more promising therapeutic compound for brain diseases such as AD. This chapter will discuss the significance of these findings, and the implication in the current context of drug development for PIO in AD.

4.2. Introduction

4.2.1. Therapeutic potential of ROSI and PIO against AD

In chapter 2 and chapter 3, I have discussed at length the therapeutic potential of PPARγ agonists for treatment of AD, and gathered both *in vitro* (chapter 2) and *in vivo* (chapter 3) data to support the therapeutic application of PPARγ agonists, in particular PIO, in AD therapy. These findings are in agreement with other preclinical findings in the existing literatures, where a wealth of information demonstrates the wide-ranging therapeutic strength of PPARγ agonists against AD, from lowering Aβ plaque load to alleviating mitochondrial dysfunction associated with AD [70, 79, 81]. Taken all together, PPARγ agonists represent a promising class of drugs that could be developed into therapeutics in the field of AD, where currently there is no approved drug that can effectively halt the disease progression.

4.2.2. Lost in translation: Failure of ROSI to achieve clinical trial success

Despite having their therapeutic benefits in AD well documented in preclinical studies, drug development for PPARγ agonists in the field of AD is still being hampered by their poor translation of preclinical successes into positive clinical outcomes, in particular by the failure of ROSI in a Phase III AD clinical trial.. Research interest on PPARγ agonist for AD was first heightened after ROSI demonstrated promising treatment effects in a preliminary clinical trial for AD patients in 2005 [74], which was quickly followed by another positive phase II clinical trial outcome [72]. However, a subsequent phase III clinical trial for ROSI ended in dismay after it failed to detect any evidence of

treatment efficacy for ROSI in the entire AD patient population recruited for the study [29]. To account for their failure to observe any treatment effect for ROSI, the authors suggested that the target tissues in patient's brain may not have sufficient ROSI to reach the therapeutic levels [29]. They reasoned that this could be due to the fact that ROSI is a substrate to P-gp, which is a major drug efflux transporter present on the BBB. On top of that, up-regulation of P-gp expression induced by neuroinflammation could severely limit brain exposure to ROSI and obviate its potential therapeutic benefits in AD [29]. Accordingly, the authors suggested that other PPARγ agonist with higher brain penetration should be investigated.

4.2.3. Could PIO be the success story for PPARγ agonists in AD therapy?

Unfortunately, PIO, the only alternative PPARγ agonist available in the market, also demonstrated low brain penetration [84]. In a case that is uncannily similar to ROSI, PIO had also gathered substantial preclinical evidence in support of its therapeutic potential for treatment of AD [78, 85, 86]. At the time of writing, two preliminary clinical trials for PIO in AD patients had been reported, but with contradictory outcomes. An 18-month pilot clinical trial originally designed to study PIO's long-term drug safety profile in AD patient population did not detect any treatment effect in its exploratory analysis of clinical efficacy [87]. On the other hand, another preliminary clinical trial conducted in Japan reported positive treatment outcome when AD patients with comorbid type II diabetes were given PIO [73]. These discrepancies between the PIO's performances in preclinical and clinical studies remain an obstacle to its drug development process, and much

work is needed to understand the factors behind the poor brain penetration of PIO, as well as to devise a strategy against this limitation. Such knowledge is especially important and relevant now, since Takeda had recently just started recruiting 5800 subjects for a 5-year phase III clinical trial to look at therapeutic potential of PIO in AD [88].

Given the structural resemblance between ROSI and PIO, I hypothesized that similar to ROSI, drug efflux transporters present at the BBB also play a significant role in limiting brain penetration of PIO. So far, however, there is no study that shed light on this factor. Therefore in this chapter, I proposed to investigate the influence of two major and most relevant drug efflux transporters, P-gp and breast cancer resistance protein (BCRP) [141], to PIO's brain penetration. Since these two efflux drug transporters are expressed on the membrane of brain capillary endothelial cell that is in direct contact with the peripheral circulatory system [142], they could exert a significant impact on limiting brain penetration of PIO. In a nutshell, my *in vivo* experiments demonstrated that inhibition of P-gp, but not BCRP, significantly increased the brain-to-plasma ratios of PIO in mice, which translates to higher brain penetration of PIO in these mice. Therefore, co-administration of P-gp regulator together with PIO could potentially be put forward as a dosing strategy to bring more PIO across the BBB into the brain to achieve therapeutic level in target brain tissue. However, such dosing strategy for a chronic disease like AD is severely limited by poor solubility and nonspecific toxicity of even the third generation P-gp inhibitors [143]. Therefore I started

to search for an alternative strategy to overcome the poor brain penetration of PIO.

4.2.4. Alternative strategies to Enhance Brain Penetration of PIO

Since MDR1 gene (the gene that encodes for P-gp) is polymorphic, I started to explore the idea of using single nucleotide polymorphism (SNP) as a predictor for different pharmacokinetics in each individual. The aim was to hunt for a SNP that could predict less pronounced P-gp drug efflux transport function in an individual, and determine if this SNP predictor will correlate with brain penetration of PIO, since PIO is a substrate of P-gp at the BBB. However, reports showed limited functional significance for MDR1 polymorphism [144], and the limited data in current literature make the evidence for SNP predictor inconclusive. Therefore, in its current state, SNP for P-gp is not a suitable predictor for an individual's pharmacokinetics profiles.

I then focused my effort on P-gp's stereoselectivity, since P-gp has demonstrated clinically relevant stereoselectivity in its activity [145]. As PIO exists in two stereoisomers, I proposed that one of the two stereoisomers could bind less preferentially to P-gp, and therefore penetrate the brain better. In a pilot trial conducted in this chapter, I observed higher presence of (+)-PIO in brain tissue when mice were given a single dose of racemic PIO (while opposite trend was observed in their plasma samples, i.e., (+)-PIO was lower in plasma levels). Encouraged by this finding, I followed up by purifying the (+)-PIO, and administer the purified (+)-PIO to mice and compared its brain penetration profile against mice fed with racemic PIO. Interestingly, I

discovered that administration of purified (+)-PIO resulted in a significantly higher brain tissue exposure to PIO in mice as compared to administration of racemic PIO. This represents a feasible strategy for enhancing brain exposure to PIO for treatment of AD. This finding serves as an important piece of information for the development of PIO as a therapeutic compound for AD, and could prove to be helpful for research scientists involved in the PIO's phase III AD clinical trial.

4.3. Materials and Methods

4.3.1. Chemicals and reagents used

Ko143, a potent selective inhibitor of BCRP was purchased from Enzo Life Sciences (Lausen, Switzerland). LY335979, a P-gp inhibitor was a generous gift from Eli Lilly and Company. PIO and ROSI (IS) were purchased from Cell Molecular Pharmaceutical R&D (Xi'an, China). All other reagents used were of analytical grades.

4.3.2. Animal husbandry

In total, sixty adult male C57BL/6 mice (10-12 weeks of age) with body weights ranging between 23 and 28g were obtained from NUS CARE (Singapore). The mice were housed in groups (maximum of 5 mice per cage) under standard conditions of humidity, temperature and 12-h light/dark cycle with ad libitum access to food and water. All mice were maintained under constant conditions for 4 days prior to experiments. All animal experiments

were conducted in accordance with NACLAR guidelines and approved by IACUC (Reference No. 074-11).

4.3.3. Animal experiment and sample collection

A total of twenty four mice were split into four treatment groups (n = 6), with three groups receiving efflux pump inhibitors pre-treatment (P-gp inhibitor LY335979, BCRP inhibitor Ko143, and a combination of LY335979 + Ko143) and one group receiving vehicle pre-treatment as control. All test compounds (PIO, LY335979, and Ko143) were dissolved in Milli-Q water using 1% DMSO as co-solvent. Pre-treatments of LY335979 (25 mg/kg), Ko143 (5 mg/kg) or combined LY335979 (25 mg/kg) + Ko143 (5 mg/kg) were given in a single intra-peritoneal (i.p.) injection 30 minutes before PIO administration (i.p. injection, 30 mg/kg). Following another 30 minutes after PIO administration, all mice were sacrificed by CO_2 euthanization and their blood samples were collected via cardiac puncture into eppendorf tubes supplemented with heparin. Transcardial perfusion with saline was then performed on the sacrificed mice to remove traces of blood from their organs before their whole brain tissues were harvested. All biological samples were kept on ice immediately after collection. Blood samples were centrifuged at 4,000 g for 10 minutes and plasma samples were then collected from supernatants in clean eppendorf tubes. Plasma and all tissue samples were stored at -80 °C until analysis.

4.3.4. Sample preparation for quantitative measurement of PIO in biological samples

All samples were thawed and kept on ice. Brain tissue samples were homogenized with Milli-Q water in ratio of 1 part of tissue mass to 1 part of water. Plasma and brain homogenate, were then diluted 10-fold and 3-fold with Milli-Q water, respectively. 95 µl of diluted samples were transferred into clean eppendorf tubes, and ROSI (2.5 ng in 5µl of DMSO) was added as IS to each sample. 300 uL of methanol was then added to each tube to initiate protein precipitation step for extraction of analytes. All mixtures were vortex-mixed at high speed for 5 minutes, and 14,000 g centrifugation (20 minutes at 4°C) was used to pellet the precipitated protein and sample debris. Supernatants were then transferred into injection vials for subsequent analysis using ultra performance liquid chromatographic system coupled with tandem mass spectrometer (UPLC-MS/MS). For calibration standards, blank plasma and tissue homogenates (spiked with 100, 500, 1000, 2500, 5000, and 10000 ng/mL PIO) were prepared in similar manners and used to build calibration curve for each sample type.

4.3.5. Instrumental operating conditions of UPLC-MS/MS and data processing

Liquid chromatographic separations were performed using the Waters Acquity UPLC system fitted with Acquity UPLC BEH C18 1.7 µm, 2.1 (i.d.) × 50 mm column (Waters Corp., MA, USA). Temperatures of column and autosampler were maintained at 45°C and 10°C, respectively. The mobile phases consisted of 1% (v/v) formic acid in Milli-Q water (solvent A) and 1% (v/v) formic acid in acetonitrile (solvent B) delivered at 0.6 ml/minute. The elution conditions used were as follows: isocratic at 20% solvent B (0–0.2 minute), gradient of

20% to 90% solvent B (0.2–1.5 minute), isocratic at 95% solvent B (1.5–1.8 minute), isocratic at 0.1% solvent B (1.8–2.2 minute) and isocratic at 20% solvent B (2.2–2.5 minute).

API 3200 triple quadrupole mass spectrometer (AB SCIEX, MA, USA), operating in positive electrospray ionization mode, was used for detection of PIO and ROSI (IS). Multiple-reaction-monitoring (MRM) method was used to measure both PIO (target compound) and ROSI (IS). The following MS operating conditions were optimized: curtain gas, turbo gas temperature, ionspray voltage, nebulizing gas, turbo gas, declustering potential, entrance potential, collision energy, and collision cell exit potential. Integration of peak areas and data processing were carried out using Analyst version 1.4.2 software (AB SCIEX). Analyte/IS peak area ratios were used to construct calibration plots for different tissue sample types, which was then used to determine concentrations of PIO in experimental samples.

4.3.6. Exploring stereoselectivity in PIO brain penetration using chiral HPLC-MS/MS

To explore whether stereoselectivity is exerted in brain penetration of PIO, I investigated the differential distributions of (+)-PIO and (-)-PIO in both brain and plasma tissue compartments. Levels of (+)-PIO and (-)-PIO in brain and plasma samples taken from mice used in experiment above (no pre-treatment group, n = 3) were analysed. Stereoisomers of PIO were separated by reversed phase chiral high performance liquid chromatographic (HPLC) column. Brain and plasma samples from mice, as well as blank brain and plasma samples spiked with racemic PIO, were subjected to chiral HPLC separation and

quantified using tandem MS. Chiral liquid chromatographic separations were performed using Agilent 1200 HPLC system (Agilent Technologies, CA, USA) fitted with Chiralcel OD-R 10 μm particle size, 4.6 mm (i.d.) × 250 mm analytical column (Chiral Technologies Europe, Illkirch-Graffenstaden, France). Temperatures of column and autosampler were maintained at 25 °C. Mobile phase consisted of 60% (v/v) methanol in milliQ water was delivered at 1.0 ml/minute under isocratic elution mode. Detection and quantitation of PIO was carried out using API 3200 MS (AB SCIEX) according to tandem MS operating conditions described above. Ratios of both stereoisomers in relative of each other were used to determine which is higher in each sample matrix.

4.3.7. Purification and identification of (+)-PIO

Purification of (+)-PIO was carried out using HPLC system coupled with UV detector and automated fraction collector. The system used consisted of Shimadzu LC-10AT pump, SCL-10A system controller and FRC-10A fraction collector (Shimadzu Corporation, Kyoto, Japan). Chiral column used was a Chiralpak IA 5 μm particle size, 10 mm (i.d.) × 250 mm semi-preparative column (Chiral Technologies Europe, Illkirch-Graffenstaden, France). For every round of collection, 250 μL of PIO solution (5 mg/mL) was injected and separated using isocratic mobile phase elution (90 % acetonitrile and 10 % isopropanol, supplemented with 0.1 % acetic acid), and detection wavelength was set at 266 nm. HPLC elution flow rate was set to 2 mL/minute, and temperature was maintained at 40 °C. Racemic PIO was dissolved in solvent with similar composition to mobile phase to prepare the solution for injections.

The RT for (+)-PIO was around 15.00 minute, with peak width of 2 minutes for fraction collection. Purified fraction was then dried using a rotary evaporator to obtain purified powder of (+)-PIO. Purity of (+)-PIO was then examined by re-constituting them in mobile phase solvent and analysing the re-constituted solution using previously established chiral HPLC separation coupled with MS detection (API 3200 MS, AB SCIEX) using MRM method (m/z transitions of 357 to for PIO detection). The identity of purified (+)-PIO was confirmed by measuring its optical activity using DIP-1000 Spectropolarimeter (Jasco Inc., MD, USA). Optical rotation measurements were performed on PIO solution (1.11 mg/mL) in a 10 mm cell, measured at a wavelength of 589 nm and temperature of 26 °C. Specific rotation (cm2/g) was calculated using the equation of $[\alpha]\lambda T = \alpha\ /\ L\ *\ c$ (where $[\alpha]\lambda T$ is the specific rotation, α is the observed rotations in degrees, L is the cell path in dm, and c is the sample concentration in g/100mL).

4.3.8. <u>In vivo experiment to investigate brain distribution of racemic PIO and (+)-PIO</u>

A total of forty mice were split into two treatment groups (n = 20), with one group receiving single dose of racemic PIO (30 mg/kg, p.o) and another group receiving purified (+)-PIO (30 mg/kg, p.o.). Both compounds were dissolved in Milli-Q water using 1% DMSO as co-solvent. Following oral administration of the test compounds, mice from both treatment groups were split again into five subgroups (n = 4), and mice belonging to different subgroups were sacrificed at different post-dosing time points (1 hour, 2 hours, 4 hours, 6 hours, and 8 hours). All mice were sacrificed by CO_2 euthanization and their

blood samples were taken via cardiac puncture, which were then centrifuged at 4,000 g (10 minutes) to collect the plasma. Whole brains were collected following exsanguination by transcardial perfusion with saline. Sample treatment for measurement of PIO in plasma and brain samples using UPLC-MS/MS is similar to procedure described above. PIO concentrations *versus* time graphs were constructed for both brain and plasma sample, and area under curve (AUC) for both (+)-PIO and racemic PIO were then used to assess each tissue exposure to PIO. AUC was calculated from time 0 hour to infinity ($AUC_{0-\infty}$) for both types of samples using trapezoidal rule.

4.4.   Results

4.4.1. Quantitative measurement of PIO in biological samples using UPLC-MS/MS

A UPLC-MS/MS method for quantitation of PIO in both sample matrices (plasma and brain tissue) was successfully developed. MRM analyses were carried out using optimized m/z transitions for both PIO (357 to 134) and ROSI (358 to 135). The optimized operating conditions for mass spectrometer were: curtain gas, 15 psi (nitrogen); turbo gas temperature, 550 °C; ionspray voltage, 5,500 V; nebulizing gas, 40 psi; turbo gas, 40 psi; declustering potential, 54 V; entrance potential, 9 V; collision energy, 40 eV; collision cell exit potential, 4 V. The optimized RT for PIO and ROSI were determined to be 0.72 minute and 0.61 minute, respectively. Five calibration samples were used to build calibration curves for both plasma and brain tissue samples. Calibration curves were constructed from analyte/IS peak area ratios, and

weighted 1/x quadratic regression produced linear plots for plasma and brain samples over concentration ranges of 500 – 4000 ng/mL (r2 = 0.9995) and 50 – 3000 ng/mL (r2 = 0.9998), respectively. PIO concentrations for different sample matrices were then determined based on their respective calibration curves.

4.4.2. Investigating contributions of P-gp and BCRP to limiting brain penetration of PIO

No significant difference could be seen among PIO concentrations in plasma samples harvested from all four treatment groups (**Figure 16A**). However, I observed almost four times higher standard deviation in plasma concentrations in the respective groups that received LY335979 (40.34 ± 17.02 µg/mL) and combined LY335979 + Ko143 pre-treatment (37.68 ± 17.43 µg/mL), as compared to the groups that received vehicle (41.30 ± 5.17 µg/mL) and Ko143 pre-treatment (38.77 ± 4.38 µg/mL). The ratios of PIO concentrations in brain-to-plasma tissue were used to assess the extent of PIO penetration into the brain tissue. Mice that did not receive P-gp or BCRP inhibitor (pre-treated with vehicle) had a brain-to-plasma ratio of 10.65 ± 1.25 %, which did not increase significantly when mice were given pre-treatment of Ko143. Pre-treatment with LY335979 significantly increased the brain-to-plasma ratio by 16.92 % to 12.45 ± 1.15 %; whereas pre-treatment with combined LY335979 + Ko143 also significantly increased this ratio by 20.82 % to 12.87 ± 1.56 %. No significant difference could be observed between brain-to-plasma ratios of the latter two treatment groups. Data on brain-to-plasma ratios were summarized in **Figure 16B**.
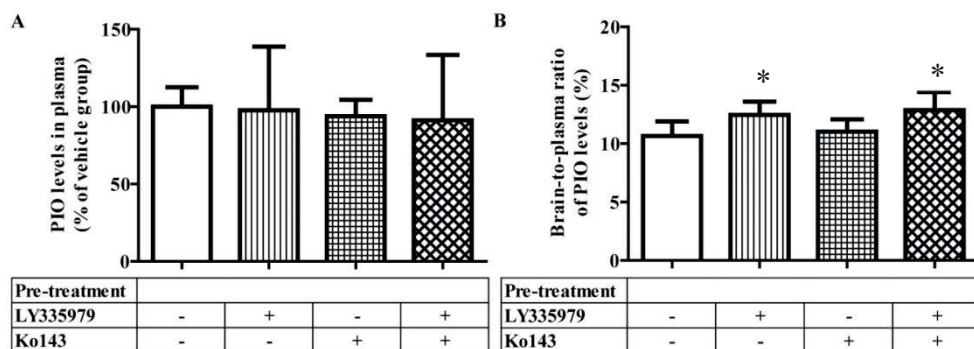
Figure 16. (A) PIO levels in plasma samples harvested from mice given intra-peritoneal PIO with or without pre-treatment of P-gp and/or BCRP blocker; **(B)** Ratios of PIO levels in brain-to-plasma in mice with or without pre-treatment of P-gp and/or BCRP blocker; * $P < 0.05$ when compared mice pre-treated with vehicle; Error bars represent one SD.

4.4.3. Investigating stereoselectivity in PIO brain penetration using chiral HPLC-MS/MS

Both (+)-PIO and (-)-PIO were successfully separated using reversed phase chiral HPLC column, with RT of approximately 28.00 minutes and 31.50 minutes, respectively. Chromatograms for both brain tissue and plasma samples that were analysed for all three mice are shown in **Figure 17**. I consistently observed a higher level of (+)-PIO in brain tissue samples (+ 46.6 %) as compared to (-)-PIO. By contrast, the opposite trend was observed for plasma samples, where (+)-PIO was always lower (- 67.7 %) as compared to (-)-PIO. No difference could be seen between amount of (+)-PIO and (-)-PIO in blank brain and plasma samples spiked with racemic PIO.
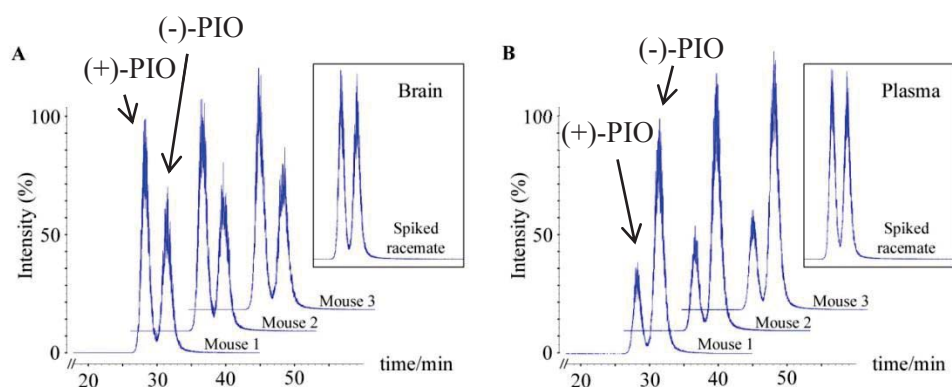
Figure 17. (A) Chiral separation of (+)-PIO and (-)-PIO in brain samples of mice administered with racemic PIO; chromatogram in box shows (+)-PIO and (-)-PIO in blank brain samples spiked with racemic PIO; **(B)** Chiral separation of (+)-PIO and (-)-PIO in plasma samples of mice administered with racemic PIO; chromatogram in box shows (+)-PIO and (-)-PIO in blank plasma samples spiked with racemic PIO.

4.4.4. Purification and identification of (+)-PIO

Purification of (+)-PIO was successfully carried out to obtain purified (+)-PIO powder. Purity was established by analysing three separate samples taken from the purified (+)-PIO powder, which was observed to have > 98.0 % purity (n = 3, 98.08 %, 98.12 %, and 98.94 %). Identity of (+)-PIO was confirmed by measuring the optical activity of purified powder dissolved in 90 % acetonitrile and 10 % isopropanol, supplemented with 0.1 % acetic acid. Solvent blank was used as a zero reference before optical activity measurements were taken from ten separately prepared (+)-PIO solutions. Specific rotation in degrees ($[\alpha]\lambda T$) for 1.11 mg/mL (+)-PIO solution was calculated to be +0.8198 cm2/g, therefore confirming the identity of purified powder to be (+)-PIO stereoisomer.

4.4.5. <u>In vivo experiment to investigate brain distribution of racemic PIO and</u> <u>(+)-PIO</u>

Our previously established UPLC-MS/MS method was used to quantify PIO concentrations in plasma and brain samples harvested at different time points (1 hour, 2 hours, 4 hours, 6 hours, and 8 hours) from mice given either racemic PIO or (+)-PIO. 8-hour plots of the mean plasma concentrations and mean brain concentrations versus time profile of PIO for both treatment groups are shown in **Figure 18A** and **Figure 18B**, respectively. Plasma PIO profile in mice that received racemic PIO showed a significantly higher C_{max} (53.53 ± 8.07 µg/mL) than mice that received (+)-PIO (C_{max} = 39.92 ± 6.20 µg/mL). Tmax of plasma PIO for mice from both treatment groups were at 1 hour after drug administration. $AUC_{0-\infty}$ of plasma PIO were determined to be 2.62×10^5 µg.hour/L and 2.74×10^5 µg.hour/L for mice that received racemic PIO and (+)-PIO, respectively. On the other hand, C_{max} for brain PIO profile were not significantly different between mice that received racemic PIO (4.88 ± 0.34 µg/mL) and mice that were given (+)-PIO (5.07 ± 0.38 µg/mL). However, brain PIO concentration was significantly higher in mice that received (+)-PIO at 4, 6 and 8 hours after drug administration. $AUC_{0-\infty}$ of brain PIO for mice that received (+)-PIO was also considerably higher (4.00×10^4 µg.hour/L), and represents a 76% increase as compared to mice that received racemic PIO (2.27×10^4 µg,hour/L).
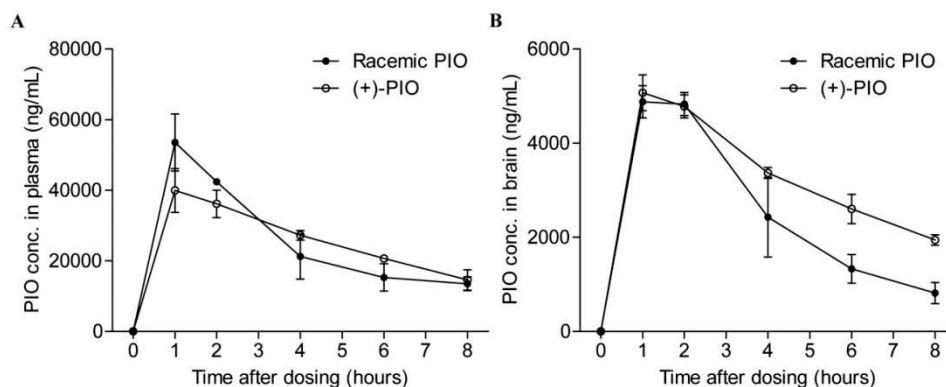
Figure 18. **(A)** PIO concentration *versus* time (hours) profile for plasma samples harvested from mice fed with either racemic PIO or purified (+)-PIO; **(B)** PIO concentration *versus* time (hours) profile for brain samples harvested from mice fed with either racemic PIO or purified (+)-PIO; Error bars represent one SD.

4.5.   Discussion

4.5.1. P-gp drug efflux transport at the BBB limits presence of PIO in brain

In this study, I investigated the effects of pre-treatment with P-gp inhibitor (LY335979), BCRP inhibitor (Ko143) or combination of both on the brain penetration of PIO. I observed significant increases in brain penetration of PIO (as demonstrated by higher brain-to-plasma ratio of PIO) when mice were given pre-treatment of P-gp inhibitor or a combination of P-gp and BCRP inhibitors. Pre-treatment with BCRP inhibitor alone did not improve the brain penetration of PIO, and pre-treatment with BCRP inhibitor did not show any synergistic effect with P-gp inhibitor in enhancing the brain penetration of PIO.

Mice that did not received any drug transporter inhibitor pre-treatment showed a brain-to-plasma PIO ratio of 10.65 %. To the best of my knowledge, this is

the first study to investigate brain penetration of PIO using C57BL/6 mice. Extent of PIO brain penetration observed in this study is in agreement with previous studies using other animals, which reported low PIO brain penetration in general. One study observed that CSF concentration for PIO in monkeys was less than 3 % of their plasma PIO [146], and another study reported about 18 % of serum PIO could be found in the CSF of rats, dogs, and monkeys [84].

I also observed that brain penetration of PIO was increased by pre-treatment with P-gp inhibitor, but not with BCRP inhibitor in this study. This is the first study to investigate contribution of P-gp and BCRP drug efflux transporters in limiting brain penetration of PIO. My findings are supported by another study which looked at ROSI, a close structural analogue of PIO. Looking at three drug efflux transporters (P-gp, BCRP and Multidrug Resistance Protein, MRP1) at human placental apical membrane, Weiss et al. found that ROSI was transporter predominantly by P-gp [141]. It should be noted that P-gp and BCRP inhibitor pre-treatments were given in a single-dose manner, and effects of chronic or sub-chronic inhibition of these drug transporters on the brain penetrability of PIO were not investigated in this study.

Our findings imply that PIO is a substrate of P-gp, and this could substantially limit the brain penetration of PIO which was observed in this study, and reported in previous studies as well [84, 146]. This limitation could be a significant barrier to drug development of PIO, since being a substrate of P-gp was cited as a reason for ROSI's failure to reach therapeutic level in the brain

tissue and thus resulting in its phase III AD trial flop [29]. Co-administration of PIO with P-gp regulators could potentially be a dosing strategy to enhance brain penetration and therapeutic effects of PIO in treating AD. However, such dosing strategy for a chronic disease like AD is severely limited by poor solubility and nonspecific toxicity of even the third generation P-gp inhibitors [143].

4.5.2. <u>Stereoselectivity in PIO brain penetration</u>

In an attempt to devise a more superior strategy for enhancing PIO's brain penetration, I next focused my effort on finding out if there is any stereoselectivity in brain penetration of PIO. Since P-gp had been reported to be stereoselective in its drug efflux transport activity, and PIO exists in two stereoisomers, (+)-PIO and (-)-PIO, these form the basis for an exploration into stereoselectivity in PIO brain penetration. First, I developed a chiral HPLC method that successfully resolves the two stereoisomers when a sample containing racemic mixture of PIO was injected. I then applied this chiral HPLC method on brain and plasma samples taken from mice that were given intra-peritoneal injection of racemic PIO. Remarkably, I observed that (+)-PIO is clearly higher than (-)-PIO in brain, and the trend is consistent in brain samples harvested from 3 individual mice that were given racemic PIO. On the other hand, (+)-PIO is evidently lower than (-)-PIO in their plasma. This represents an interesting case for (+)-PIO, since its higher presence in the brain suggests that (+)-PIO is targeted more at brain tissue, and its lower presence in plasma could potentially translate to lower drug induced toxicities in other peripheral tissue organs. Since no difference was reported between therapeutic

activities of both (+)-PIO and (-)-PIO [147], these combinations make a very promising case for (+)-PIO from a pharmacokinetics point of view, especially when it is developed for treatment of brain diseases such as AD. This encouraging piece of information is especially important now since PIO is being investigated in clinical trials for several neurodegenerative disorders, namely a phase III clinical trial for AD [88] and a pilot clinical trial for Parkinson's disease [91].

4.5.3. (+)-PIO afforded a brain exposure to PIO than racemic PIO

Naturally, the next course of action would be to determine whether administration of purified (+)-PIO could increase presence of PIO compound in the brain as compared to racemic PIO, which is the form of PIO available in the market currently. Since (+)-PIO is not commercially available, I had to purify it from racemic PIO to obtain sufficient mass for *in vivo* brain penetration experiments. Methods for purification of (+)-PIO using chiral semi-preparative column was successfully set up, which afforded me > 98 % pure (+)-PIO powder. Upon administration of both (+)-PIO and racemic PIO to groups of mice and harvesting their biological samples over five different time points (1 hour, 2 hours, 4 hours, 6 hours, and 8 hours), I observed that total PIO exposure ($AUC_{0-\infty}$) in brain of mice administered with (+)-PIO is 76 % higher than mice given racemic PIO. On the other hand, total presence of PIO in plasma of mice given (+)-PIO was just 4 % higher than mice fed with racemic PIO. This clearly demonstrates the brain targeting property of (+)-PIO, which offers two advantages to therapeutic application of (+)-PIO in treating AD or other brain diseases. Firstly, increasing brain penetration of

PIO could bring more drug compound across the BBB into brain tissue at the same dose given to patient, thus allowing higher concentration of PIO to be achieved in the brain to hit therapeutic level required for PIO to exert its treatment effects in brain tissue. Secondly, a more brain-targeting (+)-PIO allows a lower dose of PIO to be given to AD patients to achieve the same therapeutic level of PIO in their brains, giving the compound an advantage of lower drug induced toxicities in other peripheral organs. This finding represents an important piece of information for therapeutic research of PIO in AD, and opens up new and exciting possibilities to look into (+)-PIO and its applications in AD therapy.

4.6.   Conclusions

In this chapter, I looked into factors that could have contributed to limiting brain penetration of PIO. P-gp was found to be a significant contributor in keeping PIO away from brain tissue in my *in vivo* experiment, and I discovered stereoselectivity in brain penetration profile of PIO in mouse brains. Subsequently, (+)-PIO was shown to give higher brain exposure to PIO than racemic PIO, thus represents a potentially more superior drug for the treatment of AD. However, more work needs to be done if (+)-PIO is to be pursued as a therapeutic compound for AD, especially to better characterise its drug efficacy and safety profiles. Nevertheless, enhanced brain penetration of (+)-PIO makes this a promising drug compound for treating brain diseases, and future work that shed light on its safety and affinity to nuclear receptors will serve to advance this compound further in the pipeline for AD.

CHAPTER 5: GC-TOF-MS-based metabolic profiling of caffeinated and decaffeinated coffee and its implications for AD

5.1. <u>Chapter summary</u>

In this chapter, I ventured into a research topic that differs slightly from those discussed in previous chapters. It is a project that I initiated out of personal interest, after reading reports of neuroprotection offered by coffee consumption against AD. After reviewing the literature, I came across numerous findings from preclinical, epidemiology and clinical studies which indicate coffee consumption could have beneficial effects against dementia and AD. More interestingly, these benefits were observed to come from caffeinated coffee, but not from decaffeinated coffee nor pure caffeine itself. A report also suggested that caffeine could act synergistically with another unknown compound in coffee, to produce its therapeutic benefits against AD. Based on all these findings, I postulated that this unknown synergistic compound(s) could have been stripped away from the coffee beans during the decaffeination process, hence rendered the decaffeinated coffee ineffective against AD. In this case, metabolic profiling technique represents an appropriate study tool which can help to elucidate the differences between metabolites present in caffeinated and decaffeinated coffee. Therefore, the research objective of this chapter was to use metabolic profiling approach to delineate the discriminant metabolites between caffeinated and decaffeinated coffee, which could have contributed to the therapeutic differences between the two types of coffee. GC-TOF-MS was employed as the analytical instrument in this metabolic profiling study. OPLS-DA displayed clear

separation between the two types of coffee (cumulative Q^2 = 0.998), with the first predictive component modelling 84.4 % of variations in the dataset. A total of 69 discriminant metabolites were identified based on the OPLS-DA model, with 37 of them present at higher levels in caffeinated coffee, and 32 of them higher in decaffeinated coffee. Among this list of 69 metabolites, some notable ones include benzoate and cinnamate-derived phenolic compounds, organic acids, sugar, fatty acids, and amino acids. The work in this chapter successfully established GC-TOF-MS-based metabolic profiling approach as a highly robust tool suitable for analysis of coffee samples, which was exemplified by the discriminant analysis between caffeinated and decaffeinated coffee in this study. Majority of the discriminant metabolites identified in this discriminant analysis are biologically relevant and provide valuable insights into therapeutic research of coffee against AD. These findings could serve as an informative guide for future therapeutic research of coffee in AD. More importantly, my findings clearly showed that the difference between caffeinated and decaffeinated coffee is not merely caffeine, an assumption commonly made in many studies involving decaffeinated coffee. In addition, my data also hint at possible involvement of gut microbial metabolism to enhance therapeutic potential of coffee components when coffee is consumed, and this represents an interesting area for future research.

5.2. Introduction

In this chapter, I explored a research field that is slightly different from those discussed in previous chapters. I will venture into dietary research, more specifically research on coffee, and its pros to AD. Research interest in this chapter is piqued by reports of neuroprotection offered by coffee consumption against development of AD. Upon reviewing the current literature, I learnt from several studies that this neuroprotection is associated more with consumption of caffeinated coffee, and not the decaffeinated ones. Interestingly, these therapeutic benefits observed are not due to mere presence of caffeine in caffeinated coffee, which I will discuss in more details below. However, there is a lack of study that systematically profile the components present in both types of coffee, and compare their profiles to elucidate the chemical differences between caffeinated and decaffeinated coffee, which I strongly believe is not caffeine alone. Therefore in this chapter, I proposed that metabolic profiling approach is a suitable tool to study the chemical differences between these two types of coffee, and the findings will be useful to the field of coffee research, especially in research focused on AD therapy.

The benefit of coffee consumption for AD prevention or treatment is not new in AD research. There is already a growing body of epidemiological evidence that supports the therapeutic roles of coffee consumption against AD development. In one study with a follow-up of 21 years, it was observed that people who drank 3-5 cups of coffee a day during midlife had 65 % reduction in risk of developing AD later in life, when compared against those who drank little or no coffee at all [148]. Shortly after that study, a meta-analysis of

pooled epidemiological studies was carried out, and the report also supported the protective effects of coffee consumption against AD, but cautioned on the methodological heterogeneity that could limit the interpretation of their findings [149].

Recognizing that epidemiologic studies are not the most direct evidence, Cao et al. obtained the first direct clinical evidence to support the therapeutic benefits of coffee consumption in prevention of AD [150]. They observed that patients with MCI had delayed onset of dementia if they had higher plasma caffeine levels, and most of the caffeine present in the study subjects could be traced back to coffee consumption [150]. This study provided the evidence to support the therapeutic roles of coffee consumption in preventing AD, and the authors proposed coffee consumption as a prophylactic intervention early in life, far before AD symptoms surface.

Remarkably, more recent studies revealed that the therapeutic benefits of coffee consumption were not due to caffeine alone. One study showed that improvements of cognition and psychomotor behaviours in aged rats were due to coffee, and not caffeine itself [151]. In line with these observations, crude caffeine – a by-product of coffee decaffeination process – was observed to exert a greater therapeutic effect on memory impairment in AD mouse model than pure caffeine [152]. More specifically, the study reported that administration of crude caffeine reduced amyloid burden, improved antioxidant activity and enhanced glucose uptake in AD mouse model, which

were not observed with administration of pure caffeine in the mouse model [152].

Decaffeinated coffee, on the other hand, has had mixed results when it was investigated for its therapeutic potential in AD. Although it improved brain energy metabolism in mice [153], it was observed to have very limited beneficiary effect on glucose homeostasis, a metabolic process closely implicated in both type 2 diabetes and AD [154]. More recently, researchers started to systematically compare the therapeutic potential of caffeinated and decaffeinated coffee for treatment of AD. One study reported the synergistic interaction between an unknown coffee component and caffeine for stronger therapeutic potential in AD, therefore making caffeinated coffee the therapeutically superior [94]. In another study, consumption of caffeinated coffee, but not decaffeinated coffee or pure caffeine itself, was observed to be therapeutic against oxidative stress, a pathological marker commonly associated with AD development [155].

In order to delineate the component differences between caffeinated and decaffeinated coffee, one must first understand the decaffeination processes used to remove caffeine from coffee beans. Several different decaffeination processes are available to strip caffeine away from the coffee beans, namely solvent-based, water-based, and supercritical carbon dioxide-based decaffeination methods [156]. All these processes mainly differ in costs and types of solvents used to extract caffeine, although one thing in common for all three methods is that the decaffeination process removes more than just

caffeine. One example is the water-based decaffeination process, which is known to result in loss of water-soluble components that are in excess of 20 % by weight. As a result, the extraction water is supplemented with non-caffeine soluble solids to minimize loss of these water-soluble components through extraction [156]. Supercritical carbon dioxide-based decaffeination method, a process that is often touted for its high extraction selectivity for caffeine, also removes more than just caffeine, thus leaving behind a brown colour extraction residue in the crude caffeine [157]. Not surprisingly, it has been shown that the crude caffeine contains a variety of non-caffeine bioactive phytochemicals [157], which could account for its therapeutic effects in the AD mouse model [152]. Perhaps the strongest observation in support of this argument would be the drastically different aromas and flavours of decaffeinated coffee as compared to the original coffee, clearly suggesting that significant portions of non-caffeine phytochemicals have been stripped away from the coffee beans by the decaffeination process.

Despite being in the market for a long time, there are limited data on characterization of the chemical composition profiles that differentiate caffeinated and decaffeinated coffee. One study investigated alterations in chlorogenate levels in coffee following water-based decaffeination process, since chlorogenate was perceived to be one major bioactive phytochemicals present in coffee [158]. However the evidence for chlorogenate's beneficial effects was inconclusive, with one study reported no beneficial effect on glucose metabolism after chlorogenate was given to human patients at risk for type 2 diabetes [154]. Some studies set out to investigate alterations in

phenolic contents of coffee following decaffeination process, but contradictory data had been reported [159, 160]. Therefore, there exist significant research gaps in the current literatures between the compositions of the coffee's bioactive chemical components and evidence of their therapeutic benefits in AD. Bridging this gap is especially important with the emergence of aforementioned reports on therapeutic differences between caffeinated and decaffeinated coffee, which could be useful for research on prevention or even treatment of AD.

One suitable tool that could be employed for characterization of the chemical composition in coffee samples would be the metabolic profiling approach. This approach systematically profiles all small molecules present in samples and utilizes data mining tool to sieve out meaningful data by comparing metabolic profiles of caffeinated and decaffeinated coffee. Two recent studies applied this technique on coffee samples to determine the coffee beans' origins [161, 162], while another study uses this approach to authenticate the prized coffee product [163]. However, none of them used metabolic profiling approach to investigate the chemical differences between caffeinated and decaffeinated coffee, and applied it with an objective to discern its beneficial/therapeutic origins. Therefore, this study endeavoured to employ metabolic profiling tool to discern the chemical differences in coffee rendered by decaffeination process. The discriminant chemical compounds identified could have contributed to the beneficial effects of caffeinated over decaffeinated coffee for AD.

With the availability of a variety of high-throughput analytical instruments, metabolic profiling approach has to be appropriately matched with the right choice of analytical platform to achieve study's aims more efficiently. As I had discussed in previous chapters, GC-MS represents an excellent tool of choice for its high sensitivity and the availability of large commercial electron ionization (EI) spectral libraries, which was made possible by highly robust and reproducible EI mass spectra. As a result, highly efficient and straightforward identification of metabolic peaks is a strong advantage for GC-MS-based metabolic profiling approach, especially for a non-targeted approach. Therefore, this study proposed to employ GC-TOF-MS as the platform for metabolic profiling of both caffeinated and decaffeinated coffee. A recent report by Jumhawan et al. used GC-quadrupole-MS for metabolic profiling of coffee samples [163]. However, a quadrupole MS loses its sensitivity when operated in scanning mode due to compromised duty cycle, and TOF-MS could be a better alternative when employed in a non-targeted metabolic profiling setting.

In this chapter, my work successfully demonstrated the suitability of GC-TOF-MS as an analytical platform for metabolic profiling analysis of coffee samples. On top of that, metabolic profiling approach was found to be an effective method in elucidating the chemical differences between caffeinated and decaffeinated coffee. My findings in this chapter could be useful for research on optimization of decaffeination processes, as well as for therapeutic research on coffee consumption for prevention or even treatment of AD. More importantly, this study raises the awareness that caffeine is not the only

difference between the two types of coffee, an assumption commonly made in research involving decaffeinated coffee.

5.3. Materials and methods

5.3.1. Chemicals and reagents used

MOX reagent and MSTFA with 1 % TCMS used for GC-TOF-MS sample derivatisation were purchased from Thermo Fisher Scientific (Waltham, MA). All other reagents used were of analytical grades.

5.3.2. Caffeinated and decaffeinated coffee samples

In this study, I used NESCAFÉ GOLD caffeinated and decaffeinated coffees (Nestlé, Singapore) as my coffee samples. Both types of coffee were available commercially as freeze-dried granules, and the decaffeinated option utilised water-based decaffeination method to remove caffeine as claimed by the manufacturer. 400 mg of freeze-dried granules for both caffeinated and decaffeinated coffee were transferred into a clean 50-mL falcon tube, and 40 mL of warm Milli-Q water (80°C) was added to the tube to make a coffee solution. The solution was vortex-mixed to ensure complete dissolution of the freeze-dried granules. This process was repeated five times to prepare five replicates for both caffeinated and decaffeinated coffee. Coffee solutions were then allowed to cool to room temperature over 30 minutes, after which they were immediately subjected to sample preparation and derivatisation step for subsequent GC-TOF-MS-based metabolic profiling analysis.

5.3.3. Coffee sample preparation for metabolic profiling analysis

200 μL of caffeinated and decaffeinated coffee sample (n = 5) was transferred into clean 2-mL centrifuge tube and 1.0 mL of chilled methanol was added to each tube for protein precipitation. All mixtures were vortex-mixed at high speed for 5 minutes, followed by centrifugation (14,000 g) for 20 minutes at 4°C to pellet any precipitated protein. 950 μL of supernatant from each sample was then carefully transferred into a clean, pre-silanised glass tube for drying. Subsequent sample derivatisation procedures were similar to those described under section 2.3.5.

5.3.4. GC-TOF-MS data acquisition and preprocessing

Data acquisition and preprocessing for GC-TOF-MS analyses in this chapter were similar to procedure detailed under section 2.3.6, with some slight variations. Caffeinated and decaffeinated coffee samples were used as their own QC samples, and both caffeinated and decaffeinated coffee samples were injected in an interspersed manner to minimize introduction of procedural artefacts and ensure good data reliability in QC and subsequent analyses. Resulting metabolic data were processed using total area normalization, where area of each peak in one sample was divided by the sum of all peaks in the same sample.

5.3.5. Multivariate data analysis

Multivariate data analysis used to build a discriminant model between caffeinated and decaffeinated coffee was similar to procedure described under section 2.3.7. Biologically relevant information regarding the identified

discriminant metabolites were then sought from past literature for interpretation and discussion of my findings in this chapter.

5.4. <u>Results</u>

5.4.1. <u>GC-TOF-MS for metabolic profiling of caffeinated and decaffeinated coffee</u>

First, I established the suitability of GC-TOF-MS as an analytical platform for metabolic profiling analysis of coffee samples by performing analysis on QC samples. The five replicates that were made for both caffeinated and decaffeinated coffee were used as their own respective QC samples. GC-TOF-MS total ion chromatograms (TIC) of injected samples for both caffeinated and decaffeinated coffee were displayed in **Figure 19A and 19B**, respectively. Upon visual inspection, both TICs displayed extensive overlapping regions, suggesting that both caffeinated and decaffeinated coffee were derived from similar or close source of coffee beans. A total of 332 small molecule peaks were detected in both caffeinated and decaffeinated coffee after peak deconvolution of GC chromatograms. 97 Out of these 332 distinct peaks were assigned putative metabolite identities based on pre-defined matching criteria (SI against mass spectral libraries $\geq$ 70 %). QC analysis was carried out on these 97 identified metabolites, and it was observed that none of them had CV more than 15 % in both caffeinated and decaffeinated groups. The data reliability is high because almost all metabolites had CV lower than 10 %, with the exception of 2-deoxy-D-galactose (CV = 11.5 %, QC for caffeinated coffee) and L-proline (CV = 10.8 %, QC for decaffeinated coffee). This

indicates that the sample preparation and data acquisition are very robust, reflected by the minimal presence of variations in my metabolic data. Therefore, this QC sample analysis had successfully established GC-TOF-MS as a robust and highly reproducible platform for metabolic profiling analysis of coffee samples.
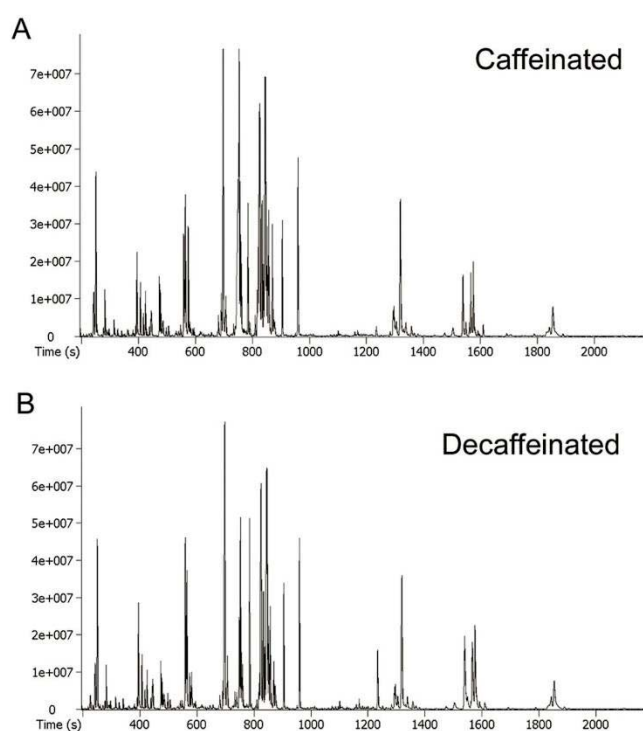
Figure 19. (A) Representative GC-TOF-MS chromatogram of caffeinated coffee sample; **(B)** Representative GC-TOF-MS chromatogram of decaffeinated coffee sample.

5.4.2. Multivariate data analysis of metabolic data in coffee

After suitability of GC-TOF-MS for metabolic profiling analysis of coffee samples had been established, I went on to carry out multivariate data analysis on metabolic data taken from both caffeinated and decaffeinated coffee samples. The first step was to do a non-supervised PCA, which was used to

observe presence of clustering among samples, or any drift in samples due to technical variations that could have been introduced during sample preparation step. PCA of both caffeinated and decaffeinated coffee samples displayed distinct clustering trend on the scores plot for each type of coffee, suggesting that their metabolic profiles differ extensively from each other (**Figure 20A**). First component of PCA modelled 84.5 % of variations among the 97 identified metabolites, while second component modelled only 5.3 % of the variations. This demonstrates that majority of metabolic alterations among the samples can be explained by the difference between caffeinated and decaffeinated coffee.

A PLS-DA was then performed for both caffeinated and decaffeinated coffee, and randomly Y-permuted validation plot for the PLS-DA model showed clearly that the model is valid, with little or no risk of over-fitting of data in the model. This is exemplified by all the lower Q^2 values calculated for the Y-permuted datasets and the regression line of all Q^2 values intersected y-axis below zero (**Figure 20B**). After the model is shown to be valid, an OPLS-DA model was constructed using the same dataset to generate a list discriminant metabolites. The OPLS-DA model is presented in **Figure 20C** (1 predictive component, 1 orthogonal component, $R^2(Y)$ and Q^2(cum) were 1 and 0.998, respectively). The high Q^2(cum) value obtained for the OPLS-DA model indicates that separation between metabolic profiles of the caffeinated and decaffeinated coffee is strong and highly robust. Predictive component modelled 84.4 % of variation among the 97 identified metabolites, while orthogonal component modelled only 4.0 % of the variation. This also goes to

show that most of the variations in metabolic data could be explained by the separation between caffeinated and decaffeinated coffee. Therefore, the OPLS-DA model built using metabolic data from both coffee groups was shown to be valid and subsequently used for discovery of discriminant metabolites.
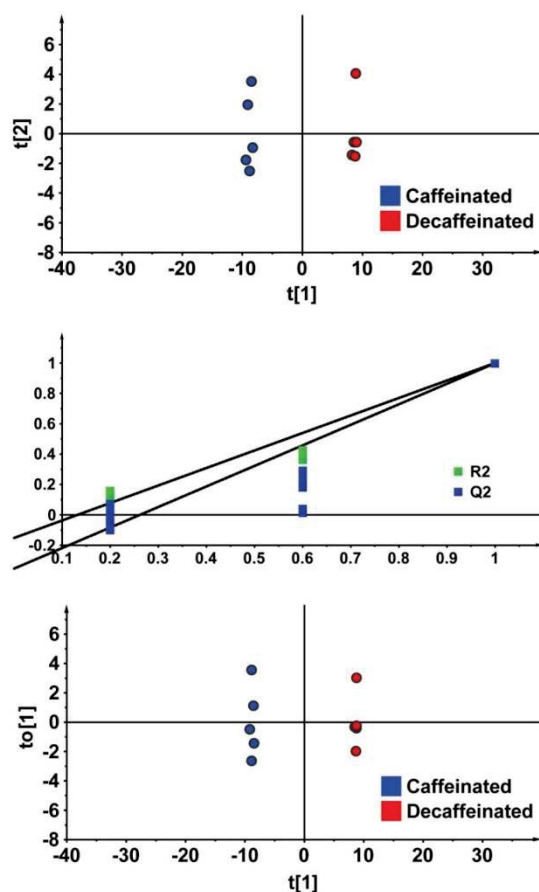
Figure 20. (A) PCA scores plot for caffeinated and decaffeinated coffee samples **(B)** Model validation plot for PLS-DA model between caffeinated and decaffeinated coffee samples **(C)** OPLS-DA between caffeinated and decaffeinated coffee samples (1 predictive component, 1 orthogonal component, $R^2(Y) = 1$, $Q^2(\text{cum}) = 0.998$)

5.4.3. Discriminant metabolites that differentiate caffeinated from decaffeinated coffee

149

Based on the OPLS-DA model discussed in previous section, a list of 69 potential discriminant metabolites (VIP $\geq$ 1.00) that were responsible for separation in the OPLS-DA model was generated. All of these 69 metabolites achieved significance (P < 0.0007, Bonferroni-adjusted significance level) when their means were compared using two-tailed independent t-tests with Welch's correction, confirming their significant contributions as discriminant metabolites to separation between caffeinated and decaffeinated coffee. A summary of these 69 discriminant metabolites, including their identities and similarity indices, as well as the amount present in each type of coffee (relative to caffeinated coffee) can be found in **Table 7.**

Table 7. List of 69 discriminant metabolites that differentiate caffeinated from decaffeinated coffee samples.

	Metabolite	VIP [a]	SI (%) [b]	% metabolite levels relative to caffeinated coffee, mean ± SD	
				Caffeinated	Decaffeinated [c]
1	Caffeine	1.0873	91.0	100.00 ± 3.48	12.26 ± 0.46
2	Fumarate	1.0883	77.6	100.00 ± 1.31	33.85 ± 0.56
3	4-Hydroxybutyrate	1.0884	91.6	100.00 ± 0.96	35.50 ± 0.86
4	Malonate	1.0884	80.2	100.00 ± 0.83	35.60 ± 0.97
5	3-Hydroxybenzoate	1.0869	91.0	100.00 ± 2.19	39.88 ± 1.60
6	2-(2-Hydroxyphenyl)ethanol	1.0883	77.0	100.00 ± 1.16	41.29 ± 0.67
7	5-Hydroxyvalerate	1.0865	74.2	100.00 ± 2.78	42.00 ± 0.92
8	2-Deoxy-D-galactose	1.0459	81.8	100.00 ± 11.51	46.22 ± 4.29
9	Deoxyribose 1-phosphate	1.0865	78.9	100.00 ± 2.25	49.05 ± 1.25
10	Arabinose	1.088	73.6	100.00 ± 1.18	50.50 ± 0.80
11	2-Hydroxyglutarate	1.0882	90.7	100.00 ± 0.99	52.32 ± 0.56
12	2-Deoxy-erythro-pentonate	1.0881	72.4	100.00 ± 0.91	54.73 ± 0.78
13	2-methylpipecolate	1.0867	88.6	100.00 ± 1.19	56.47 ± 1.75
14	Uracil	1.0866	86.1	100.00 ± 1.69	59.20 ± 1.05
15	4,6-dimethoxy-5-(acetyl)pyrimidine	1.0846	81.1	100.00 ± 2.53	59.77 ± 1.12
16	Erythronate	1.0853	84.9	100.00 ± 1.84	59.98 ± 1.73

17	Levoglucosan	1.0817	80.0	100.00 ± 3.00	62.06 ± 1.63
18	2-Hydroxyaniline	1.0879	80.2	100.00 ± 0.70	62.07 ± 0.87
19	Methylsuccinate	1.0865	91.5	100.00 ± 1.62	62.25 ± 0.95
20	Shikimate	1.0867	77.1	100.00 ± 1.69	62.59 ± 0.58
21	Rhamnose	1.0431	83.1	100.00 ± 7.82	63.06 ± 3.89
22	Hydroxyisocaproate	1.0795	82.7	100.00 ± 3.50	64.09 ± 1.28
23	2-Furanpropanoate	1.0859	82.3	100.00 ± 1.61	68.57 ± 0.75
24	Glucose	1.0796	94.4	100.00 ± 2.71	69.54 ± 1.57
25	2-Hydroxybutyrate	1.0692	88.4	100.00 ± 2.05	72.76 ± 3.60
26	4-Hydroxybenzoate	1.0512	88.9	100.00 ± 2.26	74.95 ± 4.84
27	Galactose	1.0766	95.2	100.00 ± 2.50	75.11 ± 1.60
28	Picolinate	1.0043	82.3	100.00 ± 5.25	76.46 ± 5.76
29	Lactic acid dimer	1.0637	74.8	100.00 ± 2.51	81.31 ± 2.03
30	Benzoate	1.0599	77.5	100.00 ± 2.75	82.48 ± 1.74
31	Succinate	1.0851	94.1	100.00 ± 0.72	83.13 ± 0.83
32	2-Furoate	1.0831	94.3	100.00 ± 1.00	83.17 ± 0.92
33	Fructose	1.0692	89.6	100.00 ± 2.09	83.20 ± 1.47
34	4-Hydroxy-2-pentenoate	1.0758	78.5	100.00 ± 1.46	83.45 ± 1.41
35	3-Deoxytetronate	1.0812	89.6	100.00 ± 0.47	85.59 ± 1.27
36	2,3-Dimethyl-3-hydroxyglutarate	1.0187	76.9	100.00 ± 2.36	91.48 ± 0.96
37	Lactate	1.0264	95.5	100.00 ± 1.08	95.09 ± 0.85
38	Parabanate	1.0644	77.0	100.00 ± 1.43	109.43 ± 0.73
39	3-Deoxy-ribo-hexonate, 1,4-lactone	1.0124	81.6	100.00 ± 1.77	109.54 ± 2.40
40	Protocatechuate	1.0535	80.2	100.00 ± 1.79	111.12 ± 1.43
41	2-Deoxytetronate	1.0689	81.6	100.00 ± 1.04	114.08 ± 1.89
42	Ribose	1.0578	87.2	100.00 ± 1.82	115.76 ± 2.43
43	2,3-Hydroxypropanoate	1.083	90.9	100.00 ± 1.82	119.78 ± 1.20
44	Gentisate	1.0825	79.0	100.00 ± 1.41	119.90 ± 0.93
45	1-Methyl-2-piperidinemethanol	1.0804	86.5	100.00 ± 0.60	120.84 ± 1.96
46	Fucose	1.0834	84.3	100.00 ± 0.76	122.60 ± 1.61
47	Methylmaleate	1.0342	88.8	100.00 ± 3.52	125.82 ± 5.73
48	Sumiki's acid	1.0866	93.6	100.00 ± 0.58	129.10 ± 1.30
49	Hydroxypropionate	1.0841	90.3	100.00 ± 1.56	133.39 ± 1.89
50	Uridine	1.0589	82.4	100.00 ± 3.46	136.20 ± 5.90
51	Maleate	1.0752	86.6	100.00 ± 2.13	138.46 ± 4.35
52	Trigonelline	1.0305	84.4	100.00 ± 8.17	141.00 ± 7.45
53	Ribitol	1.0694	88.6	100.00 ± 3.80	141.90 ± 5.05
54	Xylonate 1,4-lactone	1.0788	81.8	100.00 ± 2.24	150.64 ± 4.96
55	Glycine	1.0842	85.9	100.00 ± 2.78	152.85 ± 2.62

56	Valine	1.0559	89.4	100.00 ± 7.80	153.73 ± 7.29
57	Glucuronate	1.0419	82.9	100.00 ± 8.61	155.21 ± 10.05
58	Alanine	1.062	88.4	100.00 ± 5.81	158.97 ± 8.77
59	Xylopyranose	1.0663	75.1	100.00 ± 4.86	161.74 ± 8.80
60	Phenylalanine	1.0685	77.4	100.00 ± 4.74	176.39 ± 10.81
61	N-formylglycine	1.0604	79.0	100.00 ± 4.90	181.39 ± 14.14
62	Proline	1.0392	79.8	100.00 ± 6.32	184.75 ± 19.95
63	Furazan	1.0686	97.8	100.00 ± 9.10	186.00 ± 9.62
64	2-Deoxy-pentos-3-ulose	1.0765	82.4	100.00 ± 1.65	188.39 ± 10.42
65	Malate	1.0869	92.3	100.00 ± 2.86	196.25 ± 3.37
66	Aspartate	1.0612	88.3	100.00 ± 8.17	228.83 ± 21.89
67	2-Ketobutyrate	1.0885	83.9	100.00 ± 4.54	408.99 ± 2.23
68	Guaiacol-alpha-glucoside	1.0881	74.7	100.00 ± 3.67	688.59 ± 14.56
69	Pyruvate	1.0885	81.2	100.00 ± 4.87	885.53 ± 10.34

[a] VIP values were generated from OPLS-DA.
[b] SI indicates percentage match between the mass spectrum of identified compound in samples versus mass spectrum in libraries.
[c] All 69 metabolites achieved significance ($P < 0.0007$, Bonferroni-adjusted significance level). Means were compared using two-tailed independent t-tests with Welch's correction.

5.5. Discussion

5.5.1. GC-TOF-MS as a suitable platform for metabolic profiling of coffee samples

The caffeinated and decaffeinated QC samples analysis clearly showed that GC-TOF-MS is a suitable analytical platform for metabolic profiling analysis of coffee samples. The majority of putatively identified metabolites detected in the coffee samples have CV values lower than 10%, indicating good reliability in sample preparation and data acquisition using the GC-TOF-MS. On top of good reproducibility, analytical platform used in this study also demonstrated high sensitivity when compared against GC-quadrupole-MS used in a recent metabolic profiling study on coffee samples [163]. In their attempt to perform

non-targeted metabolic profiling as a novel method to authenticate the highly prized Civet coffee, Jumhawan et al. detected a total of 182 metabolic peaks and identified 26 of them by matching against mass spectral libraries [163]. In comparison, 332 metabolic peaks were detected in this study and 97 putative metabolite identities were successfully assigned by library matching, even though a lower MS scan speed was used during acquisition (15 Hz) as compared to the much higher scan speed used in Jumhawan's study (10000 Hz). This could be due to the compromised duty cycle when quadrupole MS is operated in scanning mode, as only one mass ion can be selected by the quadrupole mass analyser at every single time point during scanning. In addition, longer GC run time employed in this study might offer better separation of peaks, hence offering better peak resolution during analysis.

5.5.2. Discriminant metabolites between caffeinated and decaffeinated coffee

In total, 69 discriminant metabolites that differentiated caffeinated and decaffeinated coffee had been identified. 37 out of these 69 metabolites were present at higher levels in caffeinated coffee. Besides the well-known caffeine molecule, they also include phenolic compounds which are derivatives of benzoate and cinnamate. In particular, benzoate itself was higher (+21 %) in caffeinated coffee, and two other monohydroxybenzoates, namely 3-hydroxybenzoate and 4-hydroxybenzoate were 151 % and 33 % higher in caffeinated coffee, respectively. On the other hand, two dihydroxybenzoates, namely gentisate and protocatechuate were 20 % and 11 % higher in decaffeinated coffee. Dihydroxybenzoates were reported to possess higher antioxidative capacities than monohydroxybenzoates [164, 165]. However, the

metabolic findings in this study clearly showed that only monohydroxybenzoates were higher in caffeinated coffee; whereas dihydroxybenzoates were higher in decaffeinated coffee instead. Coupled with previous reports of the therapeutic superiority of caffeinated over decaffeinated coffee for prevention of AD, this study suggests that therapeutic advantages of caffeinated coffee could be due to presence of markedly higher levels of monohydroxybenzoates. One possibility that holds the potential for further exploration is the involvement of gut microbial activity in converting the monohydroxybenzoates into stronger bioactive compounds, since it had been shown that monohydroxybenzoates could be metabolized via microbial degradation in the gut into other phenolic compounds or constituents of citrate cycle [166]. This factor plays an important role, especially when tens of trillions of gut microbes could serve as the connector between diet and health in human [167]. Caffeate (a cinnamate derivative) was also detected by the GC-TOF-MS analysis, but no difference in caffeate could be seen between caffeinated and decaffeinated coffee. Even though cinnamate-derived compounds had been reported to offer more antioxidative capacity than benzoate-derived ones [164], metabolic data in this chapter suggest that caffeate might not have contributed significantly to the therapeutic superiority of caffeinated coffee over its decaffeinated counterpart. This finding is in agreement with previous report, which showed that chlorogenate (another cinnamate derivative) has no observable beneficial effect on glucose metabolism in patients at risk for type 2 diabetes [154]. Taken all together, findings here suggest that antioxidative capacities of benzoic and cinnamate-derived phenolic compounds could be further modified by extensive gut

microbial metabolism upon consumption. Future work could aim to uncover these missing links, which, if proven valid, would have a considerable impact on how we relate coffee consumption to clinical health outcome.

Besides the phenolic compounds, discriminant metabolites also include some organic acids, which were shown to be higher in caffeinated coffee. These include L-2-hydroxyglutarate (+91 %), erythronate (+67 %), methylsuccinate (+61 %), and succinate (+20 %). Since all these compounds had been reported to be decreasing in urinary concentrations with increasing age in a previous study [168], their dietary supplementation via coffee consumption could be a potential explanation for the therapeutic benefits of coffee. It should be noted that the age of subjects employed in that particular study was only up to 12 years old, but their findings indicated a clear downward trends in urinary excretion of these compounds with increasing age in these subjects, demonstrating the relevance of these compounds to developmental health. Nevertheless, even though my metabolic data showed that these compounds were higher in caffeinated coffee, their beneficial dietary effects if consumed over the long term remained yet to be defined. 5-hydroxyvalerate is another organic acid which was detected at higher concentration in caffeinated coffee (+138 %). This compound was previously reported as an antioxidant present in citrus peel [169], and its higher level in caffeinated coffee could offer additional antioxidative activity and free radical scavenging capacity, therefore conferring caffeinated coffee its therapeutic superiority over decaffeinated coffee.

Fumarate, a fatty acid which is also a component of citrate cycle, was another compound found to be higher in caffeinated coffee (+195 %). Interestingly, fumarate and its esters had been investigated for their neuroprotective and antioxidative effects, which was believed to be due to its salvaging effect on perturbed citrate cycle [170]. Another compound, shikimate was detected to be 60 % higher in caffeinated coffee than decaffeinated one. This compound is widely present in edible plants, and its production in plant is increased as an antioxidative response to wounding stress [171]. It had also been shown that shikimate can be metabolized by gut microbes to cyclohexanecarboxylate, which will then be aromatized in mammalian tissues [172].

Besides offering additional antioxidative protection, other detected compounds gave clues of alternative mechanisms that can give caffeinated coffee its therapeutic advantage over decaffeinated coffee. L-rhamnose, a deoxy sugar which has been shown to exert inhibitory effects on lipogenesis upon consumption [173], was observed to be higher in caffeinated coffee (+59 %). 2-Furoate, which was reported to possess lipid lowering effects in a previous study [174], was also higher in caffeinated coffee (+20 %). Since dysregulation of lipid metabolism is closely associated with AD development and it is a potential therapeutic target for treating AD [175], these findings suggest that L-rhamnose and 2-furoate could act as lipid metabolism regulators, hence making caffeinated coffee the more desirable option for AD prevention. Another potential therapeutic mechanism could be coming from the higher picolinate in caffeinated coffee (+31 %). It had already been shown that dietary picolinate enhances absorption of dietary zinc in human [176], and

zinc deficiency had been previously discussed as a factor for AD pathogenesis [177]. A higher level of picolinate in caffeinated coffee could potentially enhance zinc absorption over long-term consumption and contribute to prevention of AD.

5.5.3. <u>Decaffeination process enhanced levels of some metabolites present in coffee</u>

In contrast to my original expectation, decaffeination process did more than just stripping components away from the beans. Several compounds actually had elevated concentrations in decaffeinated coffee. Some of these compounds include pyruvate (+785 %), 2-ketobutyrate (+309 %), and malate (+96 %), which are closely associated with energy metabolism. Several amino acids were also detected at higher levels in decaffeinated coffee, namely L-aspartate (+129 %), L-proline (+85 %), L-phenylalanine (+76 %), L-alanine (+59 %), L-valine (+54 %), and glycine (+53 %). Interestingly, trigonelline was observed to be higher in decaffeinated coffee (+41 %). Trigonelline is a vitamin B3 precursor which is often described as a major component of coffee that exerts beneficial effect on glucose metabolism, a trait that is closely associated with AD development [178]. However, contradictory evidence showed that it had limited anti-diabetic effects in human patients [154], which led some to question its role in AD prevention. All in all, a total of 32 compounds were observed to be present at higher levels in decaffeinated coffee. Although data in this study clearly demonstrated the increased presence of these compounds in decaffeinated coffee, I could not tell if this was due to the decaffeination

process or post-decaffeination modification processes employed by the manufacturer.

5.6. Conclusions

The study reported in this chapter, though deviated slightly from the main stream of the whole thesis, the findings shed lights on the beneficial effects of caffeinated coffee for AD. The decaffeination process could strip away the active components in coffee for AD. This study also substantiated that GC-TOF-MS is a suitable platform for metabolic profiling analysis, and metabolic profiling approach was demonstrated to be a highly robust tool to discriminate the chemical components between the caffeinated and decaffeinated coffee samples. Their chemical differences include several phenolic compounds, organic acids, sugar, fatty acids, and amino acids. All these compounds are biologically relevant and findings here provide important revelations into research of the therapeutic potential of coffee against AD. My data also hinted at the possible involvement of gut microbial metabolism of compounds present in caffeinated coffee, which could have enhanced its therapeutic potential against AD when consumed over a long period of time. This represents an interesting area for future exploration, which could aim to uncover the links between coffee compositions, gut microbial metabolism, and clinical health outcome.

5.7. Limitations

This study has few limitations; one is that the absolute concentrations of each discriminant metabolite were not measured. That would require a different

methodology and it is not in line with my research objectives in this chapter. Another limitation is that although GC-TOF-MS offers the sensitivity to cover a wide metabolic space, its metabolic coverage is definitely not exhaustive. However, to the best of my knowledge, the analytical method employed in this study offers the widest coverage of coffee metabolites using a single analytical platform assisted with the commercially available spectral libraries.

Despite having these limitations, the findings generated in this study remain significant. It is the first study to evidently demonstrate the wide-ranging chemical differences between caffeinated and decaffeinated coffee, and clearly showed that caffeine is not the only discriminant metabolite between caffeinated and decaffeinated coffee. As this assumption is often made in research that involves decaffeinated coffee, this study contributes to the scientific community by raising awareness that one should look beyond caffeine when comparing the two types of coffee.

CHAPTER 6: Concluding remarks, limitations of my study and future perspectives

In chapter 1, I gave an overview on AD characteristics, and discussed in more detail the clinical challenges imposed on therapeutic research for AD. Several recent failures of major phase III AD clinical trials highlighted the need for a different approach to treating this seemingly intractable disease, and one such example is the currently ongoing clinical trial that initiates clinical intervention even before the subjects exhibit any AD symptom. The basis of this "AD prevention trial" is to stop the disease progression at its early stages, a notion that resonates well in the AD research community nowadays, as more and more AD researchers are focusing on investigating early-stage AD. In this respect, metabolic profiling approach presents itself as a suitable tool as it offers superb sensitivity that could detect subtle fluctuations in a biological system. Therefore in this thesis, I proposed to employ metabolic profiling technique on appropriately selected AD models to pick up early-stage AD signals projected by these models. This did not just help me understand AD pathogenesis better, but also allowed me to use the models in elucidating treatment effects of compound of interest. In this thesis, I investigated the treatment effects of PPARγ agonist in AD. PPARγ agonist holds tremendous potential as a therapeutic molecule for AD, but the apparent failure to translate its preclinical successes into positive clinical outcomes remains as an obstacle to its development in the AD drug pipeline.

In chapter 2 and 3, I explored the application of GC-TOF-MS-based metabolic profiling in studying metabolic alterations that occurred in *in vitro* (CHO-APP$_{695}$) and *in vivo* (APP/PS1) AD models. Metabolic profiling was used as a bottom-up approach to further investigate what processes had gone awry in these two models. Several pathological processes observed were common to both models, namely impaired energy metabolism and dysregulated amino acid metabolism. Mitochondrial dysfunction was observed to have preceded amyloid-β induced toxicity in the *in vitro* model, which was then attributed to the possibility of toxicity induced by accumulation of APP in mitochondria membrane. The accumulation of mitochondrial APP was similarly observed in the cortex of APP/PS1 transgenic mice, lending support to the findings based on my *in vitro* model. More interestingly, PIO was observed to have exerted a larger extent of treatment effect than ROSI when tested using *in vitro* AD model, even though ROSI is a stronger and more selective agonist of PPARγ nuclear receptor. Therapeutic superiority of PIO was attributed to its double agonistic properties on both PPARγ and PPARα nuclear receptors, and the compound was further investigated for its therapeutic mechanism using subsequent *in vivo* model (APP/PS1 transgenic mice). By investigating four brain regions (cortex, hippocampus, cerebellum and midbrain) separately, the *in vivo* experimental design allowed me to discover the brain region-specific treatment effects of PIO, which was observed to exert extensive treatment effects in cortex and cerebellum tissue of APP/PS1 mice. This novel finding would no doubt be useful for researchers working in the field of AD therapeutic research, in particular those who have an interest in PPARγ and PPARα nuclear receptor agonisms. However, it should be noted that most of

my findings in chapter 2 and 3 originated from disease models that are based on the amyloid cascade hypothesis, and therefore may not be directly translatable to clinical interpretations if other unrelated pathophysiological processes are involved.

With the spotlight focused on PIO, I then attempted to tackle one major obstacle that could limit its drug development process in AD research – PIO's poor brain penetration. In chapter 4, I confirmed that P-gp's drug efflux transport at the BBB played a significant role in keeping PIO away from the brain. Co-administration of P-gp regulators together with PIO therefore presented itself as a plausible dosing strategy to overcome poor brain penetration problem of PIO, but the poor solubility and long-term drug toxicities of P-gp inhibitors imposed a serious challenge to this dosing regimen. Not satisfied with this strategy, I explored the possibility of stereoselectivity in PIO's brain penetration, and discovered that (+)-PIO is present at a higher concentration in brain tissue, but lower in plasma of normal healthy mouse given a single dose of PIO. I then proceeded to purify (+)-PIO and compared its brain pharmacokinetic profile against racemic PIO. Judging based on the AUC of brain concentration vs time graphs, I observed a higher brain exposure to PIO in mice when they were dosed with purified (+)-PIO as compared to racemic PIO. This suggests that (+)-PIO is potentially a better drug candidate for treating AD than racemic PIO, due to its larger presence in brain tissue demonstrated in mice. This is the first study to shed light on stereoselectivity in PIO's brain penetration, and the discovery of (+)-PIO being a potentially better brain drug than racemic PIO is definitely a

significant finding in this field, especially when two active clinical trials are now being run to look at PIO in AD and Parkinson's disease. However, (+)-PIO's current application in AD therapy is severely limited by the lack of efficacy and safety study on this particular stereoisomer, especially for long-term drug administration which is commonly associated for chronic disease like AD.

The work in chapter 2 to 4 serves as a good foundation for future work to continue building on the findings. In particular, accumulation of APP in brain mitochondria, if validated properly in clinical studies, could potentially be a drug target for treating AD while it is still at an early disease stage. On top of that, studies that investigate further the brain region specificity of PIO's treatment effect, and factors behind this particular observation, would contribute significantly to therapeutic research of PPARγ agonist, particularly PIO. Last but not least, future studies that compare therapeutic efficacy and drug safety of (+)-PIO directly against racemic PIO in preclinical and/or clinical settings would help to validate, or rule out, the application of (+)-PIO in AD therapeutic research.

In chapter 5, I ventured into a slightly different research topic, using metabolic profiling approach to study the metabolic alterations in coffee rendered by decaffeination process. My findings demonstrated clear differences between caffeinated and decaffeinated coffee, and the difference is more than just caffeine. Based on previous reports of therapeutic superiority of caffeinated coffee in AD over pure caffeine or decaffeinated coffee, this list of

discriminant metabolites could potentially be holding the key to a promising therapeutic molecule for treating or preventing AD. Future work would contribute substantially to this topic by profiling the metabolites in extracts obtained from decaffeination process, to account for the loss of those metabolites from coffee. Biological relevance of these chemical differences should also be established to widen the knowledge with regard to coffee consumption as prevention against AD development.

REFERENCES

[1]   Fratiglioni L, Qiu C (2009) Prevention of common neurodegenerative disorders in the elderly. *Exp Gerontol* **44**, 46-50.

[2]   Abbott A (2011) Dementia: a problem for our age. *Nature* **475**, S2-4.

[3]   Holtzman JL (2010) Are we prepared to deal with the Alzheimer's disease pandemic? *Clin Pharmacol Ther* **88**, 563-565.

[4]   LaFerla FM, Green KN, Oddo S (2007) Intracellular amyloid-beta in Alzheimer's disease. *Nat Rev Neurosci* **8**, 499-509.

[5]   Gamblin TC, Chen F, Zambrano A, Abraha A, Lagalwar S, Guillozet AL, Lu M, Fu Y, Garcia-Sierra F, LaPointe N, Miller R, Berry RW, Binder LI, Cryns VL (2003) Caspase cleavage of tau: linking amyloid and neurofibrillary tangles in Alzheimer's disease. *Proc Natl Acad Sci U S A* **100**, 10032-10037.

[6]   Hanger DP, Anderton BH, Noble W (2009) Tau phosphorylation: the therapeutic challenge for neurodegenerative disease. *Trends Mol Med* **15**, 112-119.

[7]   Oddo S, Caccamo A, Kitazawa M, Tseng BP, LaFerla FM (2003) Amyloid deposition precedes tangle formation in a triple transgenic model of Alzheimer's disease. *Neurobiol Aging* **24**, 1063-1070.

[8]   Wray S, Noble W (2009) Linking amyloid and tau pathology in Alzheimer's disease: the role of membrane cholesterol in Abeta-mediated tau toxicity. *J Neurosci* **29**, 9665-9667.

[9]   McGeer PL, Rogers J, McGeer EG (2006) Inflammation, anti-inflammatory agents and Alzheimer disease: the last 12 years. *J Alzheimers Dis* **9**, 271-276.

[10]   Pratico D, Clark CM, Liun F, Rokach J, Lee VY, Trojanowski JQ (2002) Increase of brain oxidative stress in mild cognitive impairment: a possible predictor of Alzheimer disease. *Arch Neurol* **59**, 972-976.

[11]   Wyss-Coray T (2006) Inflammation in Alzheimer disease: driving force, bystander or beneficial response? *Nat Med* **12**, 1005-1015.

[12]   Wang X, Wang W, Li L, Perry G, Lee HG, Zhu X (2014) Oxidative stress and mitochondrial dysfunction in Alzheimer's disease. *Biochim Biophys Acta* **1842**, 1240-1247.

[13]   Chaturvedi RK, Flint Beal M (2013) Mitochondrial diseases of the brain. *Free Radic Biol Med* **63**, 1-29.

[14]   Sochocka M, Koutsouraki ES, Gasiorowski K, Leszek J (2013) Vascular oxidative stress and mitochondrial failure in the pathobiology of Alzheimer's disease: a new approach to therapy. *CNS Neurol Disord Drug Targets* **12**, 870-881.

[15]   Budson AE, Solomon PR (2012) New diagnostic criteria for Alzheimer's disease and mild cognitive impairment for the practical neurologist. *Pract Neurol* **12**, 88-96.

[16]   Pearson SD, Ollendorf DA, Colby JA (2014) Amyloid-beta positron emission tomography in the diagnostic evaluation of alzheimer disease: summary of primary findings and conclusions. *JAMA Intern Med* **174**, 133-134.

[17]   Jack CR, Jr., Lowe VJ, Weigand SD, Wiste HJ, Senjem ML, Knopman DS, Shiung MM, Gunter JL, Boeve BF, Kemp BJ, Weiner M, Petersen RC (2009) Serial PIB and MRI in normal, mild cognitive impairment

and Alzheimer's disease: implications for sequence of pathological events in Alzheimer's disease. *Brain* **132**, 1355-1365.

[18]   Hardy J, Selkoe DJ (2002) The amyloid hypothesis of Alzheimer's disease: progress and problems on the road to therapeutics. *Science* **297**, 353-356.

[19]   Hardy JA, Higgins GA (1992) Alzheimer's disease: the amyloid cascade hypothesis. *Science* **256**, 184-185.

[20]   Karran E, Mercken M, De Strooper B (2011) The amyloid cascade hypothesis for Alzheimer's disease: an appraisal for the development of therapeutics. *Nat Rev Drug Discov* **10**, 698-712.

[21]   Doody RS, Raman R, Farlow M, Iwatsubo T, Vellas B, Joffe S, Kieburtz K, He F, Sun X, Thomas RG, Aisen PS, Siemers E, Sethuraman G, Mohs R (2013) A phase 3 trial of semagacestat for treatment of Alzheimer's disease. *N Engl J Med* **369**, 341-350.

[22]   Doody RS, Thomas RG, Farlow M, Iwatsubo T, Vellas B, Joffe S, Kieburtz K, Raman R, Sun X, Aisen PS, Siemers E, Liu-Seifert H, Mohs R (2014) Phase 3 trials of solanezumab for mild-to-moderate Alzheimer's disease. *N Engl J Med* **370**, 311-321.

[23]   Salloway S, Sperling R, Fox NC, Blennow K, Klunk W, Raskind M, Sabbagh M, Honig LS, Porsteinsson AP, Ferris S, Reichert M, Ketter N, Nejadnik B, Guenzler V, Miloslavsky M, Wang D, Lu Y, Lull J, Tudor IC, Liu E, Grundman M, Yuen E, Black R, Brashear HR (2014) Two phase 3 trials of bapineuzumab in mild-to-moderate Alzheimer's disease. *N Engl J Med* **370**, 322-333.

[24]   Iqbal K, Liu F, Gong CX (2014) Alzheimer disease therapeutics: focus on the disease and not just plaques and tangles. *Biochem Pharmacol* **88**, 631-639.

[25]   Medina M, Avila J (2014) New perspectives on the role of tau in Alzheimer's disease. Implications for therapy. *Biochem Pharmacol* **88**, 540-547.

[26]   Bloom GS (2014) Amyloid-beta and tau: the trigger and bullet in Alzheimer disease pathogenesis. *JAMA Neurol* **71**, 505-508.

[27]   Pasqualetti P, Bonomini C, Dal Forno G, Paulon L, Sinforiani E, Marra C, Zanetti O, Rossini PM (2009) A randomized controlled study on effects of ibuprofen on cognitive progression of Alzheimer's disease. *Aging Clin Exp Res* **21**, 102-110.

[28]   Sano M, Bell KL, Galasko D, Galvin JE, Thomas RG, van Dyck CH, Aisen PS (2011) A randomized, double-blind, placebo-controlled trial of simvastatin to treat Alzheimer disease. *Neurology* **77**, 556-563.

[29]   Gold M, Alderton C, Zvartau-Hind M, Egginton S, Saunders AM, Irizarry M, Craft S, Landreth G, Linnamagi U, Sawchak S (2010) Rosiglitazone monotherapy in mild-to-moderate Alzheimer's disease: results from a randomized, double-blind, placebo-controlled phase III study. *Dement Geriatr Cogn Disord* **30**, 131-146.

[30]   Genentech (2014) A Study of Crenezumab Versus Placebo in Preclinical PSEN1 E280A Mutation Carriers to Evaluate Efficacy and Safety in the Treatment of Autosomal-Dominant Alzheimer Disease, Including a Placebo-Treated Noncarrier Cohort.

[31]   Nicholson JK, Lindon JC (2008) Systems biology: Metabonomics. *Nature* **455**, 1054-1056.

[32] Zhao S, Iyengar R (2012) Systems pharmacology: network analysis to identify multiscale mechanisms of drug action. *Annu Rev Pharmacol Toxicol* **52**, 505-521.

[33] Oliver SG, Winson MK, Kell DB, Baganz F (1998) Systematic functional analysis of the yeast genome. *Trends Biotechnol* **16**, 373-378.

[34] Nicholson JK, Lindon JC, Holmes E (1999) 'Metabonomics': understanding the metabolic responses of living systems to pathophysiological stimuli via multivariate statistical analysis of biological NMR spectroscopic data. *Xenobiotica* **29**, 1181-1189.

[35] Atkinson AJ, Colburn WA, DeGruttola VG, DeMets DL, Downing GJ, Hoth DF, Oates JA, Peck CC, Schooley RT, Spilker BA, Woodcock J, Zeger SL (2001) Biomarkers and surrogate endpoints: Preferred definitions and conceptual framework*. *Clin Pharmacol Ther* **69**, 89-95.

[36] Bundy JG, Spurgeon DJ, Svendsen C, Hankard PK, Osborn D, Lindon JC, Nicholson JK (2002) Earthworm species of the genus Eisenia can be phenotypically differentiated by metabolic profiling. *FEBS Lett* **521**, 115-120.

[37] Urbanczyk-Wochniak E, Luedemann A, Kopka J, Selbig J, Roessner-Tunali U, Willmitzer L, Fernie AR (2003) Parallel analysis of transcript and metabolic profiles: a new approach in systems biology. *EMBO Rep* **4**, 989-993.

[38] ter Kuile BH, Westerhoff HV (2001) Transcriptome meets metabolome: hierarchical and metabolic regulation of the glycolytic pathway. *FEBS Lett* **500**, 169-171.

[39] Pasikanti KK, Ho PC, Chan EC (2008) Gas chromatography/mass spectrometry in metabolic profiling of biological fluids. *J Chromatogr B Analyt Technol Biomed Life Sci* **871**, 202-211.

[40] Babushok VI, Linstrom PJ, Reed JJ, Zenkevich IG, Brown RL, Mallard WG, Stein SE (2007) Development of a database of gas chromatographic retention properties of organic compounds. *J Chromatogr A* **1157**, 414-421.

[41] Kind T, Wohlgemuth G, Lee do Y, Lu Y, Palazoglu M, Shahbaz S, Fiehn O (2009) FiehnLib: mass spectral and retention index libraries for metabolomics based on quadrupole and time-of-flight gas chromatography/mass spectrometry. *Anal Chem* **81**, 10038-10048.

[42] Palma P, Famiglini G, Trufelli H, Pierini E, Termopoli V, Cappiello A (2011) Electron ionization in LC-MS: recent developments and applications of the direct-EI LC-MS interface. *Anal Bioanal Chem* **399**, 2683-2693.

[43] Taylor PJ (2005) Matrix effects: the Achilles heel of quantitative high-performance liquid chromatography-electrospray-tandem mass spectrometry. *Clin Biochem* **38**, 328-334.

[44] Dunn WB, Ellis DI (2005) Metabolomics: Current analytical platforms and methodologies. *TrAC Trends in Analytical Chemistry* **24**, 285-294.

[45] Teul J, Ruperez FJ, Garcia A, Vaysse J, Balayssac S, Gilard V, Malet-Martino M, Martin-Ventura JL, Blanco-Colio LM, Tunon J, Egido J, Barbas C (2009) Improving metabolite knowledge in stable

atherosclerosis patients by association and correlation of GC-MS and 1H NMR fingerprints. *J Proteome Res* **8**, 5580-5589.

[46] Sperling R, Johnson K (2013) Biomarkers of Alzheimer disease: current and future applications to diagnostic criteria. *Continuum (Minneap Minn)* **19**, 325-338.

[47] Peters KR, Lynn Beattie B, Feldman HH, Illes J (2013) A conceptual framework and ethics analysis for prevention trials of Alzheimer Disease. *Prog Neurobiol* **110**, 114-123.

[48] Xu XH, Huang Y, Wang G, Chen SD (2012) Metabolomics: a novel approach to identify potential diagnostic biomarkers and pathogenesis in Alzheimer's disease. *Neurosci Bull* **28**, 641-648.

[49] Kaddurah-Daouk R, McEvoy J, Baillie RA, Lee D, Yao JK, Doraiswamy PM, Krishnan KR (2007) Metabolomic mapping of atypical antipsychotic effects in schizophrenia. *Mol Psychiatry* **12**, 934-945.

[50] Ji Y, Hebbring S, Zhu H, Jenkins GD, Biernacka J, Snyder K, Drews M, Fiehn O, Zeng Z, Schaid D, Mrazek DA, Kaddurah-Daouk R, Weinshilboum RM (2011) Glycine and a glycine dehydrogenase (GLDC) SNP as citalopram/escitalopram response biomarkers in depression: pharmacometabolomics-informed pharmacogenomics. *Clin Pharmacol Ther* **89**, 97-104.

[51] Belyaev ND, Kellett KA, Beckett C, Makova NZ, Revett TJ, Nalivaeva NN, Hooper NM, Turner AJ (2010) The transcriptionally active amyloid precursor protein (APP) intracellular domain is preferentially produced from the 695 isoform of APP in a {beta}-secretase-dependent pathway. *J Biol Chem* **285**, 41443-41454.

[52] Holcomb L, Gordon MN, McGowan E, Yu X, Benkovic S, Jantzen P, Wright K, Saad I, Mueller R, Morgan D, Sanders S, Zehr C, O'Campo K, Hardy J, Prada CM, Eckman C, Younkin S, Hsiao K, Duff K (1998) Accelerated Alzheimer-type phenotype in transgenic mice carrying both mutant amyloid precursor protein and presenilin 1 transgenes. *Nat Med* **4**, 97-100.

[53] Duyckaerts C, Potier MC, Delatour B (2008) Alzheimer disease models and human neuropathology: similarities and differences. *Acta Neuropathol* **115**, 5-38.

[54] Howlett DR (2011) APP transgenic mice and their application to drug discovery. *Histol Histopathol* **26**, 1611-1632.

[55] Hu ZP, Browne ER, Liu T, Angel TE, Ho PC, Chan EC (2012) Metabonomic profiling of TASTPM transgenic Alzheimer's disease mouse model. *J Proteome Res* **11**, 5903-5913.

[56] Trushina E, Nemutlu E, Zhang S, Christensen T, Camp J, Mesa J, Siddiqui A, Tamura Y, Sesaki H, Wengenack TM, Dzeja PP, Poduslo JF (2012) Defects in mitochondrial dynamics and metabolomic signatures of evolving energetic stress in mouse models of familial Alzheimer's disease. *PLoS One* **7**, e32737.

[57] Czech C, Berndt P, Busch K, Schmitz O, Wiemer J, Most V, Hampel H, Kastler J, Senn H (2012) Metabolite profiling of Alzheimer's disease cerebrospinal fluid. *PLoS One* **7**, e31501.

[58] Lalande J, Halley H, Balayssac S, Gilard V, Dejean S, Martino R, Frances B, Lassalle JM, Malet-Martino M (2014) 1H NMR

metabolomic signatures in five brain regions of the AbetaPPswe Tg2576 mouse model of Alzheimer's disease at four ages. *J Alzheimers Dis* **39**, 121-143.

[59]   Salek RM, Xia J, Innes A, Sweatman BC, Adalbert R, Randle S, McGowan E, Emson PC, Griffin JL (2010) A metabolomic study of the CRND8 transgenic mouse model of Alzheimer's disease. *Neurochem Int* **56**, 937-947.

[60]   Jiang N, Yan X, Zhou W, Zhang Q, Chen H, Zhang Y, Zhang X (2008) NMR-based metabonomic investigations into the metabolic profile of the senescence-accelerated mouse. *J Proteome Res* **7**, 3678-3686.

[61]   Tukiainen T, Tynkkynen T, Makinen VP, Jylanki P, Kangas A, Hokkanen J, Vehtari A, Grohn O, Hallikainen M, Soininen H, Kivipelto M, Groop PH, Kaski K, Laatikainen R, Soininen P, Pirttila T, Ala-Korpela M (2008) A multi-metabolite analysis of serum by 1H NMR spectroscopy: early systemic signs of Alzheimer's disease. *Biochem Biophys Res Commun* **375**, 356-361.

[62]   Kummer MP, Heneka MT (2008) PPARs in Alzheimer's Disease. *PPAR Res* **2008**, 403896.

[63]   Heneka MT, Landreth GE, Feinstein DL (2001) Role for peroxisome proliferator-activated receptor-gamma in Alzheimer's disease. *Ann Neurol* **49**, 276.

[64]   Kielian T, Drew PD (2003) Effects of peroxisome proliferator-activated receptor-gamma agonists on central nervous system inflammation. *J Neurosci Res* **71**, 315-325.

[65]   Landreth GE, Heneka MT (2001) Anti-inflammatory actions of peroxisome proliferator-activated receptor gamma agonists in Alzheimer's disease. *Neurobiol Aging* **22**, 937-944.

[66]   in t' Veld BA, Ruitenberg A, Hofman A, Launer LJ, van Duijn CM, Stijnen T, Breteler MM, Stricker BH (2001) Nonsteroidal antiinflammatory drugs and the risk of Alzheimer's disease. *N Engl J Med* **345**, 1515-1521.

[67]   Lehmann JM, Lenhard JM, Oliver BB, Ringold GM, Kliewer SA (1997) Peroxisome proliferator-activated receptors alpha and gamma are activated by indomethacin and other non-steroidal anti-inflammatory drugs. *J Biol Chem* **272**, 3406-3410.

[68]   Cameron B, Landreth GE (2010) Inflammation, microglia, and Alzheimer's disease. *Neurobiol Dis* **37**, 503-509.

[69]   Jiang Q, Lee CY, Mandrekar S, Wilkinson B, Cramer P, Zelcer N, Mann K, Lamb B, Willson TM, Collins JL, Richardson JC, Smith JD, Comery TA, Riddell D, Holtzman DM, Tontonoz P, Landreth GE (2008) ApoE promotes the proteolytic degradation of Abeta. *Neuron* **58**, 681-693.

[70]   Mandrekar-Colucci S, Landreth GE (2011) Nuclear receptors as therapeutic targets for Alzheimer's disease. *Expert Opin Ther Targets* **15**, 1085-1097.

[71]   Landreth G, Jiang Q, Mandrekar S, Heneka M (2008) PPARgamma agonists as therapeutics for the treatment of Alzheimer's disease. *Neurotherapeutics* **5**, 481-489.

[72]   Risner ME, Saunders AM, Altman JF, Ormandy GC, Craft S, Foley IM, Zvartau-Hind ME, Hosford DA, Roses AD (2006) Efficacy of

rosiglitazone in a genetically defined population with mild-to-moderate Alzheimer's disease. *Pharmacogenomics J* **6**, 246-254.

[73] Sato T, Hanyu H, Hirao K, Kanetaka H, Sakurai H, Iwamoto T (2011) Efficacy of PPAR-gamma agonist pioglitazone in mild Alzheimer disease. *Neurobiol Aging* **32**, 1626-1633.

[74] Watson GS, Cholerton BA, Reger MA, Baker LD, Plymate SR, Asthana S, Fishel MA, Kulstad JJ, Green PS, Cook DG, Kahn SE, Keeling ML, Craft S (2005) Preserved cognition in patients with early Alzheimer disease and amnestic mild cognitive impairment during treatment with rosiglitazone: a preliminary study. *Am J Geriatr Psychiatry* **13**, 950-958.

[75] Kersten S, Desvergne B, Wahli W (2000) Roles of PPARs in health and disease. *Nature* **405**, 421-424.

[76] Aleshin S, Reiser G (2013) Role of the peroxisome proliferator-activated receptors (PPAR)-alpha, beta/delta and gamma triad in regulation of reactive oxygen species signaling in brain. *Biol Chem* **394**, 1553-1570.

[77] Escribano L, Simon AM, Gimeno E, Cuadrado-Tejedor M, Lopez de Maturana R, Garcia-Osta A, Ricobaraza A, Perez-Mediavilla A, Del Rio J, Frechilla D (2010) Rosiglitazone rescues memory impairment in Alzheimer's transgenic mice: mechanisms involving a reduced amyloid and tau pathology. *Neuropsychopharmacology* **35**, 1593-1604.

[78] Nicolakakis N, Aboulkassim T, Ongali B, Lecrux C, Fernandes P, Rosa-Neto P, Tong XK, Hamel E (2008) Complete rescue of cerebrovascular function in aged Alzheimer's disease transgenic mice by antioxidants and pioglitazone, a peroxisome proliferator-activated receptor gamma agonist. *J Neurosci* **28**, 9287-9296.

[79] Jiang Q, Heneka M, Landreth GE (2008) The role of peroxisome proliferator-activated receptor-gamma (PPARgamma) in Alzheimer's disease: therapeutic implications. *CNS Drugs* **22**, 1-14.

[80] Qin W, Haroutunian V, Katsel P, Cardozo CP, Ho L, Buxbaum JD, Pasinetti GM (2009) PGC-1alpha expression decreases in the Alzheimer disease brain as a function of dementia. *Arch Neurol* **66**, 352-361.

[81] Strum JC, Shehee R, Virley D, Richardson J, Mattie M, Selley P, Ghosh S, Nock C, Saunders A, Roses A (2007) Rosiglitazone induces mitochondrial biogenesis in mouse brain. *J Alzheimers Dis* **11**, 45-51.

[82] Sime M, Allan AC, Chapman P, Fieldhouse C, Giblin GM, Healy MP, Lambert MH, Leesnitzer LM, Lewis A, Merrihew RV, Rutter RA, Sasse R, Shearer BG, Willson TM, Xu RX, Virley DJ (2011) Discovery of GSK1997132B a novel centrally penetrant benzimidazole PPARgamma partial agonist. *Bioorg Med Chem Lett* **21**, 5568-5572.

[83] Schinkel AH (1999) P-Glycoprotein, a gatekeeper in the blood-brain barrier. *Adv Drug Deliv Rev* **36**, 179-194.

[84] Maeshiba Y, Kiyota Y, Yamashita K, Yoshimura Y, Motohashi M, Tanayama S (1997) Disposition of the new antidiabetic agent pioglitazone in rats, dogs, and monkeys. *Arzneimittelforschung* **47**, 29-35.

[85] Papadopoulos P, Rosa-Neto P, Rochford J, Hamel E (2013) Pioglitazone improves reversal learning and exerts mixed

cerebrovascular effects in a mouse model of Alzheimer's disease with combined amyloid-beta and cerebrovascular pathology. *PLoS One* **8**, e68612.

[86] Sastre M, Dewachter I, Rossner S, Bogdanovic N, Rosen E, Borghgraef P, Evert BO, Dumitrescu-Ozimek L, Thal DR, Landreth G, Walter J, Klockgether T, van Leuven F, Heneka MT (2006) Nonsteroidal anti-inflammatory drugs repress beta-secretase gene promoter activity by the activation of PPARgamma. *Proc Natl Acad Sci U S A* **103**, 443-448.

[87] Geldmacher DS, Fritsch T, McClendon MJ, Landreth G (2011) A randomized pilot clinical trial of the safety of pioglitazone in treatment of patients with Alzheimer disease. *Arch Neurol* **68**, 45-50.

[88] Takeda (2013) Biomarker Qualification for Risk of Mild Cognitive Impairment (MCI) Due to Alzheimer's Disease (AD) and Safety and Efficacy Evaluation of Pioglitazone in Delaying Its Onset. In: ClinicalTrials.gov [Internet]. Bethesda (MD): National Library of Medicine (US). 2000- [cited 2013 Dec 03]. Available from: http://clinicaltrials.gov/show/NCT01931566 NLM Identifier: NCT01931566.

[89] Woodcock J, Sharfstein JM, Hamburg M (2010) Regulatory action on rosiglitazone by the U.S. Food and Drug Administration. *N Engl J Med* **363**, 1489-1491.

[90] Luo Y, He Q, Kuang G, Jiang Q, Yang J (2014) PPAR-alpha and PPAR-beta expression changes in the hippocampus of rats undergoing global cerebral ischemia/reperfusion due to PPAR-gamma status. *Behav Brain Funct* **10**, 21.

[91] Rochester U (2013) Pioglitazone in Early Parkinson's Disease. In: ClinicalTrials.gov [Internet]. Bethesda (MD): National Library of Medicine (US). 2000- [cited 2014 July 31]. Available from: http://clinicaltrials.gov/show/NCT01280123 NLM Identifier: NCT01280123.

[92] Orasanu G, Ziouzenkova O, Devchand PR, Nehra V, Hamdy O, Horton ES, Plutzky J (2008) The peroxisome proliferator-activated receptor-gamma agonist pioglitazone represses inflammation in a peroxisome proliferator-activated receptor-alpha-dependent manner in vitro and in vivo in mice. *J Am Coll Cardiol* **52**, 869-881.

[93] Kell DB, Brown M, Davey HM, Dunn WB, Spasic I, Oliver SG (2005) Metabolic footprinting and systems biology: the medium is the message. *Nat Rev Microbiol* **3**, 557-565.

[94] Cao C, Wang L, Lin X, Mamcarz M, Zhang C, Bai G, Nong J, Sussman S, Arendash G (2011) Caffeine synergizes with another coffee component to increase plasma GCSF: linkage to cognitive benefits in Alzheimer's mice. *J Alzheimers Dis* **25**, 323-335.

[95] Kovalevich J, Langford D (2013) Considerations for the use of SH-SY5Y neuroblastoma cells in neurobiology. *Methods Mol Biol* **1078**, 9-21.

[96] Hazra S, Batra RK, Tai HH, Sharma S, Cui X, Dubinett SM (2007) Pioglitazone and rosiglitazone decrease prostaglandin E2 in non-small-cell lung cancer cells by up-regulating 15-hydroxyprostaglandin dehydrogenase. *Mol Pharmacol* **71**, 1715-1720.

[97] Lee G, Elwood F, McNally J, Weiszmann J, Lindstrom M, Amaral K, Nakamura M, Miao S, Cao P, Learned RM, Chen JL, Li Y (2002) T0070907, a selective ligand for peroxisome proliferator-activated receptor gamma, functions as an antagonist of biochemical and cellular activities. *J Biol Chem* **277**, 19649-19657.

[98] Zaytseva YY, Wallis NK, Southard RC, Kilgore MW (2011) The PPARgamma antagonist T0070907 suppresses breast cancer cell proliferation and motility via both PPARgamma-dependent and -independent mechanisms. *Anticancer Res* **31**, 813-823.

[99] Ding L, Liang XG, Lou YJ (2007) Time-dependence of cardiomyocyte differentiation disturbed by peroxisome proliferator-activated receptor alpha inhibitor GW6471 in murine embryonic stem cells in vitro. *Acta Pharmacol Sin* **28**, 634-642.

[100] Garrido-Urbani S, Jemelin S, Deffert C, Carnesecchi S, Basset O, Szyndralewiez C, Heitz F, Page P, Montet X, Michalik L, Arbiser J, Ruegg C, Krause KH, Imhof BA (2011) Targeting vascular NADPH oxidase 1 blocks tumor angiogenesis through a PPARalpha mediated mechanism. *PLoS One* **6**, e14665.

[101] Chan EC, Pasikanti KK, Nicholson JK (2011) Global urinary metabolic profiling procedures using gas chromatography-mass spectrometry. *Nat Protoc* **6**, 1483-1499.

[102] Ejigu BA, Valkenborg D, Baggerman G, Vanaerschot M, Witters E, Dujardin JC, Burzykowski T, Berg M (2013) Evaluation of normalization methods to pave the way towards large-scale LC-MS-based metabolomics profiling experiments. *OMICS* **17**, 473-485.

[103] Wishart DS, Jewison T, Guo AC, Wilson M, Knox C, Liu Y, Djoumbou Y, Mandal R, Aziat F, Dong E, Bouatra S, Sinelnikov I, Arndt D, Xia J, Liu P, Yallou F, Bjorndahl T, Perez-Pineiro R, Eisner R, Allen F, Neveu V, Greiner R, Scalbert A (2013) HMDB 3.0--The Human Metabolome Database in 2013. *Nucleic Acids Res* **41**, D801-807.

[104] Kanehisa M, Goto S, Sato Y, Furumichi M, Tanabe M (2012) KEGG for integration and interpretation of large-scale molecular data sets. *Nucleic Acids Res* **40**, D109-114.

[105] Abu-Amero KK, Bosley TM (2005) Detection of mitochondrial respiratory dysfunction in circulating lymphocytes using resazurin. *Arch Pathol Lab Med* **129**, 1295-1298.

[106] Marroquin LD, Hynes J, Dykens JA, Jamieson JD, Will Y (2007) Circumventing the Crabtree effect: replacing media glucose with galactose increases susceptibility of HepG2 cells to mitochondrial toxicants. *Toxicol Sci* **97**, 539-547.

[107] Han KL, Choi JS, Lee JY, Song J, Joe MK, Jung MH, Hwang JK (2008) Therapeutic potential of peroxisome proliferators--activated receptor-alpha/gamma dual agonist with alleviation of endoplasmic reticulum stress for the treatment of diabetes. *Diabetes* **57**, 737-745.

[108] Anandatheerthavarada HK, Biswas G, Robin MA, Avadhani NG (2003) Mitochondrial targeting and a novel transmembrane arrest of Alzheimer's amyloid precursor protein impairs mitochondrial function in neuronal cells. *J Cell Biol* **161**, 41-54.

[109] Pavlov PF, Wiehager B, Sakai J, Frykman S, Behbahani H, Winblad B, Ankarcrona M (2011) Mitochondrial gamma-secretase participates in the metabolism of mitochondria-associated amyloid precursor protein. *FASEB J* **25**, 78-88.

[110] Ferreira IL, Resende R, Ferreiro E, Rego AC, Pereira CF (2010) Multiple defects in energy metabolism in Alzheimer's disease. *Curr Drug Targets* **11**, 1193-1206.

[111] Chen JX, Yan SS (2010) Role of mitochondrial amyloid-beta in Alzheimer's disease. *J Alzheimers Dis* **20 Suppl 2**, S569-578.

[112] Kim EJ, Cho SS, Jeong Y, Park KC, Kang SJ, Kang E, Kim SE, Lee KH, Na DL (2005) Glucose metabolism in early onset versus late onset Alzheimer's disease: an SPM analysis of 120 patients. *Brain* **128**, 1790-1801.

[113] Chen JX, Yan SD (2007) Amyloid-beta-induced mitochondrial dysfunction. *J Alzheimers Dis* **12**, 177-184.

[114] Galindo MF, Ikuta I, Zhu X, Casadesus G, Jordan J (2010) Mitochondrial biology in Alzheimer's disease pathogenesis. *J Neurochem* **114**, 933-945.

[115] Greene JG, Greenamyre JT (1995) Characterization of the excitotoxic potential of the reversible succinate dehydrogenase inhibitor malonate. *J Neurochem* **64**, 430-436.

[116] Greene JG, Porter RH, Eller RV, Greenamyre JT (1993) Inhibition of succinate dehydrogenase by malonic acid produces an "excitotoxic" lesion in rat striatum. *J Neurochem* **61**, 1151-1154.

[117] Morath MA, Okun JG, Muller IB, Sauer SW, Horster F, Hoffmann GF, Kolker S (2008) Neurodegeneration and chronic renal failure in methylmalonic aciduria--a pathophysiological approach. *J Inherit Metab Dis* **31**, 35-43.

[118] McCracken C, Hudson P, Ellis R, McCaddon A (2006) Methylmalonic acid and cognitive function in the Medical Research Council Cognitive Function and Ageing Study. *Am J Clin Nutr* **84**, 1406-1411.

[119] Fonteh AN, Harrington RJ, Tsai A, Liao P, Harrington MG (2007) Free amino acid and dipeptide changes in the body fluids from Alzheimer's disease subjects. *Amino Acids* **32**, 213-224.

[120] Masciopinto F, Di Pietro N, Corona C, Bomba M, Pipino C, Curcio M, Di Castelnuovo A, Ciavardelli D, Silvestri E, Canzoniero LM, Sekler I, Pandolfi A, Sensi SL (2012) Effects of long-term treatment with pioglitazone on cognition and glucose metabolism of PS1-KI, 3xTg-AD, and wild-type mice. *Cell Death Dis* **3**, e448.

[121] Reifel-Miller A, Otto K, Hawkins E, Barr R, Bensch WR, Bull C, Dana S, Klausing K, Martin JA, Rafaeloff-Phail R, Rafizadeh-Montrose C, Rhodes G, Robey R, Rojo I, Rungta D, Snyder D, Wilbur K, Zhang T, Zink R, Warshawsky A, Brozinick JT (2005) A peroxisome proliferator-activated receptor alpha/gamma dual agonist with a unique in vitro profile and potent glucose and lipid effects in rodent models of type 2 diabetes and dyslipidemia. *Mol Endocrinol* **19**, 1593-1605.

[122] Atherton HJ, Bailey NJ, Zhang W, Taylor J, Major H, Shockcor J, Clarke K, Griffin JL (2006) A combined 1H-NMR spectroscopy- and mass spectrometry-based metabolomic study of the PPAR-alpha null

mutant mouse defines profound systemic changes in metabolism linked to the metabolic syndrome. *Physiol Genomics* **27**, 178-186.

[123] Satapati S, He T, Inagaki T, Potthoff M, Merritt ME, Esser V, Mangelsdorf DJ, Kliewer SA, Browning JD, Burgess SC (2008) Partial resistance to peroxisome proliferator-activated receptor-alpha agonists in ZDF rats is associated with defective hepatic mitochondrial metabolism. *Diabetes* **57**, 2012-2021.

[124] Liu LP, Yan TH, Jiang LY, Hu W, Hu M, Wang C, Zhang Q, Long Y, Wang JQ, Li YQ, Hu M, Hong H (2013) Pioglitazone ameliorates memory deficits in streptozotocin-induced diabetic mice by reducing brain beta-amyloid through PPARgamma activation. *Acta Pharmacol Sin* **34**, 455-463.

[125] Minnich A, Tian N, Byan L, Bilder G (2001) A potent PPARalpha agonist stimulates mitochondrial fatty acid beta-oxidation in liver and skeletal muscle. *Am J Physiol Endocrinol Metab* **280**, E270-279.

[126] Cree MG, Newcomer BR, Herndon DN, Qian T, Sun D, Morio B, Zwetsloot JJ, Dohm GL, Fram RY, Mlcak RP, Aarsland A, Wolfe RR (2007) PPAR-alpha agonism improves whole body and muscle mitochondrial fat oxidation, but does not alter intracellular fat concentrations in burn trauma children in a randomized controlled trial. *Nutr Metab (Lond)* **4**, 9.

[127] Zhang X, Liu H, Wu J, Zhang X, Liu M, Wang Y (2009) Metabonomic alterations in hippocampus, temporal and prefrontal cortex with age in rats. *Neurochem Int* **54**, 481-487.

[128] Garcia-Alloza M, Robbins EM, Zhang-Nunes SX, Purcell SM, Betensky RA, Raju S, Prada C, Greenberg SM, Bacskai BJ, Frosch MP (2006) Characterization of amyloid deposition in the APPswe/PS1dE9 mouse model of Alzheimer disease. *Neurobiol Dis* **24**, 516-524.

[129] van Groen T, Kiliaan AJ, Kadish I (2006) Deposition of mouse amyloid beta in human APP/PS1 double and single AD model transgenic mice. *Neurobiol Dis* **23**, 653-662.

[130] Alexander G, Hanna A, Serna V, Younkin L, Younkin S, Janus C (2011) Increased aggression in males in transgenic Tg2576 mouse model of Alzheimer's disease. *Behav Brain Res* **216**, 77-83.

[131] Lalonde R, Fukuchi K, Strazielle C (2012) APP transgenic mice for modelling behavioural and psychological symptoms of dementia (BPSD). *Neurosci Biobehav Rev* **36**, 1357-1375.

[132] Ballard C, Corbett A (2013) Agitation and aggression in people with Alzheimer's disease. *Curr Opin Psychiatry* **26**, 252-259.

[133] Zahodne LB, Ornstein K, Cosentino S, Devanand DP, Stern Y (2013) Longitudinal Relationships Between Alzheimer Disease Progression and Psychosis, Depressed Mood, and Agitation/Aggression. *Am J Geriatr Psychiatry*.

[134] Molina JA, Jimenez-Jimenez FJ, Vargas C, Gomez P, de Bustos F, Orti-Pareja M, Tallon-Barranco A, Benito-Leon J, Arenas J, Enriquez-de-Salamanca R (1998) Cerebrospinal fluid levels of non-neurotransmitter amino acids in patients with Alzheimer's disease. *J Neural Transm* **105**, 279-286.

[135] Paban V, Manrique C, Filali M, Maunoir-Regimbal S, Fauvelle F, Alescio-Lautier B (2014) Therapeutic and preventive effects of

methylene blue on Alzheimer's disease pathology in a transgenic mouse model. *Neuropharmacology* **76 Pt A**, 68-79.

[136] Ross JM, Oberg J, Brene S, Coppotelli G, Terzioglu M, Pernold K, Goiny M, Sitnikov R, Kehr J, Trifunovic A, Larsson NG, Hoffer BJ, Olson L (2010) High brain lactate is a hallmark of aging and caused by a shift in the lactate dehydrogenase A/B ratio. *Proc Natl Acad Sci U S A* **107**, 20087-20092.

[137] Bittner DM, Heinze HJ, Kaufmann J (2013) Association of 1H-MR spectroscopy and cerebrospinal fluid biomarkers in Alzheimer's disease: diverging behavior at three different brain regions. *J Alzheimers Dis* **36**, 155-163.

[138] Jessen F, Lewczuk P, Gur O, Block W, Ende G, Frolich L, Hammen T, Arlt S, Kornhuber J, Kucinski T, Popp J, Peters O, Maier W, Traber F, Wiltfang J (2011) Association of N-acetylaspartate and cerebrospinal fluid Abeta42 in dementia. *J Alzheimers Dis* **27**, 393-399.

[139] Haass C, Selkoe DJ (2007) Soluble protein oligomers in neurodegeneration: lessons from the Alzheimer's amyloid beta-peptide. *Nat Rev Mol Cell Biol* **8**, 101-112.

[140] Iglesias-Gonzalez J, Sanchez-Iglesias S, Mendez-Alvarez E, Rose S, Hikima A, Jenner P, Soto-Otero R (2012) Differential toxicity of 6-hydroxydopamine in SH-SY5Y human neuroblastoma cells and rat brain mitochondria: protective role of catalase and superoxide dismutase. *Neurochem Res* **37**, 2150-2160.

[141] Weiss J, Sauer A, Herzog M, Boger RH, Haefeli WE, Benndorf RA (2009) Interaction of thiazolidinediones (glitazones) with the ATP-binding cassette transporters P-glycoprotein and breast cancer resistance protein. *Pharmacology* **84**, 264-270.

[142] Girardin F (2006) Membrane transporter proteins: a challenge for CNS drug development. *Dialogues Clin Neurosci* **8**, 311-321.

[143] Saneja A, Khare V, Alam N, Dubey RD, Gupta PN (2014) Advances in P-glycoprotein-based approaches for delivering anticancer drugs: pharmacokinetic perspective and clinical relevance. *Expert Opin Drug Deliv* **11**, 121-138.

[144] Cascorbi I (2011) P-glycoprotein: tissue distribution, substrates, and functional consequences of genetic variations. *Handb Exp Pharmacol*, 261-283.

[145] Choong E, Dobrinas M, Carrupt PA, Eap CB (2010) The permeability P-glycoprotein: a focus on enantioselectivity and brain distribution. *Expert Opin Drug Metab Toxicol* **6**, 953-965.

[146] Swanson CR, Joers V, Bondarenko V, Brunner K, Simmons HA, Ziegler TE, Kemnitz JW, Johnson JA, Emborg ME (2011) The PPAR-gamma agonist pioglitazone modulates inflammation and induces neuroprotection in parkinsonian monkeys. *J Neuroinflammation* **8**, 91.

[147] Takeda Pharmaceuticals America I (2008) ACTOS - pioglitazone hydrochloride tablet [package insert].

[148] Eskelinen MH, Ngandu T, Tuomilehto J, Soininen H, Kivipelto M (2009) Midlife coffee and tea drinking and the risk of late-life dementia: a population-based CAIDE study. *J Alzheimers Dis* **16**, 85-91.

[149] Santos C, Costa J, Santos J, Vaz-Carneiro A, Lunet N (2010) Caffeine intake and dementia: systematic review and meta-analysis. *J Alzheimers Dis* **20 Suppl 1**, S187-204.

[150] Cao C, Loewenstein DA, Lin X, Zhang C, Wang L, Duara R, Wu Y, Giannini A, Bai G, Cai J, Greig M, Schofield E, Ashok R, Small B, Potter H, Arendash GW (2012) High Blood caffeine levels in MCI linked to lack of progression to dementia. *J Alzheimers Dis* **30**, 559-572.

[151] Shukitt-Hale B, Miller MG, Chu YF, Lyle BJ, Joseph JA (2013) Coffee, but not caffeine, has positive effects on cognition and psychomotor behavior in aging. *Age (Dordr)* **35**, 2183-2192.

[152] Chu Y-F, Chang WH, Black RM, Liu JR, Sompol P, Chen Y, Wei H, Zhao Q, Cheng IH (2012) Crude caffeine reduces memory impairment and amyloid beta(1-42) levels in an Alzheimer's mouse model. *Food Chem* **135**, 2095-2102.

[153] Ho L, Varghese M, Wang J, Zhao W, Chen F, Knable LA, Ferruzzi M, Pasinetti GM (2012) Dietary supplementation with decaffeinated green coffee improves diet-induced insulin resistance and brain energy metabolism in mice. *Nutr Neurosci* **15**, 37-45.

[154] Olthof MR, van Dijk AE, Deacon CF, Heine RJ, van Dam RM (2011) Acute effects of decaffeinated coffee and the major coffee components chlorogenic acid and trigonelline on incretin hormones. *Nutr Metab (Lond)* **8**, 10.

[155] Viana AL, Fonseca M, Meireles EL, Duarte SM, Rodrigues MR, Paula FB (2012) Effects of the consumption of caffeinated and decaffeinated instant coffee beverages on oxidative stress induced by strenuous exercise in rats. *Plant Foods Hum Nutr* **67**, 82-87.

[156] Katz SN (1987) Decaffeination of Coffee In *Coffee*, Clarke RJ, Macrae R, eds. Springer Netherlands, pp. 59-71.

[157] Chu Y-F, Chen Y, Brown PH, Lyle BJ, Black RM, Cheng IH, Ou B, Prior RL (2012) Bioactivities of crude caffeine: Antioxidant activity, cyclooxygenase-2 inhibition, and enhanced glucose uptake. *Food Chem* **131**, 564-568.

[158] Farah A, de Paulis T, Moreira DP, Trugo LC, Martin PR (2006) Chlorogenic acids and lactones in regular and water-decaffeinated arabica coffees. *J Agric Food Chem* **54**, 374-381.

[159] Alves RC, Costa AS, Jerez M, Casal S, Sineiro J, Nunez MJ, Oliveira B (2010) Antiradical Activity, Phenolics Profile, and Hydroxymethylfurfural in Espresso Coffee: Influence of Technological Factors. *J Agric Food Chem*.

[160] Silverio Ados S, Pereira RG, Lima AR, Paula FB, Rodrigues MR, Baldissera L, Jr., Duarte SM (2013) The effects of the decaffeination of coffee samples on platelet aggregation in hyperlipidemic rats. *Plant Foods Hum Nutr* **68**, 268-273.

[161] Choi M-Y, Choi W, Park JH, Lim J, Kwon SW (2010) Determination of coffee origins by integrated metabolomic approach of combining multiple analytical data. *Food Chemistry* **121**, 1260-1268.

[162] Wei F, Furihata K, Koda M, Hu F, Kato R, Miyakawa T, Tanokura M (2012) (13)C NMR-Based Metabolomics for the Classification of

Green Coffee Beans According to Variety and Origin. *J Agric Food Chem*.

[163] Jumhawan U, Putri SP, Yusianto, Marwani E, Bamba T, Fukusaki E (2013) Selection of discriminant markers for authentication of asian palm civet coffee (kopi luwak): a metabolomics approach. *J Agric Food Chem* **61**, 7994-8001.

[164] Natella F, Nardini M, Di Felice M, Scaccini C (1999) Benzoic and cinnamic acid derivatives as antioxidants: structure-activity relation. *J Agric Food Chem* **47**, 1453-1459.

[165] Sroka Z, Cisowski W (2003) Hydrogen peroxide scavenging, antioxidant and anti-radical activity of some phenolic acids. *Food Chem Toxicol* **41**, 753-758.

[166] Karegoudar TB, Kim C-K (2000) Microbial degradation of monohydroxybenzoic acids. *Journal of microbiology (Seoul, Korea)* **38**, 53-61.

[167] Kau AL, Ahern PP, Griffin NW, Goodman AL, Gordon JI (2011) Human nutrition, the gut microbiome and the immune system. *Nature* **474**, 327-336.

[168] Guneral F, Bachmann C (1994) Age-related reference values for urinary organic acids in a healthy Turkish pediatric population. *Clin Chem* **40**, 862-866.

[169] Jeong SM, Kim SY, Kim DR, Jo SC, Nam KC, Ahn DU, Lee SC (2004) Effect of heat treatment on the antioxidant activity of extracts from citrus peels. *J Agric Food Chem* **52**, 3389-3393.

[170] Gold R, Linker RA, Stangel M (2012) Fumaric acid and its esters: an emerging treatment for multiple sclerosis with antioxidative mechanism of action. *Clin Immunol* **142**, 44-48.

[171] Becerra-Moreno A, Benavides J, Cisneros-Zevallos L, Jacobo-Velazquez DA (2012) Plants as biofactories: glyphosate-induced production of shikimic acid and phenolic antioxidants in wounded carrot tissue. *J Agric Food Chem* **60**, 11378-11386.

[172] Wheeler LA, Halula M, DeMeo M, Sutter VL, Finegold SM (1979) Metabolism of shikimic, quinic, and cyclohexanecarboxylic acids in germfree, conventional, and gnotobiotic rats. *Current Microbiology* **2**, 85-90.

[173] Vogt JA, Pencharz PB, Wolever TM (2004) L-Rhamnose increases serum propionate in humans. *Am J Clin Nutr* **80**, 89-94.

[174] Hall IH, Wong OT, Reynolds DJ, Chang JJ (1993) The hypolipidemic effects of 2-furoic acid in Sprague-Dawley rats. *Arch Pharm (Weinheim)* **326**, 15-23.

[175] Di Paolo G, Kim TW (2011) Linking lipids to Alzheimer's disease: cholesterol and beyond. *Nat Rev Neurosci* **12**, 284-296.

[176] Barrie SA, Wright JV, Pizzorno JE, Kutter E, Barron PC (1987) Comparative absorption of zinc picolinate, zinc citrate and zinc gluconate in humans. *Agents Actions* **21**, 223-228.

[177] Brewer GJ (2012) Copper excess, zinc deficiency, and cognition loss in Alzheimer's disease. *Biofactors* **38**, 107-113.

[178] Zhou J, Zhou S, Zeng S (2013) Experimental diabetes treated with trigonelline: effect on beta cell and pancreatic oxidative parameters. *Fundam Clin Pharmacol* **27**, 279-287.

Dataset for *in vitro* metabolic profiling experiments performed in Chapter 2

	Vehicle-treated CHO-WT									
2,3,4-Trihydroxybutyric acid tetrakis(trimethylsilyl) deriv.	7.40E-05	6.99E-05	7.04E-05	7.04E-05	6.62E-05	7.23E-05	7.20E-05	7.04E-05	7.32E-05	7.02E-05
2-Piperidinecarboxylic acid, trimethylsilyl ester	3.51E-03	4.56E-03	2.97E-03	3.69E-03	3.01E-03	2.55E-03	4.04E-03	3.33E-03	3.03E-03	3.76E-03
3,8-Dioxa-2,9-disiladecane, 2,2,9,9-tetramethyl-5,6-bis[(trimethylsilyl)oxy]-, (R*,S*)-	1.25E-03	1.26E-03	1.23E-03	1.24E-03	1.20E-03	1.24E-03	1.25E-03	1.23E-03	1.24E-03	1.24E-03
3à-(Trimethylsiloxy)cholest-5-ene	1.34E-04	1.30E-04	1.23E-04	1.17E-04	1.09E-04	1.08E-04	1.32E-04	1.20E-04	1.21E-04	1.27E-04
Acetic acid, [(trimethylsilyl)oxy]-, trimethylsilyl ester	4.27E-05	3.36E-05	3.40E-05	3.20E-05	3.12E-05	3.11E-05	3.82E-05	3.30E-05	3.69E-05	3.38E-05
Alanine, phenyl-, trimethylsilyl ester, dl-	7.71E-03	8.29E-03	6.74E-03	6.97E-03	5.86E-03	5.26E-03	8.00E-03	6.86E-03	6.49E-03	7.52E-03
Aminomalonic acid, tris(trimethylsilyl)-	4.26E-04	3.63E-04	3.45E-04	3.83E-04	4.02E-04	5.33E-04	3.95E-04	3.64E-04	4.80E-04	3.54E-04
Benzoic acid trimethylsilyl ester	8.00E-04	8.11E-04	7.94E-04	7.70E-04	8.43E-04	8.00E-04	8.06E-04	7.82E-04	8.00E-04	8.03E-04
Butanoic acid, 2-[(trimethylsilyl)amino]-, trimethylsilyl ester	1.12E-04	1.15E-04	1.15E-04	1.09E-04	1.18E-04	1.18E-04	1.13E-04	1.12E-04	1.15E-04	1.15E-04
Citric acid, tetrakis(trimethylsilyl) deriv. (mainlib)	4.58E-04	5.14E-04	5.24E-04	5.22E-04	4.31E-04	5.15E-04	4.86E-04	5.23E-04	4.86E-04	5.19E-04

Compound										
d-Galactose, 2,3,4,5,6-pentakis-O-(trimethylsilyl)-, o-methyloxyme, (1Z)-	1.82E-03	1.52E-03	1.46E-03	1.76E-03	1.30E-03	1.70E-03	1.67E-03	1.61E-03	1.76E-03	1.49E-03
D-Glucitol, 6-deoxy-1,2,3,4,5-pentakis-O-(trimethylsilyl)-	8.69E-05	7.75E-05	7.59E-05	8.02E-05	6.74E-05	7.72E-05	8.22E-05	7.81E-05	8.20E-05	7.67E-05
D-Ribose, 2,3,4,5-tetrakis-O-(trimethylsilyl)-	3.03E-02	3.00E-02	2.98E-02	3.01E-02	2.88E-02	2.96E-02	3.02E-02	2.99E-02	3.00E-02	2.99E-02
Ethanedioic acid, bis(trimethylsilyl) ester	2.61E-04	3.42E-04	2.73E-04	2.34E-04	3.59E-04	4.16E-04	3.01E-04	2.53E-04	3.38E-04	3.07E-04
d-glucose	3.67E-04	3.86E-04	3.78E-04	3.93E-04	3.81E-04	3.81E-04	3.76E-04	3.86E-04	3.74E-04	3.82E-04
Glutamic acid, N,O,O'-tris(trimethylsilyl)-I (mainlib)	8.40E-04	6.62E-04	9.17E-04	7.42E-04	9.30E-04	9.36E-04	7.51E-04	8.30E-04	8.88E-04	7.90E-04
Glycine, N,N-bis(trimethylsilyl)-, trimethylsilyl ester	2.25E-02	2.38E-02	2.32E-02	2.30E-02	2.31E-02	2.26E-02	2.31E-02	2.31E-02	2.25E-02	2.35E-02
Glycine, N-formyl-, trimethylsilyl ester	3.65E-04	3.69E-04	3.12E-04	3.37E-04	2.67E-04	3.08E-04	3.67E-04	3.24E-04	3.37E-04	3.40E-04
Hexadecanoic acid, trimethylsilyl ester	1.84E-03	1.35E-03	1.18E-03	1.01E-03	7.32E-04	6.58E-04	1.59E-03	1.09E-03	1.25E-03	1.26E-03
Hexanoic acid, 2-(methoxyimino)-, trimethylsilyl ester	3.63E-04	4.31E-04	3.68E-04	3.79E-04	3.46E-04	3.30E-04	3.97E-04	3.73E-04	3.46E-04	3.99E-04
Lactic acid, bis(trimethylsilyl)oxy-, ester (mainlib)	4.56E-01	4.68E-01	4.52E-01	4.56E-01	4.72E-01	4.71E-01	4.62E-01	4.54E-01	4.64E-01	4.60E-01
l-Alanine, N-(trimethylsilyl)-, trimethylsilyl ester	2.99E-02	3.17E-02	3.15E-02	3.01E-02	3.31E-02	3.17E-02	3.08E-02	3.08E-02	3.08E-02	3.16E-02
L-Aspartic acid, N-(trimethylsilyl)-, bis(trimethylsilyl) ester	4.76E	4.20E	4.99E	5.26E	5.11E	7.70E	4.48E	5.12E	6.23E	4.59E

-04	-04	-04	-04	-04	-04	-04	-04	-04	-04
L-Cystine, N,N'-bis(trimethylsilyl)-, bis(trimethylsilyl) ester	5.09E -04	6.11E -04	7.04E -04	7.72E -04	7.81E -04	8.70E -04	5.60E -04	7.38E -04	6.90E -04	6.57E -04
L-Isoleucine, N-(trimethylsilyl)-, trimethylsilyl ester	4.44E -02	4.63E -02	4.48E -02	4.40E -02	4.36E -02	4.33E -02	4.54E -02	4.44E -02	4.39E -02	4.55E -02
L-Leucine, N-(trimethylsilyl)-, trimethylsilyl ester	1.70E -02	1.90E -02	1.85E -02	1.80E -02	1.78E -02	1.86E -02	1.90E -02	1.82E -02	1.78E -02	1.77E -02
L-Lysine, N2,N6,N6-tris(trimethylsilyl)-, trimethylsilyl ester	1.27E -02	1.27E -02	1.35E -02	1.29E -02	1.37E -02	1.35E -02	1.27E -02	1.32E -02	1.31E -02	1.31E -02
L-Methionine, ethyl ester	2.65E -03	3.18E -03	2.41E -03	2.54E -03	2.16E -03	2.19E -03	2.92E -03	2.48E -03	2.42E -03	2.80E -03
L-Methionine, N-(trimethylsilyl)-, trimethylsilyl ester	7.85E -04	8.51E -04	8.46E -04	8.10E -04	8.08E -04	9.47E -04	8.18E -04	8.28E -04	8.66E -04	8.49E -04
L-Ornithine, N2,N5,N5-tris(trimethylsilyl)-, trimethylsilyl ester	5.37E -04	7.03E -04	6.17E -04	6.00E -04	7.03E -04	7.21E -04	7.70E -04	6.09E -04	6.29E -04	5.10E -04
L-Proline, 1-(trimethylsilyl)-, trimethylsilyl ester	3.59E -04	3.38E -04	3.74E -04	3.56E -04	3.63E -04	3.51E -04	3.48E -04	3.65E -04	3.55E -04	3.56E -04
L-Proline, 5-oxo-1-(trimethylsilyl)-, trimethylsilyl ester	1.37E -01	1.36E -01	1.41E -01	1.40E -01	1.27E -01	1.27E -01	1.36E -01	1.40E -01	1.32E -01	1.38E -01
L-Proline, ethyl ester	1.10E -03	1.13E -03	1.02E -03	1.00E -03	9.55E -04	8.44E -04	1.12E -03	1.01E -03	9.74E -04	1.07E -01
L-Serine, N,O-bis(trimethylsilyl)-, trimethylsilyl ester	9.28E -04	9.17E -04	1.03E -03	9.92E -04	1.02E -03	1.09E -03	9.23E -04	1.01E -03	1.01E -03	9.76E -04
l-Threonine, O-(trimethylsilyl)-, trimethylsilyl ester	1.48E -02	1.56E -02	1.42E -02	1.41E -02	1.36E -02	1.27E -02	1.52E -02	1.42E -02	1.38E -02	1.49E -02

Compound										
L-Tyrosine, N,O-bis(trimethylsilyl)-, trimethylsilyl ester	1.04E-02	1.05E-02	1.06E-02	1.01E-02	1.06E-02	1.07E-02	1.04E-02	1.09E-02	9.96E-03	1.03E-02
L-Valine, N-(trimethylsilyl)-, trimethylsilyl ester (Kishore-STDS)	3.33E-02	3.38E-02	3.39E-02	3.23E-02	3.55E-02	3.49E-02	3.37E-02	3.41E-02	3.25E-02	3.21E-02
Malic acid, tris(trimethylsilyl) ester	1.20E-04	1.15E-04	1.14E-04	1.26E-04	1.05E-04	1.09E-04	1.15E-04	1.13E-04	1.27E-04	1.25E-04
Malonic acid, bis(2-trimethylsilylethyl ester	5.56E-06	5.32E-06	5.31E-06	5.84E-06	5.19E-06	6.37E-06	5.73E-06	4.89E-06	6.23E-06	5.46E-06
N,O,O-Tris(trimethylsilyl)-L-threonine	6.22E-03	6.46E-03	6.49E-03	5.88E-03	6.99E-03	6.55E-03	6.37E-03	6.61E-03	5.83E-03	5.93E-03
N,O-Bis(trimethylsilyl)-L-phenylalanine	3.18E-03	3.43E-03	3.36E-03	2.97E-03	3.82E-03	3.58E-03	3.26E-03	3.46E-03	2.90E-03	3.04E-03
n-Butylamine, N,N-bis(trimethylsilyl)	1.52E-04	1.49E-04	1.44E-04	1.64E-04	1.39E-04	1.56E-04	1.53E-04	1.35E-04	1.69E-04	1.59E-04
Octadecanoic acid, trimethylsilyl ester	8.17E-04	7.91E-04	7.27E-04	9.85E-04	4.74E-04	5.59E-04	6.83E-04	7.72E-04	8.62E-04	1.11E-03
Oleic acid, trimethylsilyl ester	9.35E-05	1.21E-04	9.05E-05	1.40E-04	5.12E-05	4.91E-05	8.39E-05	9.71E-05	8.99E-05	1.90E-04
Pantothenic acid, O,O,O-tris(trimethylsilyl) deriv.	9.27E-05	9.56E-05	9.22E-05	9.70E-05	9.18E-05	8.81E-05	9.36E-05	9.08E-05	9.46E-05	9.93E-05
Pentanedioic acid, 2-[(trimethylsilyl)oxy]-, bis(trimethylsilyl) ester	1.09E-04	1.07E-04	1.12E-04	1.06E-04	1.07E-04	1.11E-04	1.10E-04	1.13E-04	1.05E-04	1.07E-04
Pentanoic acid, 2-(methoxyimino)-3-methyl-, trimethylsilyl ester	3.20E-04	2.68E-04	2.97E-04	3.17E-04	2.52E-04	2.68E-04	3.04E-04	2.91E-04	3.49E-04	2.84E-04
Pentasiloxane, dodecamethyl-	4.22E-04	4.68E-04	4.33E-04	4.58E-04	4.66E-04	3.90E-04	4.67E-04	3.99E-04	4.46E-04	4.69E-04

Compound										
Propanedioic acid, bis(trimethylsilyl) ester:2	7.53E-04	7.42E-04	7.25E-04	7.73E-04	7.35E-04	7.65E-04	7.47E-04	7.49E-04	7.59E-04	7.34E-04
Propanedioic acid, methyl-, bis(trimethylsilyl) ester	1.43E-04	1.29E-04	1.26E-04	1.28E-04	1.24E-04	1.30E-04	1.46E-04	1.27E-04	1.36E-04	1.37E-04
Propanoic acid, 2-(methoxyimino)-, trimethylsilyl ester	4.60E-03	5.52E-03	5.11E-03	4.94E-03	4.67E-03	4.33E-03	5.06E-03	5.03E-03	4.47E-03	5.31E-03
Propanoic acid, 2,3-bis[(trimethylsilyl)oxy]-, trimethylsilyl ester	5.22E-05	4.89E-05	4.69E-05	4.71E-05	4.53E-05	4.56E-05	5.05E-05	4.70E-05	4.89E-05	4.79E-05
Propanoic acid, 2-[(trimethylsilyl)oxy]-, trimethylsilyl ester:	3.23E-02	1.13E-02	3.30E-02	3.30E-02	3.45E-02	3.51E-02	2.18E-02	3.30E-02	3.37E-02	2.22E-02
Propanoic acid, 2-[(trimethylsilyl)oxy]-, trimethylsilyl ester	5.44E-04	5.59E-04	5.43E-04	5.41E-04	5.47E-04	5.61E-04	5.51E-04	5.42E-04	5.52E-04	5.51E-04
Pyrimidine, 2,4-bis[(trimethylsilyl)oxy]-	4.17E-04	4.10E-04	3.92E-04	3.86E-04	3.65E-04	3.69E-04	4.13E-04	3.89E-04	3.93E-04	4.01E-04
Ribitol, 1,2,3,4,5-pentakis-O-(trimethylsilyl)-	1.00E-03	7.29E-04	7.08E-04	8.79E-04	1.04E-03	8.09E-04	8.64E-04	7.93E-04	9.05E-04	7.18E-04
Silanamine, N-[2-[3,4-bis[(trimethylsilyl)oxy]phenyl]ethyl]-1,1,1-trimethyl-N-(trimethylsilyl)-	7.61E-05	6.79E-05	9.10E-05	7.98E-05	6.04E-05	6.33E-05	7.20E-05	8.54E-05	6.97E-05	7.94E-05
Succinic acid (tms) (mainlib)	2.18E-04	2.27E-04	2.15E-04	2.06E-04	2.03E-04	2.08E-04	2.23E-04	2.10E-04	2.13E-04	2.21E-04
Trimethylsilyl ether of glycerol	1.31E-03	1.53E-03	1.49E-03	1.49E-03	1.50E-03	1.32E-03	1.52E-03	1.49E-03	1.32E-03	1.31E-03
Tryptophan, bis(trimethylsilyl)-	4.37E-05	4.84E-05	3.71E-05	3.73E-05	3.20E-05	4.37E-05	3.72E-05	3.37E-05	3.37E-05	4.28E-05

Tyrosine, O-trimethylsilyl-, trimethylsilyl ester	1.65E-03	2.15E-03	1.26E-03	1.40E-03	1.04E-03	9.61E-04	1.90E-03	1.33E-03	1.31E-03	1.70E-03
Urea, N,N'-bis(trimethylsilyl)-	7.17E-03	7.52E-03	7.83E-03	7.88E-03	8.41E-03	8.89E-03	7.35E-03	7.85E-03	8.03E-03	7.68E-03
Uridine 3TMS (Kishore-STDS)	4.91E-04	3.43E-04	2.89E-04	2.83E-04	2.71E-04	3.16E-04	4.17E-04	2.86E-04	4.04E-04	3.16E-04

Vehicle-treated CHO-APP										
2,3,4-Trihydroxybutyric acid tetrakis(trimethylsilyl) deriv.	7.72E-05	6.47E-05	7.44E-05	7.09E-05	6.50E-05	6.73E-05	7.30E-05	6.67E-05	6.92E-05	8.07E-05
2-Piperidinecarboxylic acid, trimethylsilyl ester	3.41E-03	2.68E-03	3.80E-03	2.65E-03	3.81E-03	3.02E-03	3.81E-03	2.93E-03	2.73E-03	3.76E-03
3,8-Dioxa-2,9-disiladecane, 2,2,9,9-tetramethyl-5,6-bis[(trimethylsilyl)oxy]-, (R*,S*)-	1.25E-03	1.26E-03	1.25E-03	1.24E-03	1.22E-03	1.20E-03	1.23E-03	1.23E-03	1.22E-03	1.21E-03
3à-(Trimethylsiloxy)cholest-5-ene	1.37E-04	1.42E-04	1.23E-04	1.17E-04	1.10E-04	1.12E-04	1.10E-04	1.15E-04	1.17E-04	1.19E-04
Acetic acid, [(trimethylsilyl)oxy]-, trimethylsilyl ester	2.88E-05	2.95E-05	3.21E-05	3.93E-05	3.02E-05	3.10E-05	2.75E-05	2.82E-05	3.06E-05	4.44E-05
Alanine, phenyl-, trimethylsilyl ester, dl-	6.70E-03	4.99E-03	7.08E-03	5.57E-03	7.00E-03	5.33E-03	6.19E-03	7.00E-03	5.12E-03	7.35E-03
Aminomalonic acid, tris(trimethylsilyl)-	5.41E-04	7.52E-04	5.28E-04	4.58E-04	2.91E-04	4.60E-04	4.92E-04	3.89E-04	5.47E-04	5.08E-04
Benzoic acid trimethylsilyl ester	8.31E-04	8.51E-04	8.14E-04	8.23E-04	7.47E-04	8.09E-04	8.19E-04	7.98E-04	8.63E-04	8.36E-04

Compound										
Butanoic acid, 2-[(trimethylsilyl)amino]-, trimethylsilyl ester	1.20E-04	1.01E-04	1.11E-04	1.09E-04	1.06E-04	1.14E-04	1.20E-04	1.22E-04	1.24E-04	1.09E-04
Citric acid, tetrakis(trimethylsilyl) deriv. (mainlib)	5.37E-04	5.27E-04	5.47E-04	5.47E-04	5.48E-04	5.88E-04	5.58E-04	5.59E-04	6.08E-04	6.92E-04
d-Galactose, 2,3,4,5,6-pentakis-O-(trimethylsilyl)-, o-methyloxyme, (1Z)-	1.40E-03	1.82E-03	1.80E-03	1.80E-03	1.70E-03	1.77E-03	1.40E-03	1.55E-03	1.32E-03	1.38E-03
D-Glucitol, 6-deoxy-1,2,3,4,5-pentakis-O-(trimethylsilyl)-	7.61E-05	8.84E-05	8.05E-05	8.27E-05	7.36E-05	7.62E-05	7.00E-05	7.57E-05	6.87E-05	6.57E-05
D-Ribose, 2,3,4,5-tetrakis-O-(trimethylsilyl)-	2.96E-02	3.04E-02	2.96E-02	3.00E-02	3.04E-02	2.89E-02	2.91E-02	2.95E-02	2.90E-02	2.90E-02
Ethanedioic acid, bis(trimethylsilyl) ester	3.54E-04	3.43E-04	2.79E-04	2.85E-04	2.42E-04	4.40E-04	4.27E-04	4.29E-04	4.60E-04	4.60E-04
d-glucose	6.86E-04	6.49E-04	6.14E-04	6.73E-04	6.06E-04	5.83E-04	6.71E-04	5.75E-04	7.49E-04	6.81E-04
Glutamic acid, N,O,O'-tris(trimethylsilyl)-I (mainlib)	9.29E-04	6.41E-04	6.24E-04	5.14E-04	5.06E-04	9.89E-04	8.42E-04	9.03E-04	8.76E-04	8.59E-04
Glycine, N,N-bis(trimethylsilyl)-, trimethylsilyl ester	2.18E-02	1.89E-02	2.13E-02	2.09E-02	2.22E-02	2.10E-02	2.23E-02	2.27E-02	2.16E-02	2.13E-02
Glycine, N-formyl-, trimethylsilyl ester	3.44E-04	2.50E-04	2.44E-04	3.44E-04	3.33E-04	3.77E-04	2.84E-04	4.36E-04	2.78E-04	2.91E-04
Hexadecanoic acid, trimethylsilyl ester	6.18E-04	1.35E-03	5.91E-04	9.29E-04	6.64E-04	7.84E-04	6.92E-04	1.00E-03	6.31E-04	1.44E-03
Hexanoic acid, 2-(methoxyimino)-, trimethylsilyl ester	3.95E-04	3.38E-04	4.44E-04	3.42E-04	4.58E-04	3.08E-04	3.14E-04	3.49E-04	3.23E-04	3.46E-04
Lactic acid, bis(trimethylsilyl)oxy-, ester (mainlib)	4.46E-04	4.84E-04	4.52E-04	4.59E-04	4.42E-04	4.59E-04	4.58E-04	4.48E-04	4.64E-04	4.69E-04

	-01	-01	-01	-01	-01	-01	-01	-01	-01	-01
l-Alanine, N-(trimethylsilyl)-, trimethylsilyl ester	2.87E-02	2.54E-02	2.60E-02	2.62E-02	2.33E-02	2.77E-02	2.81E-02	2.97E-02	2.77E-02	2.69E-02
L-Aspartic acid, N-(trimethylsilyl)-, bis(trimethylsilyl) ester	6.36E-04	7.93E-04	6.13E-04	5.50E-04	5.52E-04	5.25E-04	5.79E-04	5.24E-04	7.47E-04	7.50E-04
L-Cystine, N,N'-bis(trimethylsilyl)-, bis(trimethylsilyl) ester	6.69E-04	7.83E-04	8.66E-04	7.47E-04	6.96E-04	8.55E-04	8.08E-04	8.73E-04	9.34E-04	9.34E-04
L-Isoleucine, N-(trimethylsilyl)-, trimethylsilyl ester	4.35E-02	3.99E-02	4.28E-02	4.23E-02	4.31E-02	4.17E-02	4.33E-02	4.36E-02	4.28E-02	4.15E-02
L-Leucine, N-(trimethylsilyl)-, trimethylsilyl ester	1.75E-02	1.45E-02	1.53E-02	1.48E-02	1.56E-02	1.62E-02	1.84E-02	1.87E-02	1.85E-02	1.62E-02
L-Lysine, N2,N6,N6-tris(trimethylsilyl)-, trimethylsilyl ester	1.10E-02	1.26E-02	1.09E-02	1.18E-02	1.15E-02	1.17E-02	1.18E-02	1.03E-02	1.14E-02	1.03E-02
L-Methionine, ethyl ester	2.76E-03	2.59E-03	3.24E-03	2.61E-03	3.22E-03	2.18E-03	2.20E-03	2.19E-03	1.93E-03	2.08E-03
L-Methionine, N-(trimethylsilyl)-, trimethylsilyl ester	1.06E-03	7.92E-04	1.01E-03	7.61E-04	1.01E-03	8.75E-04	8.36E-04	9.55E-04	8.63E-04	8.89E-04
L-Ornithine, N2,N5,N5-tris(trimethylsilyl)-, trimethylsilyl ester	5.27E-04	4.24E-04	4.15E-04	3.62E-04	4.28E-04	5.26E-04	5.08E-04	5.55E-04	5.52E-04	5.25E-04
L-Proline, 1-(trimethylsilyl)-, trimethylsilyl ester	3.64E-04	3.04E-04	3.24E-04	3.11E-04	2.98E-04	3.63E-04	3.70E-04	3.94E-04	3.51E-04	3.09E-04
L-Proline, 5-oxo-1-(trimethylsilyl)-, trimethylsilyl ester	1.43E-01	1.23E-01	1.40E-01	1.37E-01	1.53E-01	1.39E-01	1.32E-01	1.39E-01	1.33E-01	1.34E-01
L-Proline, ethyl ester	9.42E-04	8.75E-04	9.17E-04	9.15E-04	8.49E-04	8.67E-04	8.63E-04	8.36E-04	7.35E-04	7.27E-04

Compound										
L-Serine, N,O-bis(trimethylsilyl)-, trimethylsilyl ester	1.31E-03	1.08E-03	1.11E-03	1.11E-03	1.13E-03	1.32E-03	1.36E-03	1.42E-03	1.39E-03	1.29E-03
l-Threonine, O-(trimethylsilyl)-, trimethylsilyl ester	1.37E-02	1.32E-02	1.41E-02	1.40E-02	1.41E-02	1.30E-02	1.30E-02	1.28E-02	1.24E-02	1.27E-02
L-Tyrosine, N,O-bis(trimethylsilyl)-, trimethylsilyl ester	1.11E-02	1.02E-02	1.03E-02	9.99E-03	9.66E-03	1.05E-02	1.07E-02	1.09E-02	1.07E-02	1.04E-02
L-Valine, N-(trimethylsilyl)-, trimethylsilyl ester (Kishore-STDS)	3.54E-02	3.21E-02	3.30E-02	3.30E-02	3.32E-02	3.50E-02	3.68E-02	3.81E-02	3.77E-02	3.52E-02
Malic acid, tris(trimethylsilyl) ester	1.24E-04	1.33E-04	1.21E-04	1.13E-04	9.08E-05	1.09E-04	1.14E-04	1.06E-04	1.02E-04	1.05E-04
Malonic acid, bis(2-trimethylsilylethyl ester	8.16E-06	5.03E-06	7.03E-06	6.82E-06	8.40E-06	5.25E-06	5.00E-06	7.33E-06	4.41E-06	5.99E-06
N,O,O-Tris(trimethylsilyl)-L-threonine	6.95E-03	7.73E-03	6.91E-03	5.93E-03	6.17E-03	6.83E-03	7.29E-03	6.00E-03	7.47E-03	5.82E-03
N,O-Bis(trimethylsilyl)-L-phenylalanine	3.60E-03	3.00E-03	3.19E-03	3.56E-03	3.16E-03	3.88E-03	3.54E-03	3.81E-03	3.54E-03	3.55E-03
n-Butylamine, N,N-bis(trimethylsilyl)	1.46E-04	1.60E-04	1.62E-04	1.54E-04	1.53E-04	1.39E-04	1.61E-04	1.45E-04	1.53E-04	1.44E-04
Octadecanoic acid, trimethylsilyl ester	8.91E-04	8.68E-04	6.67E-04	6.46E-04	4.13E-04	5.46E-04	4.92E-04	4.75E-04	4.90E-04	4.70E-04
Oleic acid, trimethylsilyl ester	1.24E-04	9.98E-05	8.08E-05	6.18E-05	2.84E-05	5.65E-05	4.64E-05	4.35E-05	5.01E-05	4.67E-05
Pantothenic acid, O,O,O-tris(trimethylsilyl) deriv.	9.56E-05	9.56E-05	9.48E-05	9.17E-05	8.96E-05	8.93E-05	8.63E-05	9.01E-05	8.52E-05	8.60E-05
Pentanedioic acid, 2-[(trimethylsilyl)oxy]-, bis(trimethylsilyl)	1.13E-04	1.14E-04	1.17E-04	1.19E-04	1.22E-04	1.15E-04	1.12E-04	1.18E-04	1.12E-04	1.16E-04

ester	-04	-04	-04	-04	-04	-04	-04	-04	-04	-04
Pentanoic acid, 2-(methoxyimino)-3-methyl-, trimethylsilyl ester	3.16E-04	2.98E-04	3.56E-04	2.64E-04	3.29E-04	2.37E-04	2.28E-04	2.45E-04	2.50E-04	2.60E-04
Pentasiloxane, dodecamethyl-	4.23E-04	4.29E-04	4.43E-04	4.47E-04	4.81E-04	4.38E-04	4.40E-04	4.31E-04	4.12E-04	4.20E-04
Propanedioic acid, bis(trimethylsilyl) ester:2	8.15E-04	8.16E-04	7.96E-04	7.87E-04	8.08E-04	7.61E-04	8.36E-04	7.65E-04	8.31E-04	8.43E-04
Propanedioic acid, methyl-, bis(trimethylsilyl) ester	1.44E-04	1.55E-04	1.40E-04	1.42E-04	1.68E-04	1.69E-04	1.55E-04	1.53E-04	1.57E-04	1.52E-04
Propanoic acid, 2-(methoxyimino)-, trimethylsilyl ester	4.84E-03	3.95E-03	5.03E-03	4.16E-03	5.45E-03	3.97E-03	4.30E-03	4.62E-03	4.40E-03	4.53E-03
Propanoic acid, 2,3-bis[(trimethylsilyl)oxy]-, trimethylsilyl ester	4.77E-05	5.87E-05	4.73E-05	5.40E-05	4.55E-05	4.68E-05	4.67E-05	4.66E-05	4.59E-05	4.46E-05
Propanoic acid, 2-[(trimethylsilyl)oxy]-, trimethylsilyl ester:	3.06E-02	3.21E-02	3.23E-02	3.19E-02	3.08E-02	3.13E-02	3.29E-02	3.24E-02	3.31E-02	3.26E-02
Propanoic acid, 2-[(trimethylsilyl)oxy]-, trimethylsilyl ester	5.32E-04	5.49E-04	5.39E-04	5.42E-04	5.20E-04	5.22E-04	5.50E-04	5.35E-04	5.46E-04	5.37E-04
Pyrimidine, 2,4-bis[(trimethylsilyl)oxy]-	3.69E-04	3.57E-04	3.53E-04	3.39E-04	3.35E-04	3.28E-04	3.38E-04	3.33E-04	3.31E-04	3.21E-04
Ribitol, 1,2,3,4,5-pentakis-O-(trimethylsilyl)-	7.34E-04	6.56E-04	8.50E-04	7.30E-04	8.62E-04	8.31E-04	7.08E-04	7.64E-04	6.80E-04	6.69E-04
Silanamine, N-[2-[3,4-bis[(trimethylsilyl)oxy]phenyl]ethyl]-1,1,1-trimethyl-N-(trimethylsilyl)-	6.16E-05	6.46E-05	5.20E-05	5.85E-05	4.48E-05	5.18E-05	5.66E-05	5.71E-05	6.42E-05	5.91E-05
Succinic acid (tms) (mainlib)	2.02E-04	1.98E-04	2.04E-04	1.99E-04	2.00E-04	1.91E-04	1.91E-04	1.90E-04	2.06E-04	1.96E-04

Trimethylsilyl ether of glycerol	1.34E-03	1.36E-03	1.33E-03	1.32E-03	1.29E-03	1.29E-03	1.35E-03	1.33E-03	1.34E-03	1.32E-03
Tryptophan, bis(trimethylsilyl)-	3.42E-05	2.23E-05	3.10E-05	3.06E-05	4.13E-05	2.19E-05	3.56E-05	3.14E-05	2.79E-05	3.45E-05
Tyrosine, O-trimethylsilyl-, trimethylsilyl ester	1.31E-03	1.15E-03	9.04E-04	1.42E-03	9.43E-04	1.71E-03	1.11E-03	9.62E-04	1.40E-03	9.62E-04
Urea, N,N'-bis(trimethylsilyl)-	7.79E-03	8.93E-03	8.01E-03	8.83E-03	8.07E-03	8.25E-03	7.77E-03	8.70E-03	7.92E-03	8.60E-03
Uridine 3TMS (Kishore-STDS)	5.43E-04	2.71E-04	4.41E-04	3.50E-04	2.12E-04	3.47E-04	3.91E-04	5.91E-04	3.87E-04	4.28E-04

188

PIO-treated CHO-APP										
2,3,4-Trihydroxybutyric acid tetrakis(trimethylsilyl) deriv.	6.99E-05	7.57E-05	7.09E-05	7.17E-05	6.79E-05	6.74E-05	7.85E-05	7.65E-05	7.55E-05	6.13E-05
2-Piperidinecarboxylic acid, trimethylsilyl ester	5.63E-03	3.56E-03	2.99E-03	4.53E-03	3.35E-03	3.08E-03	4.46E-03	4.19E-03	3.26E-03	2.86E-03
3,8-Dioxa-2,9-disiladecane, 2,2,9,9-tetramethyl-5,6-bis[(trimethylsilyl)oxy]-, (R*,S*)-	1.22E-03	1.24E-03	1.23E-03	1.23E-03	1.22E-03	1.20E-03	1.15E-03	1.19E-03	1.27E-03	1.19E-03
3à-(Trimethylsiloxy)cholest-5-ene	1.37E-04	1.28E-04	1.34E-04	1.09E-04	1.07E-04	1.22E-04	1.01E-04	1.22E-04	1.11E-04	1.07E-04
Acetic acid, [(trimethylsilyl)oxy]-, trimethylsilyl ester	3.32E-05	3.60E-05	3.73E-05	3.29E-05	3.51E-05	2.99E-05	3.84E-05	4.24E-05	3.72E-05	2.67E-05
Alanine, phenyl-, trimethylsilyl ester, dl-	7.91E-03	6.94E-03	5.79E-03	7.06E-03	5.94E-03	5.94E-03	6.98E-03	6.19E-03	6.30E-03	5.26E-03

Compound										
Aminomalonic acid, tris(trimethylsilyl)-	5.25E-04	6.65E-04	5.37E-04	4.96E-04	5.91E-04	5.31E-04	2.51E-04	5.13E-04	6.75E-04	6.10E-04
Benzoic acid trimethylsilyl ester	7.35E-04	7.46E-04	7.77E-04	7.45E-04	7.61E-04	7.59E-04	7.31E-04	8.03E-04	8.01E-04	8.08E-04
Butanoic acid, 2-[(trimethylsilyl)amino]-, trimethylsilyl ester	1.04E-04	1.24E-04	1.19E-04	1.11E-04	1.13E-04	1.10E-04	9.47E-05	8.91E-05	1.14E-04	1.13E-04
Citric acid, tetrakis(trimethylsilyl) deriv. (mainlib)	4.52E-04	4.69E-04	5.12E-04	4.27E-04	4.91E-04	5.02E-04	3.67E-04	4.08E-04	4.19E-04	4.72E-04
d-Galactose, 2,3,4,5,6-pentakis-O-(trimethylsilyl)-, o-methyloxyme, (1Z)-	1.47E-03	1.85E-03	1.80E-03	1.81E-03	1.80E-03	1.49E-03	1.66E-03	1.65E-03	1.72E-03	1.42E-03
D-Glucitol, 6-deoxy-1,2,3,4,5-pentakis-O-(trimethylsilyl)-	7.22E-05	8.67E-05	8.13E-05	8.32E-05	7.83E-05	6.95E-05	7.19E-05	7.41E-05	8.05E-05	6.82E-05
D-Ribose, 2,3,4,5-tetrakis-O-(trimethylsilyl)-	2.99E-02	3.05E-02	3.00E-02	2.99E-02	3.02E-02	3.05E-02	2.92E-02	2.87E-02	2.96E-02	2.85E-02
Ethanedioic acid, bis(trimethylsilyl) ester	4.04E-04	5.42E-04	4.62E-04	3.50E-04	4.36E-04	3.74E-04	4.41E-04	3.08E-04	3.17E-04	3.25E-04
d-glucose	6.05E-04	5.14E-04	4.75E-04	6.94E-04	5.66E-04	6.98E-04	6.26E-04	6.83E-04	5.19E-04	7.03E-04
Glutamic acid, N,O,O'-tris(trimethylsilyl)-I (mainlib)	7.60E-04	9.48E-04	1.05E-03	7.81E-04	9.50E-04	9.48E-04	4.08E-04	5.39E-04	7.84E-04	8.85E-04
Glycine, N,N-bis(trimethylsilyl)-, trimethylsilyl ester	2.08E-02	2.01E-02	1.95E-02	2.04E-02	2.01E-02	2.03E-02	1.93E-02	1.68E-02	1.94E-02	2.03E-02
Glycine, N-formyl-, trimethylsilyl ester	2.47E-04	2.39E-04	2.66E-04	2.74E-04	2.61E-04	2.57E-04	2.63E-04	3.36E-04	3.18E-04	2.22E-04
Hexadecanoic acid, trimethylsilyl ester	1.45E-04	1.25E-04	1.14E-04	7.87E-04	7.48E-04	7.08E-04	6.70E-04	7.12E-04	6.04E-04	5.35E-04

-03	-03	-03	-04	-04	-04	-04	-04	-04	-04
Hexanoic acid, 2-(methoxyimino)-, trimethylsilyl ester									
4.95E-04	4.35E-04	4.86E-04	4.31E-04	4.35E-04	4.59E-04	1.82E-04	1.81E-04	1.27E-04	2.41E-04
Lactic acid, bis(trimethylsilyl)oxy-, ester (mainlib)									
4.24E-01	4.15E-01	4.38E-01	4.28E-01	4.36E-01	4.38E-01	4.98E-01	5.09E-01	4.62E-01	4.58E-01
l-Alanine, N-(trimethylsilyl)-, trimethylsilyl ester									
2.20E-02	2.52E-02	2.54E-02	2.20E-02	2.44E-02	2.48E-02	2.02E-02	1.87E-02	2.42E-02	2.31E-02
L-Aspartic acid, N-(trimethylsilyl)-, bis(trimethylsilyl) ester									
2.38E-04	3.40E-04	4.71E-04	3.38E-04	4.79E-04	4.49E-04	2.29E-04	4.08E-04	4.72E-04	5.29E-04
L-Cystine, N,N'-bis(trimethylsilyl)-, bis(trimethylsilyl) ester									
3.85E-04	7.02E-04	7.73E-04	6.04E-04	6.87E-04	6.23E-04	2.62E-04	3.99E-04	5.46E-04	7.30E-04
L-Isoleucine, N-(trimethylsilyl)-, trimethylsilyl ester									
4.56E-02	4.60E-02	4.41E-02	4.51E-02	4.40E-02	4.37E-02	4.22E-02	4.45E-02	4.41E-02	4.41E-02
L-Leucine, N-(trimethylsilyl)-, trimethylsilyl ester									
1.69E-02	2.06E-02	1.96E-02	1.82E-02	1.91E-02	1.85E-02	1.71E-02	1.80E-02	1.80E-02	2.26E-02
L-Lysine, N2,N6,N6-tris(trimethylsilyl)-, trimethylsilyl ester									
1.30E-02	1.40E-02	1.40E-02	1.32E-02	1.34E-02	1.39E-02	1.29E-02	1.08E-02	1.26E-02	1.35E-02
L-Methionine, ethyl ester									
3.73E-03	3.14E-03	3.17E-03	3.22E-03	2.76E-03	2.96E-03	2.08E-03	1.82E-03	1.79E-03	1.96E-03
L-Methionine, N-(trimethylsilyl)-, trimethylsilyl ester									
1.01E-03	1.18E-03	1.23E-03	1.00E-03	1.05E-03	1.13E-03	5.49E-04	5.28E-04	6.11E-04	1.01E-03
L-Ornithine, N2,N5,N5-tris(trimethylsilyl)-, trimethylsilyl ester									
3.93E-04	5.68E-04	6.28E-04	4.47E-04	5.64E-04	5.68E-04	4.37E-04	3.91E-04	5.04E-04	5.52E-04
L-Proline, 1-(trimethylsilyl)-, trimethylsilyl ester									
2.91E-04	3.63E-04	3.40E-04	2.74E-04	2.98E-04	3.04E-04	1.99E-04	1.82E-04	2.60E-04	3.53E-04

Compound										
L-Proline, 5-oxo-1-(trimethylsilyl)-, trimethylsilyl ester	1.51E-01	1.55E-01	1.45E-01	1.52E-01	1.50E-01	1.49E-01	1.11E-01	1.17E-01	1.34E-01	1.39E-01
L-Proline, ethyl ester	1.04E-03	9.01E-04	8.40E-04	8.16E-04	7.53E-04	7.70E-04	7.28E-04	6.07E-04	6.81E-04	6.16E-04
L-Serine, N,O-bis(trimethylsilyl)-, trimethylsilyl ester	1.14E-03	1.42E-03	1.29E-03	1.21E-03	1.23E-03	1.21E-03	8.47E-04	8.47E-04	1.09E-03	1.62E-03
l-Threonine, O-(trimethylsilyl)-, trimethylsilyl ester	1.54E-02	1.39E-02	1.37E-02	1.43E-02	1.36E-02	1.37E-02	1.28E-02	1.22E-02	1.31E-02	1.13E-02
L-Tyrosine, N,O-bis(trimethylsilyl)-, trimethylsilyl ester	1.08E-02	1.17E-02	1.17E-02	1.08E-02	1.13E-02	1.15E-02	9.88E-03	9.37E-03	1.08E-02	1.10E-02
L-Valine, N-(trimethylsilyl)-, trimethylsilyl ester (Kishore-STDS)	3.18E-02	3.64E-02	3.58E-02	3.38E-02	3.47E-02	3.48E-02	2.85E-02	2.72E-02	3.44E-02	3.69E-02
Malic acid, tris(trimethylsilyl) ester	9.99E-05	1.13E-04	1.15E-04	9.69E-05	9.24E-05	9.04E-05	1.00E-04	1.06E-04	1.07E-04	1.05E-04
Malonic acid, bis(2-trimethylsilylethyl ester	8.22E-06	8.08E-06	7.77E-06	7.70E-06	6.00E-06	6.31E-06	3.52E-06	3.66E-06	3.95E-06	7.73E-06
N,O,O-Tris(trimethylsilyl)-L-threonine	5.85E-03	7.30E-03	6.79E-03	6.22E-03	6.56E-03	6.55E-03	4.37E-03	4.48E-03	5.88E-03	8.64E-03
N,O-Bis(trimethylsilyl)-L-phenylalanine	3.04E-03	3.54E-03	3.94E-03	3.24E-03	3.69E-03	3.71E-03	2.60E-03	2.70E-03	3.28E-03	3.84E-03
n-Butylamine, N,N-bis(trimethylsilyl)	1.31E-04	1.28E-04	1.29E-04	1.55E-04	1.35E-04	1.36E-04	2.01E-04	2.11E-04	1.55E-04	1.36E-04
Octadecanoic acid, trimethylsilyl ester	8.44E-04	8.40E-04	7.55E-04	5.15E-04	4.73E-04	4.72E-04	5.23E-04	5.70E-04	5.01E-04	4.58E-04
Oleic acid, trimethylsilyl ester	1.50E-04	1.20E-04	1.12E-04	7.74E-04	4.25E-04	6.52E-04	4.38E-04	3.25E-04	2.10E-04	3.49E-04

	-04	-04	-04	-05	-05	-05	-05	-05	-05	-05
Pantothenic acid, O,O,O-tris(trimethylsilyl) deriv.	9.38E-05	1.01E-04	9.20E-05	9.41E-05	9.40E-05	8.68E-05	8.27E-05	8.19E-05	9.19E-05	8.16E-05
Pentanedioic acid, 2-[(trimethylsilyl)oxy]-, bis(trimethylsilyl) ester	1.03E-04	9.54E-05	9.34E-05	9.65E-05	1.05E-04	1.00E-04	9.17E-05	9.91E-05	1.01E-04	1.06E-04
Pentanoic acid, 2-(methoxyimino)-3-methyl-, trimethylsilyl ester	3.85E-04	3.39E-04	3.86E-04	3.26E-04	3.47E-04	3.48E-04	1.26E-04	1.40E-04	9.93E-05	1.74E-04
Pentasiloxane, dodecamethyl-	4.06E-04	4.70E-04	4.60E-04	4.91E-04	4.76E-04	4.30E-04	5.00E-04	4.60E-04	4.99E-04	4.08E-04
Propanedioic acid, bis(trimethylsilyl) ester:2	7.04E-04	8.24E-04	8.78E-04	6.72E-04	8.35E-04	7.11E-04	8.35E-04	8.78E-04	8.89E-04	7.19E-04
Propanedioic acid, methyl-, bis(trimethylsilyl) ester	1.20E-04	1.32E-04	1.25E-04	1.35E-04	1.30E-04	1.47E-04	1.44E-04	1.21E-04	1.31E-04	1.37E-04
Propanoic acid, 2-(methoxyimino)-, trimethylsilyl ester	6.48E-03	5.38E-03	5.64E-03	5.41E-03	5.65E-03	6.16E-03	3.85E-03	3.59E-03	3.41E-03	3.89E-03
Propanoic acid, 2,3-bis[(trimethylsilyl)oxy]-, trimethylsilyl ester	4.21E-05	4.94E-05	4.88E-05	4.86E-05	4.64E-05	4.18E-05	5.62E-05	5.74E-05	5.45E-05	4.19E-05
Propanoic acid, 2-[(trimethylsilyl)oxy]-, trimethylsilyl ester:	2.86E-02	2.88E-02	2.92E-02	2.88E-02	3.01E-02	3.05E-02	3.02E-02	3.00E-02	3.26E-02	3.12E-02
Propanoic acid, 2-[(trimethylsilyl)oxy]-, trimethylsilyl ester	5.57E-04	5.34E-04	5.36E-04	5.58E-04	5.23E-04	5.50E-04	5.65E-04	5.44E-04	5.58E-04	5.32E-04
Pyrimidine, 2,4-bis[(trimethylsilyl)oxy]-	3.49E-04	3.49E-04	3.49E-04	3.36E-04	3.33E-04	3.28E-04	3.06E-04	3.12E-04	3.45E-04	3.16E-04
Ribitol, 1,2,3,4,5-pentakis-O-(trimethylsilyl)-	7.04E-04	6.24E-04	7.78E-04	7.72E-04	6.35E-04	7.11E-04	9.35E-04	8.78E-04	8.89E-04	7.19E-04

Compound										
Silanamine, N-[2-[3,4-bis[(trimethylsilyl)oxy]phenyl]ethyl]-1,1,1-trimethyl-N-(trimethylsilyl)-	3.57E-05	4.74E-05	4.64E-05	4.41E-05	6.22E-05	5.27E-05	2.99E-05	4.67E-05	5.30E-05	6.36E-05
Succinic acid (tms) (mainlib)	2.05E-04	2.13E-04	2.06E-04	2.07E-04	2.02E-04	1.98E-04	2.16E-04	2.17E-04	2.16E-04	2.13E-04
Trimethylsilyl ether of glycerol	1.22E-03	1.26E-03	1.27E-03	1.24E-03	1.23E-03	1.21E-03	1.18E-03	1.27E-03	1.32E-03	1.25E-03
Tryptophan, bis(trimethylsilyl)-	6.74E-05	4.23E-05	3.99E-05	4.46E-05	3.63E-05	5.24E-05	5.53E-05	5.67E-05	4.21E-05	3.82E-05
Tyrosine, O-trimethylsilyl-, trimethylsilyl ester	1.57E-03	9.58E-04	7.68E-04	1.16E-03	8.45E-04	9.26E-04	1.01E-03	1.09E-03	8.15E-04	7.43E-04
Urea, N,N'-bis(trimethylsilyl)-	7.15E-03	7.72E-03	8.08E-03	7.88E-03	8.27E-03	8.27E-03	7.56E-03	8.09E-03	8.80E-03	8.78E-03
Uridine 3TMS (Kishore-STDS)	3.51E-04	3.28E-04	3.82E-04	2.01E-04	2.55E-04	2.34E-04	9.57E-05	2.73E-04	2.07E-04	2.97E-04

ROSI-treated CHO-APP										
2,3,4-Trihydroxybutyric acid tetrakis(trimethylsilyl) deriv.	7.00E-05	7.33E-05	7.19E-05	6.56E-05	8.05E-05	6.75E-05	8.05E-05	7.62E-05	6.48E-05	7.24E-05
2-Piperidinecarboxylic acid, trimethylsilyl ester	2.86E-03	2.82E-03	2.96E-03	3.78E-03	3.73E-03	3.42E-03	3.12E-03	3.26E-03	3.52E-03	2.90E-03
3,8-Dioxa-2,9-disiladecane, 2,2,9,9-tetramethyl-5,6-bis[(trimethylsilyl)oxy]-, (R*,S*)-	1.26E-03	1.22E-03	1.20E-03	1.21E-03	1.21E-03	1.25E-03	1.21E-03	1.24E-03	1.21E-03	1.21E-03
3à-(Trimethylsiloxy)cholest-5-ene	1.19E-04	1.31E-04	1.22E-04	1.39E-04	1.14E-04	1.39E-04	1.31E-04	1.10E-04	1.38E-04	1.17E-04

Compound										
Acetic acid, [(trimethylsilyl)oxy]-, trimethylsilyl ester	2.93E-05	3.13E-05	3.89E-05	3.01E-05	3.64E-05	4.21E-05	3.60E-05	2.89E-05	4.21E-05	2.91E-05
Alanine, phenyl-, trimethylsilyl ester, dl-	6.15E-03	5.00E-03	5.21E-03	5.49E-03	5.84E-03	5.63E-03	5.48E-03	5.83E-03	7.17E-03	5.81E-03
Aminomalonic acid, tris(trimethylsilyl)-	6.06E-04	6.73E-04	6.36E-04	3.83E-04	6.44E-04	6.51E-04	6.72E-04	7.02E-04	4.19E-04	4.23E-04
Benzoic acid trimethylsilyl ester	8.48E-04	7.79E-04	7.74E-04	8.44E-04	7.94E-04	8.21E-04	7.93E-04	8.44E-04	7.86E-04	8.39E-04
Butanoic acid, 2-[(trimethylsilyl)amino]-, trimethylsilyl ester	1.03E-04	1.11E-04	1.15E-04	1.20E-04	1.05E-04	1.19E-04	1.03E-04	1.02E-04	1.13E-04	1.12E-04
Citric acid, tetrakis(trimethylsilyl) deriv. (mainlib)	5.45E-04	6.43E-04	6.83E-04	6.63E-04	5.32E-04	6.56E-04	6.09E-04	6.13E-04	6.77E-04	6.82E-04
d-Galactose, 2,3,4,5,6-pentakis-O-(trimethylsilyl)-, o-methyloxyme, (1Z)-	1.49E-03	1.71E-03	1.34E-03	1.43E-03	1.81E-03	1.38E-03	1.78E-03	1.72E-03	1.35E-03	1.59E-03
D-Glucitol, 6-deoxy-1,2,3,4,5-pentakis-O-(trimethylsilyl)-	7.82E-05	8.30E-05	8.07E-05	6.72E-05	7.90E-05	7.55E-05	7.56E-05	6.91E-05	8.02E-05	7.19E-05
D-Ribose, 2,3,4,5-tetrakis-O-(trimethylsilyl)-	2.98E-02	2.91E-02	3.00E-02	3.03E-02	2.91E-02	3.00E-02	2.91E-02	3.02E-02	3.03E-02	2.98E-02
Ethanedioic acid, bis(trimethylsilyl) ester	2.87E-04	4.44E-04	3.16E-04	3.87E-04	4.02E-04	3.54E-04	3.16E-04	2.76E-04	4.47E-04	3.78E-04
d-glucose	6.25E-04	5.82E-04	6.40E-04	5.78E-04	6.61E-04	6.81E-04	6.65E-04	7.37E-04	5.87E-04	6.78E-04
Glutamic acid, N,O,O'-tris(trimethylsilyl)-I (mainlib)	9.72E-04	8.16E-04	6.19E-04	6.03E-04	9.21E-04	8.85E-04	8.38E-04	8.14E-04	6.28E-04	9.13E-04
Glycine, N,N-bis(trimethylsilyl)-, trimethylsilyl ester	2.10E	1.99E	2.16E	2.24E	2.11E	2.24E	2.08E	2.15E	1.89E	2.11E

	C1	C2	C3	C4	C5	C6	C7	C8	C9	C10
	-02	-02	-02	-02	-02	-02	-02	-02	-02	-02
Glycine, N-formyl-, trimethylsilyl ester	4.21E-04	4.11E-04	3.95E-04	4.03E-04	3.24E-04	4.06E-04	3.68E-04	4.05E-04	3.51E-04	2.90E-04
Hexadecanoic acid, trimethylsilyl ester	1.23E-03	6.69E-04	9.10E-04	1.24E-03	6.16E-04	1.32E-03	1.43E-03	9.89E-04	7.12E-04	1.34E-03
Hexanoic acid, 2-(methoxyimino)-, trimethylsilyl ester	4.38E-04	3.60E-04	3.17E-04	3.10E-04	3.66E-04	3.20E-04	3.85E-04	4.13E-04	4.56E-04	4.35E-04
Lactic acid, bis(trimethylsilyl)oxy-, ester (mainlib)	4.54E-01	4.53E-01	4.53E-01	4.50E-01	4.75E-01	4.69E-01	4.83E-01	4.79E-01	4.72E-01	4.62E-01
l-Alanine, N-(trimethylsilyl)-, trimethylsilyl ester	2.96E-02	2.86E-02	2.44E-02	2.69E-02	2.70E-02	2.54E-02	2.91E-02	2.74E-02	2.45E-02	2.77E-02
L-Aspartic acid, N-(trimethylsilyl)-, bis(trimethylsilyl) ester	7.89E-04	6.54E-04	7.68E-04	6.93E-04	6.79E-04	5.74E-04	6.71E-04	6.87E-04	6.75E-04	5.50E-04
L-Cystine, N,N'-bis(trimethylsilyl)-, bis(trimethylsilyl) ester	8.80E-04	7.47E-04	7.23E-04	7.77E-04	8.80E-04	6.93E-04	6.70E-04	7.93E-04	8.30E-04	7.08E-04
L-Isoleucine, N-(trimethylsilyl)-, trimethylsilyl ester	4.35E-02	4.29E-02	4.31E-02	4.22E-02	4.49E-02	4.69E-02	4.34E-02	4.50E-02	4.53E-02	4.33E-02
L-Leucine, N-(trimethylsilyl)-, trimethylsilyl ester	1.57E-02	1.80E-02	1.46E-02	1.63E-02	1.77E-02	1.81E-02	1.67E-02	1.77E-02	1.49E-02	1.72E-02
L-Lysine, N2,N6,N6-tris(trimethylsilyl)-, trimethylsilyl ester	1.34E-02	1.32E-02	1.31E-02	1.38E-02	1.30E-02	1.38E-02	1.42E-02	1.23E-02	1.25E-02	1.45E-02
L-Methionine, ethyl ester	3.19E-03	3.08E-03	2.73E-03	2.59E-03	2.56E-03	2.85E-03	2.02E-03	2.43E-03	2.21E-03	2.71E-03
L-Methionine, N-(trimethylsilyl)-, trimethylsilyl ester	9.44E-04	8.35E-04	9.29E-04	7.62E-04	9.09E-04	9.51E-04	7.97E-04	8.63E-04	9.01E-04	1.00E-03

Compound										
L-Ornithine, N2,N5,N5-tris(trimethylsilyl)-, trimethylsilyl ester	3.94E-04	3.86E-04	5.24E-04	4.81E-04	4.31E-04	5.01E-04	3.73E-04	3.88E-04	3.64E-04	4.14E-04
L-Proline, 1-(trimethylsilyl)-, trimethylsilyl ester	3.31E-04	3.59E-04	3.38E-04	3.78E-04	3.55E-04	3.36E-04	3.38E-04	3.43E-04	3.75E-04	3.32E-04
L-Proline, 5-oxo-1-(trimethylsilyl)-, trimethylsilyl ester	1.24E-01	1.30E-01	1.42E-01	1.49E-01	1.25E-01	1.33E-01	1.23E-01	1.50E-01	1.26E-01	1.29E-01
L-Proline, ethyl ester	8.84E-04	9.24E-04	7.84E-04	7.43E-04	8.03E-04	7.37E-04	7.87E-04	8.53E-04	7.29E-04	8.20E-04
L-Serine, N,O-bis(trimethylsilyl)-, trimethylsilyl ester	1.36E-03	1.15E-03	1.40E-03	1.13E-03	1.17E-03	1.40E-03	1.15E-03	1.14E-03	1.13E-03	1.27E-03
l-Threonine, O-(trimethylsilyl)-, trimethylsilyl ester	1.25E-02	1.27E-02	1.38E-02	1.39E-02	1.35E-02	1.35E-02	1.40E-02	1.34E-02	1.39E-02	1.28E-02
L-Tyrosine, N,O-bis(trimethylsilyl)-, trimethylsilyl ester	1.10E-02	9.78E-03	1.02E-02	9.89E-03	1.08E-02	1.03E-02	1.10E-02	1.07E-02	1.05E-02	1.05E-02
L-Valine, N-(trimethylsilyl)-, trimethylsilyl ester (Kishore-STDS)	3.25E-02	3.65E-02	3.51E-02	3.26E-02	3.68E-02	3.79E-02	3.25E-02	3.81E-02	3.23E-02	3.32E-02
Malic acid, tris(trimethylsilyl) ester	1.21E-04	1.03E-04	1.09E-04	9.99E-05	1.28E-04	1.09E-04	9.60E-05	1.30E-04	1.30E-04	1.25E-04
Malonic acid, bis(2-trimethylsilylethyl ester	4.70E-06	4.64E-06	6.85E-06	5.23E-06	5.95E-06	5.42E-06	4.92E-06	7.44E-06	5.30E-06	7.30E-06
N,O,O-Tris(trimethylsilyl)-L-threonine	6.74E-03	6.41E-03	7.62E-03	5.88E-03	6.78E-03	7.63E-03	6.62E-03	6.64E-03	6.20E-03	7.00E-03
N,O-Bis(trimethylsilyl)-L-phenylalanine	3.82E-03	3.43E-03	3.24E-03	3.34E-03	3.01E-03	3.84E-03	3.61E-03	3.85E-03	3.84E-03	3.04E-03
n-Butylamine, N,N-bis(trimethylsilyl)	1.42E-03	1.58E-03	1.54E-03	1.40E-03	1.51E-03	1.59E-03	1.50E-03	1.49E-03	1.40E-03	1.60E-03

Compound										
	-04	-04	-04	-04	-04	-04	-04	-04	-04	-04
Octadecanoic acid, trimethylsilyl ester	8.46E-04	6.23E-04	7.77E-04	7.74E-04	8.16E-04	5.74E-04	7.98E-04	4.43E-04	4.71E-04	5.65E-04
Oleic acid, trimethylsilyl ester	5.21E-05	5.38E-05	1.00E-04	8.40E-05	1.11E-04	1.20E-04	6.36E-05	5.62E-05	4.32E-05	4.40E-05
Pantothenic acid, O,O,O-tris(trimethylsilyl) deriv.	8.57E-05	8.95E-05	9.56E-05	8.91E-05	8.60E-05	8.98E-05	8.89E-05	8.86E-05	8.64E-05	8.71E-05
Pentanedioic acid, 2-[(trimethylsilyl)oxy]-, bis(trimethylsilyl) ester	1.14E-04	1.13E-04	1.13E-04	1.15E-04	1.17E-04	1.22E-04	1.21E-04	1.13E-04	1.19E-04	1.16E-04
Pentanoic acid, 2-(methoxyimino)-3-methyl-, trimethylsilyl ester	3.23E-04	2.91E-04	3.55E-04	2.94E-04	3.25E-04	3.47E-04	2.88E-04	3.56E-04	2.66E-04	3.21E-04
Pentasiloxane, dodecamethyl-	4.43E-04	4.70E-04	4.44E-04	4.24E-04	4.17E-04	4.38E-04	4.59E-04	4.60E-04	4.42E-04	4.74E-04
Propanedioic acid, bis(trimethylsilyl) ester:2	7.77E-04	8.28E-04	7.69E-04	7.76E-04	7.80E-04	7.80E-04	8.13E-04	8.05E-04	8.40E-04	8.38E-04
Propanedioic acid, methyl-, bis(trimethylsilyl) ester	1.43E-04	1.53E-04	1.67E-04	1.60E-04	1.46E-04	1.55E-04	1.59E-04	1.56E-04	1.65E-04	1.57E-04
Propanoic acid, 2-(methoxyimino)-, trimethylsilyl ester	5.02E-03	4.21E-03	4.41E-03	3.98E-03	4.64E-03	5.19E-03	4.96E-03	5.00E-03	4.07E-03	5.40E-03
Propanoic acid, 2,3-bis[(trimethylsilyl)oxy]-, trimethylsilyl ester	4.55E-05	5.81E-05	5.46E-05	5.03E-05	5.53E-05	5.08E-05	4.50E-05	4.54E-05	5.72E-05	4.89E-05
Propanoic acid, 2-[(trimethylsilyl)oxy]-, trimethylsilyl ester:	3.22E-02	3.22E-02	3.20E-02	3.13E-02	3.07E-02	3.25E-02	3.14E-02	3.26E-02	3.21E-02	3.17E-02
Propanoic acid, 2-[(trimethylsilyl)oxy]-, trimethylsilyl ester	5.42E-04	5.51E-04	5.35E-04	5.38E-04	5.33E-04	5.49E-04	5.31E-04	5.46E-04	5.38E-04	5.54E-04

Compound										
Pyrimidine, 2,4-bis[(trimethylsilyl)oxy]-	3.47E-04	3.34E-04	3.37E-04	3.63E-04	3.51E-04	3.23E-04	3.22E-04	3.61E-04	3.33E-04	3.44E-04
Ribitol, 1,2,3,4,5-pentakis-O-(trimethylsilyl)-	7.50E-04	7.69E-04	8.61E-04	8.50E-04	8.12E-04	8.26E-04	7.86E-04	8.57E-04	7.80E-04	6.62E-04
Silanamine, N-[2-[3,4-bis[(trimethylsilyl)oxy]phenyl]ethyl]-1,1,1-trimethyl-N-(trimethylsilyl)-	6.07E-05	6.14E-05	6.00E-05	5.75E-05	5.95E-05	6.15E-05	6.19E-05	5.61E-05	5.20E-05	5.76E-05
Succinic acid (tms) (mainlib)	2.03E-04	1.96E-04	1.94E-04	1.94E-04	1.92E-04	2.02E-04	1.98E-04	2.06E-04	2.00E-04	1.93E-04
Trimethylsilyl ether of glycerol	1.30E-03	1.31E-03	1.35E-03	1.33E-03	1.31E-03	1.30E-03	1.35E-03	1.29E-03	1.33E-03	1.35E-03
Tryptophan, bis(trimethylsilyl)-	2.39E-05	3.13E-05	3.05E-05	3.11E-05	3.81E-05	2.80E-05	3.91E-05	2.26E-05	3.95E-05	3.56E-05
Tyrosine, O-trimethylsilyl-, trimethylsilyl ester	9.36E-04	1.23E-03	1.63E-03	1.26E-03	1.18E-03	1.02E-03	1.22E-04	1.31E-04	1.21E-04	1.04E-04
Urea, N,N'-bis(trimethylsilyl)-	8.73E-03	8.32E-03	8.80E-03	8.02E-03	8.67E-03	7.91E-03	8.56E-03	8.20E-03	8.07E-03	8.37E-03
Uridine 3TMS (Kishore-STDS)	2.96E-04	5.47E-04	3.39E-04	5.30E-04	3.41E-04	5.84E-04	4.76E-04	2.28E-04	2.73E-04	3.95E-04